2018-04-01

Creation and Use of Software for Analysis of Kinetic Proteomic Experiments

Bradley C. Naylor
Brigham Young University

Creation and Use of Software for Analysis of Kinetic Proteomic Experiments

Bradley C. Naylor

A dissertation submitted to the faculty of
Brigham Young University
in partial fulfillment of the requirements for the degree of

Doctor of Philosophy

John C. Price, Chair
Barry M. Willardson
Steven W. Graves
Benjamin T. Bikman
Daniel E. Austin

Department of Chemistry and Biochemistry

Brigham Young University

ABSTRACT

Creation and Use of Software for Analysis of
Kinetic Proteomic Experiments

Bradley C. Naylor
Department of Chemistry and Biochemistry, BYU
Doctor of Philosophy

Proteins are constantly synthesized and destroyed to ensure sufficient functioning proteins to meet cellular needs, a process called protein turnover. Synthesis and degradation are carefully balanced over time to ensure that average protein concentrations do not change drastically. The status quo of the cell, or protein homeostasis, is required for the health of the organism. If protein homeostasis breaks down, serious diseases, such as Alzheimer's, can result when proteins aggregate instead of being degraded properly. Because protein turnover is the means to maintain protein homeostasis while keeping sufficient functioning proteins, measuring protein turnover is critical to understanding biological processes and disease states. Measuring protein turnover rates on a broad scale is possible using a method called kinetic proteomics, and the improvement of kinetic proteomics is where I have focused the work for this dissertation.

In this dissertation, I will review the history and general strategies for performing kinetic proteomics. I will then demonstrate that I have published an open source, user-friendly program for other scientists to use to perform kinetic proteomics data analysis, as well as publishing a novel discovery of key ribosomal subunits being replaced within the lifetime of the ribosome, which was discovered through use of kinetic proteomics. Finally, I will discuss work that is ongoing to improve my software tool for use in human subjects, and work being done to combine kinetic proteomics with other global analysis methods to make novel biological discoveries.

Keywords: kinetic proteomics, ribosome, software, dietary restriction

ACKNOWLEDGMENTS

I would like to acknowledge my advisor Dr. JC Price who has been very supportive, helpful in evaluating new ideas, and in teaching me about kinetic proteomics and mass spectrometry. I would also like to acknowledge Andrew Mathis, Richard Carson, and Michael Porter for the assistance and work they provided for the work presented in this dissertation. I would like to acknowledge Dr. John Dallon, who served on my committee for most of my graduate schooling. Without his help on the mathematics, the chapter "Modifications of DeuteRater for Use in Human Subjects" would not exist. I would also like to acknowledge my committee members for helpful and insightful conversations.

I acknowledge and am grateful to Brigham Young University, especially the Department of Chemistry and Biochemistry, for providing a place for me to work and funding my research and providing a stipend through various fellowships. I am immensely grateful for the financial and institutional support I have received while pursing my graduate education.

I would also like to acknowledge my family. My parents, sister, and in-laws have provided support during difficulties I encountered while pursuing my graduate work. Finally, without my wife Rachel and children James and Lizzy I would not have had the support and motivation to complete my graduate work.

TABLE OF CONTENTS

LIST OF TABLES

LIST OF FIGURES

1. **Introduction**

All biological systems are dynamic. As cells alter gene expression in response to stimuli, amounts of proteins and signaling molecules change, and old proteins undergo replacement with new copies to ensure the cell has sufficient working proteins to perform necessary functions. Loss of the dynamic controls may occur due to deregulation of synthesis or degradation [5,6], and is thought to be the cause of biological aging as well as diseases such as Alzheimer's disease, which is characterized by a lack of protein removal[10].

Large (–omics) scale studies following multiple analytes (1000's) are well suited for studying complex systems like a cell. –Omics studies attempt to see all of a certain type of a bio-molecule in a cell, tissue, or organism. Of particular interest is proteomics, because proteins are responsible for carrying out most cellular reactions and responses. Altered conditions within the cell are largely the result of a change in protein expression and behavior. These changing conditions may result from different disease states, environmental conditions, dietary inputs, and so on.

Proteomic methods for determining the presence of proteins in samples or measuring differences in protein quantity between samples are relatively mature and advanced technologies[11-1310]. In contrast, kinetic proteomics, which measures how quickly proteins are turned over, that is destroyed and replaced by new copies, is a more recent method. The underlying premise is that experimental perturbations to the proteome should also change the

turnover rates of proteins, and these kinetic changes may be far more visible than changes in protein presence or quantity. Kinetic proteomics is also useful in cases where protein quantity and expression are not changing, but the turnover rate is, such as in liver cirrhosis[12,14].

In this dissertation, I will begin by further discussing the significance and practical applications of kinetic proteomics. I will then discuss the history of kinetic proteomics in order to describe its foundations and further demonstrate its utility. Next, I will elaborate on the different ways that kinetic proteomics can be done, in order to illustrate why our lab uses some kinetic proteomics techniques and not others. Finally, I will outline the contributions I have made to the field of kinetic proteomics, namely the creation and use of software tools to analyze kinetic proteomic data.

1.1 Practical Uses of Kinetic Proteomics

The first question to be asked of any method is "what is the benefit of this method?" Kinetic Proteomics has several advantages over current proteomics methods. The first is that it is orthogonal to current tests. Because of this it can be combined with various other assays, including other mass spectrometry methods, and still provide unique information. The combination of multiple large data sets from many measurement types is an idea that is becoming more popular in proteomics. The combinations give a more holistic picture of any biological condition, so causes and effects can be better understood[14]. The most obvious method to combine with kinetic proteomics is quantitative proteomics[17], since the only way for the pool size of protein to change is for the ratio of synthesis to degradation (protein turnover rate) to change. The addition of RNA-Seq to quantify RNA amounts and compare them against the turnover rate of their protein product has also been used to investigate gene expression[19]. These

types of studies provide better understanding of disease and treatment effects, which can benefit clinical scientists and physicians.

Proteomics relies on mass spectrometry which is very practical in the clinic, where few samples should be required, and as much data as possible gleaned as rapidly as possible. The metabolic incorporation of isotopes used for kinetic proteomics methods labels many bio-molecules that can be analyzed by mass spectrometry[2,20]. A few targeted lipid and protein turnover rates from blood or limited biopsies can reveal information about diseases[2,2019], exercise and cardiac health[21], and labeled DNA can be used to measure cancer progression[20]. Models of heart disease[22], aging[23-25], metabolism[23-25], skin disease[10,26], and drug testing[10,26] have all been investigated using kinetic measurements of various bio-molecules. Some studies of proteins have been translated to clinical settings already[10,26].

A more recent, but related, idea is the virtual biopsy[28]. A patient is provided with a heavy isotope tracer to initiate metabolic labeling, and then blood is collected at predetermined time points. Since blood proteins are produced in a variety of tissues, the turnover rates of proteins in the circulatory system can be used to extract information about the organs that produced the proteins without the need for a direct biopsy. This method can be used to measure proteins directly involved in disease, such as collagen in diseases with liver cirrhosis[30,31], or to analyze protein production in specific tissues to assess overall tissue health[21,32-36].

Kinetic proteomics is useful for both clinical and basic research applications, providing unique information unavailable by other methods. However, the field of kinetic proteomics did not begin this way, and does have limitations. I will present a review of the history of this method to demonstrate its applications, its limitations, and how its limitations have been overcome.

1.2 Historical Development of Kinetic proteomics

1.2.1 The Foundation of Dynamic Measurements of Bio-Molecules

The foundation for what would become kinetic proteomics began in the 1930s when Dr. Rudolf Shoenheimer used stable isotopes to determine that lipids[21,32-36] and proteins[21,32-36] are replaced by cells over time. He also demonstrated that two different stable isotopes, ^{15}N and ^{2}H, could be incorporated into new bio-molecules of an experimental animal. Exact turnover rates could not be determined because the mass spectrometry technology was not up to the task: the quantity of an isotope could only be determined in a measurement of the pure element. Complex mixtures of molecules, such as amino acids and proteins, were beyond the reach of the technology.

In the 1980's more progress was made by Dr. Spencer Commerford, who found that both DNA and proteins incorporate ^{3}H when it was provided to laboratory animals in drinking water. While the radioactivity of the ^{3}H complicates its use in humans, it enabled the amount of isotope incorporated into different amino acids in proteins to be determined by the radioactivity they exhibited. As expected, the essential amino acids exhibited little radioactivity and the non-essential amino acids exhibited more.

1.2.2 Development of Kinetic Proteomics: From Small Molecules to Full-scale Proteomics

In the 1990s mass spectrometers had improved to the point where analyzing stable isotopes in intact biomolecules was possible. Stable isotope labeling allows many bio-molecules to have a detectable label without the hazards and instability of radioactive isotopes. Work began with small bio-molecules, such as lipids and nucleotides. Labeled small bio-molecules can be used to determine biological conditions, DNA labeling rates are a metric of cell proliferation rates for example[41,42], but the ability to perform protein analysis was still

undeveloped. It took several years to apply these techniques to proteins, but in the early 2000s researchers began to use stable isotopic metabolic labels in proteins. By isolating a specific protein[43,44] or many proteins (with the goal of getting an average rate for all proteins) [23,33,45] , then digesting them to amino acids and measuring the incorporation of label into one or more amino acids.

Proteins were more difficult to analyze by mass spectrometry because mass spectrometers can only analyze molecules in the gas phase. All of the molecules described above required chemical modification to be able to enter the gas phase. Unlike DNA, proteins exist in many forms with many different properties. Therefore, important information about cellular operations can be gained by monitoring individual protein species, but the average turnover rate less informative. Therefore, a new technology was needed to allow peptides to enter the gas phase intact, so proteins could be identified without excessive purification. The new technologies to allow peptides and proteins to enter the gas phase was actually developed in the 1980's [46-49]. Matrix Assisted Laser Desorption\Ionization (MALDI) allows the ionization of peptides within a matrix of organic acid, while Electro-Spray Ionization (ESI) allows the ionization of all peptides in a constant stream of liquid. Both of these methods allow the peptides to enter the gas phase and be analyzed by mass spectrometry. It took several years to apply these techniques to kinetic measurements, because while the peptides could be seen in the mass spectrometer, they could not be identified making analysis of individually separated proteins of known identity a better choice.

By the late 1990s and 2000s the technology and analysis software had advanced sufficiently so peptides in a mass spectrometer could be identified and matched to a database of proteins present in a given organism. With the ability to identify peptides, mass spectrometry

could be used to measure the incorporation of stable isotopes into intact peptides. These experiments used either synthetically labeled amino acids or ^{2}H, which labeled amino acid used for making proteins in the amounts detailed by Commerford[46-49], in the organism's diet. The labeled amino acids were incorporated into proteins. Once heavy label was incorporated, the proteins could be separated by two-dimensional (2-D) electrophoresis, and then analyzed using MALDI or ESI. While a few labs started targeting specific proteins using these new methods[51], dynamic measurements were still limited. Initially measuring peptide incorporation was only moderately more convenient than digesting the separated proteins to amino acids. An important step facilitating kinetic proteomics was made by Doherty et al. in the mid 2000s[24,53,54]. Instead of simplifying the analysis to one protein target, Doherty used similar experimental methods to analyze all observed proteins. The ability to measure isotope incorporation in many proteins at once paved the way for modern kinetic proteomics to measure thousands of protein turnover rates in a single experiment. Interestingly, while many of the earlier studies had relied on theoretical models[24,53,54], Doherty used an empirical method. In her experiment, labeled valine was provided to chickens, and the incorporation of the valine into proteins was measured. Peptides containing two or three valines were used to determine how much labeled valine was available, while peptides with a single valine were used to construct kinetic curves and calculate rates. This strategy worked well and set the stage for more improvements to kinetic proteomics in the early 2010s.

The first major advancement in the 2010s was the use of ^{2}H for measuring many proteins at a time. The initial work was done by the Previs lab, who first used deuterium for large scale kinetic proteomics[24,53,54]. Hellerstein followed with a more theoretical model for analyzing the dynamic proteomic data and using kinetic proteomics in humans[55,56]. Finally, Ping followed

within a few years adopting the Previs method initially, but eventually developing an improved mathematical model of deuterium incorporation in humans[57]. Because of this progress, any investigator using kinetic proteomics is faced with a variety of choices about labeling techniques, calculation methods, and analysis tools. I will analyze these below and provide justification for the approaches I have chosen in my research.

1.3 Modern Kinetic proteomics

1.3.1 Method for Label Administration

How to administer isotopic labels to experimental subjects is critical for kinetic proteomics: the isotopic labeling strategy determines analysis methods that can be used, which amino acids are labeled, which other bio-molecules are labeled, where on the bio-molecules the label is incorporated, and the software tools available to the researcher. There are two major heavy isotope labeling strategies used in kinetic proteomics. The first is metabolic labeling, in which the subject is fed raw material with an added isotopic label. This labeling is commonly done with $^{2}H_2O$, because it is non-toxic (even in humans[59]), easy to use, and will label all bio-molecules in the body that are synthesized with hydrogen[50,60]. Other commonly used materials are nitrogen(^{15}N)-containing salts[50,6027] and $H_2{}^{18}O$ [52,61]. The cell then uses the labeled molecules to create monomers, such as amino acids, incorporating the provided isotopic label into the desired polymer, such as protein.

The second strategy, Stable Isotope Labeling of Amino acids in Mammals (SILAM), is based on providing the labeled amino acids and skipping some of the metabolic steps[52,61]. While SILAM was originally intended for measuring quantities of protein, the adaptation of the method for kinetic proteomics is relatively simple. In this method, a heavy-labeled essential amino acid

is provided to the subject; usually this is leucine[23,62], although other amino acids[23] or even all amino acids[64] are possible choices. The labeled amino acid(s) are incorporated into new proteins. Advantages and disadvantages of these two methods are described in Table 1-1.

Table 1-1: Comparison of Advantages and Disadvantages of Metabolic Labeling and SILAM Style Labeling

Metabolic Labeling		SILAM Style Labeling	
Advantages	Disadvantages	Pros	Cons
Easy to use in humans[23,58,65]	Label incorporation can shift based on metabolic conditions[23,58,65]	Very useful in cell culture[66]	Large amounts of extra amino acids in the diet can disrupt metabolism[27,59,67,68]
Most peptide populations contain a labeled amino acid[27,59,67,6866]	Software is currently more limited than the SILAM method[59]	Software tools widely available that will perform calculation with minimal in-house work[55,65,69]	Only peptide fragments that contain the labeled amino acid(s) are useful for turnover calculations[59,61]
^{2}H enrichment in body water is easily determined[59,6158]	Difficult to rapidly achieve stable isotope enrichments in humans[16,59,61]	Mass spectra of labeled and unlabeled species are easily distinguishable[65]	Enrichment of amino acid pool is difficult to determine without intravenous infusion or control of the entire diet[55,7065]
All molecules biosynthesized using the heavy element are labeled[68,71]	^{2}H can cause vertigo in larger doses[68,7161]	Calculation is conceptually easy to understand	
Stable isotope enrichment causes rapid saturation of every cell with labeled amino acids[23,52,56,65]			Dietary amino acids require variable amounts of time to enter the amino acid precursor pool, complicating calculations[23,52,56,65]

In the table above, there are two points that deserve expansion. The first is the software requirement. Many commercial or freeware proteomics tools, such as PEAKs and Skyline, have been developed for the common quantitative techniques SILAM and its cell culture analogue SILAC. These methods generally rely on mixing samples both with and without a heavy isotope, and then comparing the signal abundance ratios of the distinctly separated mass spectra. In kinetic proteomics the analysis is similar: samples are analyzed, and the ratio of heavy to light (new to old) molecules can be compared over a time course. Since SILAM analysis software performs this comparison readily, mass spectrometry groups already have access to software to do this form of analysis, and simply have to the combine the results from all experimental time-points to determine a kinetic curve. Metabolic ^{2}H labeling uses a lower amount isotopic enrichment than SILAM style labeling, for reasons of both cost and safety[73,74]. As a result, the change in molecular weight is not as large as that which SILAM/SILAC software expects. In fact, peptides labeled by low enrichment ^{2}H can be misidentified by the software as contaminants due to unnaturally distributed isotope patterns.

Despite the computational difficulty, metabolic labeling with ^{2}H has a key advantage. The labeled amino acids used in the SILAM method need to make it through the gut and various other metabolic processes. They must be transported to each cell before they are attached to tRNAs and incorporated into a protein. This creates differences in availability for different organs and different locations in each organ. Measuring the progress of amino acid availability is also difficult because the amount of labeled amino acids in the blood is not necessarily indicative of the labeled amino acids in the cell[52,58,75]. The resulting incorporation speed is no longer negligible, and the turnover rates must now be modeled as two pools: one of amino acids in the diet, and the other attached to the tRNA molecules[52,58,7558]. The necessity of this two-pool

model complicates kinetic calculations significantly. The distribution of ^{2}H to each cell from drinking water or injection is much faster. The ^{2}H equilibrates rapidly and uniformly through the organism through hydrogen exchange. While there is a delay resulting from synthesis of the amino acids and loading the tRNA[13,38,73], it is more uniform and generally negligible except in very fast experiments[13,38,73].

Therefore, for my work we chose metabolic $^{2}H_2O$ labeling. Calculation with this method was simplified by the lack of a significant incorporation time compared to the length of the experiment[13,38,73]. Software for analysis of this type of data is less well known than software for SILAM experiments, so we created our own specialized software tools, which would in turn aid other researchers.

1.3.2 Measuring Label Incorporation or Decay

After a label for the kinetic proteomics experiment has been chosen, the researcher must determine if the label should be measured as it is being incorporated or as it is being removed. Label decay methods are analogous to classic pulse-chase experiments[13,14,76]. The label is applied until all the proteins of interest have incorporated enough of the label that the labeled population is easily observed as distinct from the unlabeled population. The labeling source, either labeled food or water, is removed and the amount of label in proteins is measured at various times. The amount of label present at the various times are fit to an experimental decay curve as the labeled population decreases, and a turnover rate calculated.

An alternative approach is to model label incorporation, and starts the experimental subjects with no extra heavy isotopes[24,45,53]. The isotopic label is applied at the start of the experiment and measurement of incorporation into the bio-molecules of interest begins

immediately. The data points from various time-points are fit to an exponential rise-to-plateau equation for calculation of a rate constant.

The advantage of using decay modeling is that the amount of signal early in the experiment is much higher. Since the data is fit to an exponential model in both methods the early measurements, where the plateau has not been reached, are more important in determining the fit line. Decay has more signal at these points, and thus has better signal to noise on the most critical points. However, we chose the incorporation method of labeling for my experiments and software development. This focus on label incorporation measurements was largely due to practicality; it is easily applicable to a proteome scale experiments where turnover rates vary by more than four orders of magnitude, while attempting to pre-label while ensuring significant labeling of proteins across a wide range of kinetic ranges is time-consuming and expensive[35,36]. Knowing the absolute endpoints possible for isotopic enrichment of every protein regardless of rate simplifies the modeling and allows analytical validation of the experimental isotope enrichment. The incorporation labeling method also provides confidence when observing potentially important biological deviations[35,36] from a theoretical model.

1.3.3 Theoretical vs Empirical Models

Once the metabolic labeling experiment has been performed and the isotope data extracted from the mass spectral files, the data must be analyzed. Both theoretical and empirical methods have been used to turn peptide isotopic data from a ^{2}H incorporation experiment into a functional kinetic curve from which a turnover rate can be determined.

The empirical method is conceptually straightforward. During the experiment, a steady amount of heavy isotope label is applied, and the change in the isotope pattern of target molecules at several time points is measured[23,24] (Figure 1-1). At each time-point the neutromer

peaks within the isotope pattern are weighted (normalized peak abundance multiplied by the number of extra neutrons in the peak) and summed together. The weighted sum of an isotope pattern with no heavy label added is subtracted from the weighted sums at all time-points. The data from all time points are fit to a first order rate curve to determine the turnover rate constant (Figure 1-1). This method requires that the experiment extend to sufficient times to describe each saturation curve.

The theoretical method, although more computationally intensive, removes this requirement for very long labeling times. The concept was first formalized in an approach called Mass Isotopomer Distribution Analysis (MIDA)[45]. MIDA is based on the principle that an isotopically diverse population of any molecule is detected by a mass spectrometer. For example, Figure 1A represents the natural distribution observed for a single peptide GAFGKPQGTVAR. Because isotopes of carbon, hydrogen, oxygen and other elements within the peptide were present at the time of synthesis, they were incorporated at a percentage representative of the availability. The relative intensities of the different m/z values in the molecular population are the result of the different isotope availabilities. MIDA assumes no bias exists for, or against, heavy isotopes during the creation of bio-molecules. These principles allow the use of combinatorial statistics to determine the theoretical isotope pattern without experimental measurement of the isotopic pattern before or at the endpoint of increased heavy label availability (Figure 1-1 D-E). After introducing the ^{2}H, mass spectra of the peptide can be collected to determine the amount of labeled protein at the time the data was collected. Although a single measurement allows fitting a first order rate curve (Figure 1-1 F) and determination of a turnover rate constant, combining the data from multiple time points improves signal to noise and fitting confidence.

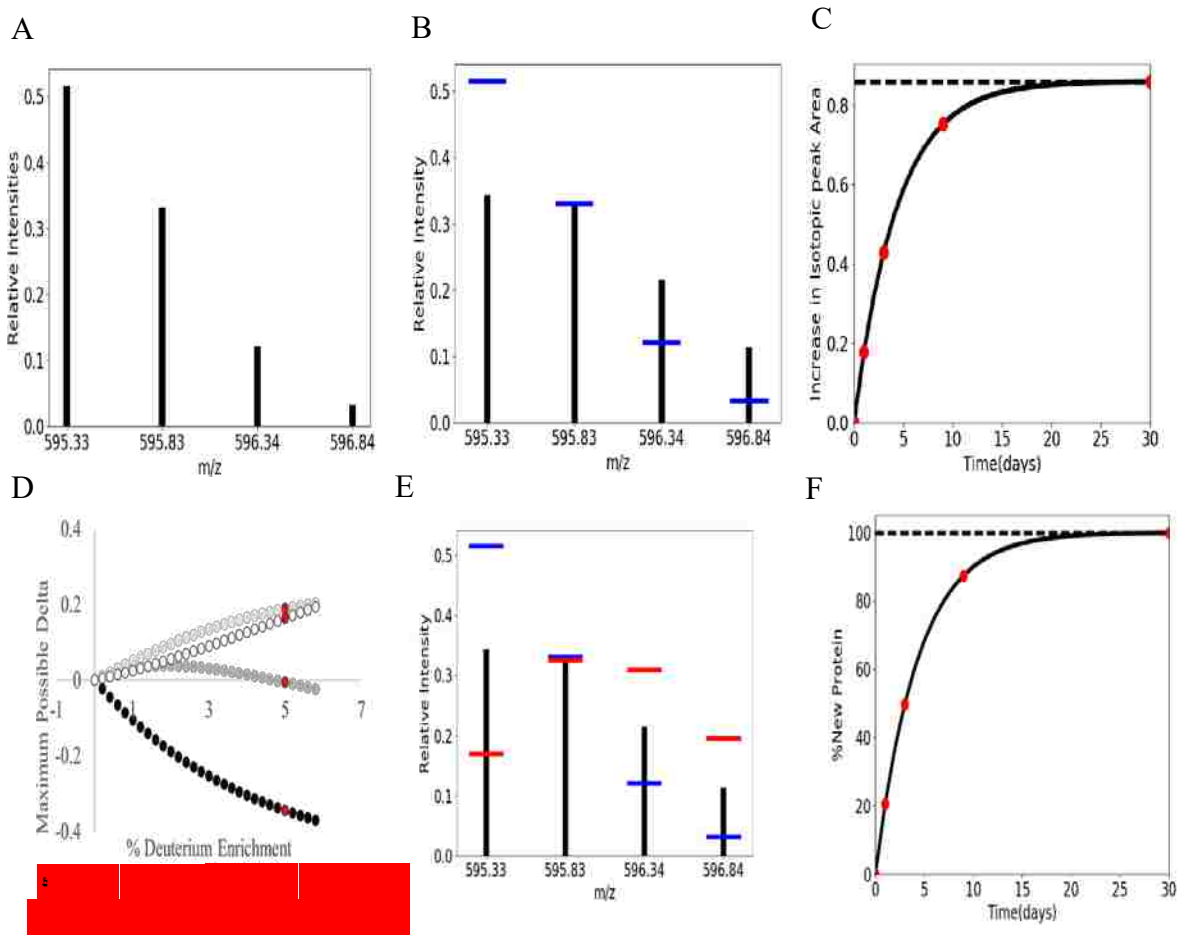

Figure 1-1 Theoretical vs Empirical Analysis Method: The difference between Empirical (B, C) and Theoretical (D, E, F) calculations using the peptide GAFGKPQGTVAR measured at charge state 2 as an example. The isotopic envelope of the peptide as detected by the mass spectrometer is shown in panel A (no extra heavy isotopes are present). The m/z values on the x-axis represent the mass to charge ratios for the sequence with different numbers of extra neutrons (0-3 extra going from left to right). In the empirical method, a weighted sum of the intensities of the peaks (intensity multiplied by the number of extra neutrons) is calculated from the black bars representing experimental endpoint measurements (Panel B). The weighted sums of the baseline intensity (blue lines) are then subtracted from the measured weighted sum (Panel B). In Panel C the weighted sums are plotted at multiple times (red dots) and a curve fit to the points (black line) which can be used to determine the turnover rate. In the more complex theoretical approach, the maximum possible change of each peak in panel A at different enrichments is calculated by combinatorial statistics (Panel D); M(number) indicates the change in the peak with (number) extra neutrons. The experimental amount of enrichment is selected (red dots). In Panel E, actual measurements at a time point (black bars) are compared with the intensities at baseline (blue lines) and the predicted change at maximum label incorporation (red lines). The difference between the experimental change (blue to black) divided by maximum theoretical change (blue to red) for each peak can be expressed as a percent. In Panel F measurements at several times are plotted in red. The black line is fit to the data, and the turnover rate determined from the equation of the curve.

Table 1-2: Comparison of Advantages and Disadvantages of Theoretical vs. Empirical calculation models

Theoretical		Empirical	
Advantages	Disadvantages	Advantages	Disadvantages
Easy to adjust to non-constant label; necessary for human labeling[24,4545]	Need to know the number of sites available for stable ^{2}H incorporation for every amino acid	Knowledge of monomer enrichment not required[77]	Requires very strict data filtering[51]
Can detect cases where labeling is incomplete[35,5151]	Susceptible to instrument bias	Conceptually easier to understand.	Cannot detect instances where the entire pool of proteins does not turnover[23,24,50]
Can use each peptide isotope pattern to calculate measurement error[23,24,5023]		If using the same instrument for all measurements, resistant to instrument bias	
The theoretical changes in isotopic incorporation can be used to calculate enrichment[23,24,50]			

For my work, we chose the theoretical method. It was attractive due to the ability to deal with a changing amount of label in the subject, and enabled filtering based on theoretical differences. The flexibility to deal with a changing amount of label deserves elaboration. If the amount of heavy isotope in the experimental subject changes over time, as is often the case when

working with humans[68], the heavy isotope incorporation will not be uniform over the time course of the experiment. As a result, the spectral changes due to the maximum isotope incorporation (red lines, Figure 1-1 E) at any point will not be stable. Not only will it vary by the amount of heavy isotope the experimental subject has consumed thus far, but it will be different for every protein depending on the turnover rate of that protein: the longer it takes for a protein to be replaced (turned over), the wider the variety in amounts of deuterium present in the amino acids of that protein's population. This makes applying a uniform correcting factor to all proteins unfeasible. Instead, any correction needs to be applied on a protein-by-protein basis[80]. The protein-by-protein correction requires mathematical modeling which cannot be applied to the empirical method, where it is necessary to assume a constant maximum label availability. The application of theoretical modeling requires software to perform individual calculations for each peptide on a proteomic scale, which is commonly 60,000 peptides at 8 time points. We will discuss these tools in the next section.

1.3.4 Software

Specialized software is utilized in every step of mass spectrometry based proteomics experiments. The amount of data generated in any experiment is simply too large and complex to fully analyze by hand. For example, SearchGUI[50] is a program that determines the identity of peptides from mass spectrometry data by accessing up to 10 different identification algorithms, each from a different research group. Several data analysis and visualization tools exist such as Skyline[45] and PeptideShaker[82] to provide statistics for identified spectra. In order to enable different programs to analyze the same data, a file format converter such as MSConvert[24] is required.

The open availability of trusted software tools such as these saves programmers from having to create software that replicates the work of others. Earlier programs can perform the basic tasks of proteomic analysis, allowing users to convert files to an appropriate file type, and provides them the choice of which search engine and analysis tool they prefer to use to perform peptide identifications. The programmer is then free to focus on creating entirely new software tools, which is beneficial for kinetic proteomics because the calculation process can be quite involved.

Several groups have already provided software to facilitate the calculations needed for the complex calculations in kinetic proteomics. Topograph[1], for example, is a program based on the SILAM style calculations used in the Doherty experiments[2]. A different program developed by the Sandygov lab uses metabolic labeling with ^{2}H based on the empirical calculations detailed in Figure 1-1 panels B-C-[3,4]. Both of these calculation types are valid, but they do not incorporate theoretical analysis of ^{2}H labeling. This leaves a rather large gap in software options because, as explained above, theoretical calculations are the best way to perform dynamic proteomic experiments in humans. In our software[3,4], I have sought to fill this gap as well as improve on what these other packages provide to allow researchers greater flexibility in their experimental methods.

There is a previous software package that can perform calculations for theoretical labeling with ^{2}H, even in humans, called ProTurn[5,6]. However, ProTurn is not openly available and is limited by only examining one portion of an isotope pattern, while DeuteRater uses the abundance of multiple isotopic peaks and the spacing between them to quantify the accuracy of its measurements. This is detailed in the "DeuteRater: a Tool for Quantifying Peptide Isotope Precision and Kinetic Proteomics" Chapter. While the initial release of DeuteRater cannot

perform calculations on human subjects, I am working to incorporate the use of changing isotope enrichment profiles. Improvements to DeuteRater for human work are detailed in the chapter "Creation of Software Tools and Methods for Measurement of Kinetic Proteomics in Humans". In addition, DeuteRater is freely available for all to use and modify, while ProTurn requires specific permission of its creators to access. Further, DeuteRater provides options for labeling different biological systems with different isotopic labels. My work provides an open source improvement that accesses more of the information available in the isotope labeling experiments.

1.4 Conclusion and My Contribution

Although initially viewed as a niche application, kinetic proteomics has developed into a practical proteomics method. As methods of kinetic proteomics have improved, the approach has become a feasible way to answer many biological questions. The technique yields unique biological information, either through analysis of protein turnover rates on their own, or by combination with other –omics techniques. Experiments can also be performed using a wide variety of isotopic labels and calculation methods in diverse biological systems.

However, one of the major limitations to performing kinetic proteomics experiments is the current lack of user-friendly openly available software tools to perform the calculations. The focus of my work has been to provide such software. DeuteRater also improves on the kinetic proteomics software currently available to researchers, and will help other scientists add kinetic proteomics capability to their labs. This dissertation details the software development for kinetic proteomics experiments involving small animals in the "DeuteRater: a Tool for Quantifying Peptide Isotope Precision and Kinetic Proteomics" chapter and humans in the "Creation of Software Tools and Methods for Measurement of Kinetic Proteomics in Humans" chapter. The

utility of the software and kinetic proteomics on its own is demonstrated in "Mechanisms of *in vivo* Ribosome Maintenance Change in Response to Nutrient Signals" and in conjunction with other –omics techniques in "Short-Term Calorie Restriction Elicits Nutrient-Specific Post-Transcriptional Regulation of Proteostasis".

1.5 Bibliography

1 Savas, J. N., Toyama, B. H., Xu, T., Yates, J. R. & Hetzer, M. W. Extremely long-lived nuclear pore proteins in the rat brain. *Science* **335**, 942, doi:10.1126/science.1217421 (2012).

2 Thompson, A. C. *et al.* Reduced in vivo hepatic proteome replacement rates but not cell proliferation rates predict maximum lifespan extension in mice. *Aging Cell* **15**, 118-127, doi:10.1111/acel.12414 (2016).

3 Verzijl, N. *et al.* Effect of collagen turnover on the accumulation of advanced glycation end products. *J. Biol. Chem.* **275**, 39027-39031, doi:10.1074/jbc.M006700200 (2000).

4 Martinez-Vicente, M., Sovak, G. & Cuervo, A. M. Protein degradation and aging. *Exp. Gerontol.* **40**, 622-633, doi:10.1016/j.exger.2005.07.005 (2005).

5 Ballard, C. *et al.* Alzheimer's disease. *Lancet* **377**, 1019-1031, doi:10.1016/S0140-6736(10)61349-9 (2011).

6 Keller, J. N. & Ding, Q. in *Prevention and Treatment of Age-related Diseases* (eds Suresh I. S. Rattan & Moustapha Kassem) 297-312 (Springer Netherlands, 2006).

7 de Groot, M. J. *et al.* Quantitative proteomics and transcriptomics of anaerobic and aerobic yeast cultures reveals post-transcriptional regulation of key cellular processes. *Microbiology* **153**, 3864-3878, doi:10.1099/mic.0.2007/009969-0 (2007).

8 Gygi, S. P., Rochon, Y., Franza, B. R. & Aebersold, R. Correlation between protein and mRNA abundance in yeast. *Mol. Cell. Biol.* **19**, 1720-1730 (1999).

9 Bergman, N. & Bergquist, J. Recent developments in proteomic methods and disease biomarkers. *Analyst* **139**, 3836-3851, doi:10.1039/c4an00627e (2014).

10 Decaris, M. L. *et al.* Turnover rates of hepatic collagen and circulating collagen-associated proteins in humans with chronic liver disease. *PLoS One* **10**, e0123311, doi:10.1371/journal.pone.0123311 (2015).

11 Miyagi, M. & Kasumov, T. Monitoring the synthesis of biomolecules using mass spectrometry. *Philos Trans A Math Phys Eng Sci* **374**, doi:10.1098/rsta.2015.0378 (2016).

12 Boisvert, F. M. *et al.* A quantitative spatial proteomics analysis of proteome turnover in human cells. *Mol. Cell. Proteomics* **11**, M111.011429, doi:10.1074/mcp.M111.011429 (2012).

13 Beynon, R. J. & Pratt, J. M. Metabolic labeling of proteins for proteomics. *Mol. Cell. Proteomics* **4**, 857-872, doi:10.1074/mcp.R400010-MCP200 (2005).

14 Schwanhäusser, B. *et al.* Global quantification of mammalian gene expression control. *Nature* **473**, 337-342, doi:10.1038/nature10098 (2011).

15 Kasumov, T. *et al.* 2H2O-based high-density lipoprotein turnover method for the assessment of dynamic high-density lipoprotein function in mice. *Arterioscler. Thromb. Vasc. Biol.* **33**, 1994-2003, doi:10.1161/ATVBAHA.113.301700 (2013).

16 Charles-Schoeman, C. *et al.* Potential mechanisms leading to the abnormal lipid profile in patients with rheumatoid arthritis versus healthy volunteers and reversal by tofacitinib. *Arthritis Rheumatol* **67**, 616-625, doi:10.1002/art.38974 (2015).

17 Scalzo, R. L. *et al.* Greater muscle protein synthesis and mitochondrial biogenesis in males compared with females during sprint interval training. *FASEB J.* **28**, 2705-2714, doi:10.1096/fj.13-246595 (2014).

18 Messmer, B. T. *et al.* In vivo measurements document the dynamic cellular kinetics of chronic lymphocytic leukemia B cells. *J. Clin. Invest.* **115**, 755-764, doi:10.1172/JCI23409 (2005).

19 Shekar, K. C. *et al.* Cardiac mitochondrial proteome dynamics with heavy water reveals stable rate of mitochondrial protein synthesis in heart failure despite decline in mitochondrial oxidative capacity. *J. Mol. Cell. Cardiol.* **75**, 88-97, doi:10.1016/j.yjmcc.2014.06.014 (2014).

20 Emson, C. L. *et al.* A pilot study demonstrating a non-invasive method for the measurement of protein turnover in skin disorders: application to psoriasis. *Clin Transl Med* **2**, 12, doi:10.1186/2001-1326-2-12 (2013).

21 Brunengraber, D. Z. *et al.* Influence of diet on the modeling of adipose tissue triglycerides during growth. *Am. J. Physiol. Endocrinol. Metab.* **285**, E917-925, doi:10.1152/ajpendo.00128.2003 (2003).

22 Shankaran, M. *et al.* Proteome-wide muscle protein fractional synthesis rates predict muscle mass gain in response to a selective androgen receptor modulator in rats. *Am. J. Physiol. Endocrinol. Metab.* **310**, E405-417, doi:10.1152/ajpendo.00257.2015 (2016).

23 Price, J. C. *et al.* Measurement of human plasma proteome dynamics with (2)H(2)O and liquid chromatography tandem mass spectrometry. *Anal. Biochem.* **420**, 73-83, doi:10.1016/j.ab.2011.09.007 (2012).

24 Lam, M. P. *et al.* Protein kinetic signatures of the remodeling heart following isoproterenol stimulation. *J. Clin. Invest.* **124**, 1734-1744, doi:10.1172/JCI73787 (2014).

25 Shankaran, M. *et al.* Circulating protein synthesis rates reveal skeletal muscle proteome dynamics. *J. Clin. Invest.* **126**, 288-302, doi:10.1172/JCI79639 (2016).

26 Decaris, M. L. *et al.* Identifying nonalcoholic fatty liver disease patients with active fibrosis by measuring extracellular matrix remodeling rates in tissue and blood. *Hepatology* **65**, 78-88, doi:10.1002/hep.28860 (2017).

27 Hsieh, E. J. *et al.* Topograph, a software platform for precursor enrichment corrected global protein turnover measurements. *Mol. Cell. Proteomics* **11**, 1468-1474, doi:10.1074/mcp.O112.017699 (2012).

28 Schoenheimer, R. & Rittenberg, D. Deuterium as an indicator in the study of intermediary metabolism. *Science* **82**, 156-157, doi:10.1126/science.82.2120.156 (1935).

29 Schoenheimer, R., Rittenberg, D., Foster, G. L., Keston, A. S. & Ratner, S. The application of the nitrogen isotope N15 for the study of protein metabolism. *Science* **88**, 599-600, doi:10.1126/science.88.2295.599 (1938).

30 Commerford, S. L., Carsten, A. L. & Cronkite, E. P. Histone turnover within nonproliferating cells. *Proc. Natl. Acad. Sci. U. S. A.* **79**, 1163-1165 (1982).

31 Commerford, S. L., Carsten, A. L. & Cronkite, E. P. The distribution of tritium among the amino acids of proteins obtained from mice exposed to tritiated water. *Radiat. Res.* **94**, 151-155 (1983).

32 Kelleher, J. K. *et al.* Isotopomer spectral analysis of cholesterol synthesis: applications in human hepatoma cells. *Am. J. Physiol.* **266**, E384-395 (1994).

33 Lee, W. N. *et al.* Measurement of fractional lipid synthesis using deuterated water (2H2O) and mass isotopomer analysis. *Am. J. Physiol.* **266**, E372-383 (1994).

34 Neese, R. A. *et al.* Measurement in vivo of proliferation rates of slow turnover cells by 2H2O labeling of the deoxyribose moiety of DNA. *Proc. Natl. Acad. Sci. U. S. A.* **99**, 15345-15350, doi:10.1073/pnas.232551499 (2002).

35 Hellerstein, M. K. Relationship between precursor enrichment and ratio of excess M2/excess M1 isotopomer frequencies in a secreted polymer. *J. Biol. Chem.* **266**, 10920-10924 (1991).

36 Hellerstein, M. K. & Neese, R. A. Mass isotopomer distribution analysis: a technique for measuring biosynthesis and turnover of polymers. *Am. J. Physiol.* **263**, E988-1001 (1992).

37 Busch, R., Siah, I. M., Gee, T. A. & Hellerstein, M. K. Heavy water labeling of DNA for measurement of cell proliferation and recruitment during primary murine lymph node responses against model antigens. *J. Immunol. Methods* **337**, 24-34, doi:10.1016/j.jim.2008.05.014 (2008).

38 Previs, S. F. *et al.* Quantifying rates of protein synthesis in humans by use of 2H2O: application to patients with end-stage renal disease. *Am. J. Physiol. Endocrinol. Metab.* **286**, E665-672, doi:10.1152/ajpendo.00271.2003 (2004).

39 Dufner, D. A. *et al.* Using 2H2O to study the influence of feeding on protein synthesis: effect of isotope equilibration in vivo vs. in cell culture. *Am. J. Physiol. Endocrinol. Metab.* **288**, E1277-1283, doi:10.1152/ajpendo.00580.2004 (2005).

40 Busch, R. *et al.* Measurement of protein turnover rates by heavy water labeling of nonessential amino acids. *Biochim. Biophys. Acta* **1760**, 730-744, doi:10.1016/j.bbagen.2005.12.023 (2006).

41 Tessari, P., Kiwanuka, E., Zanetti, M. & Barazzoni, R. Postprandial body protein synthesis and amino acid catabolism measured with leucine and phenylalanine-tyrosine tracers. *Am. J. Physiol. Endocrinol. Metab.* **284**, E1037-1042, doi:10.1152/ajpendo.00416.2002 (2003).

42 Bederman, I. R., Dufner, D. A., Alexander, J. C. & Previs, S. F. Novel application of the "doubly labeled" water method: measuring CO2 production and the tissue-specific dynamics of lipid and protein in vivo. *Am. J. Physiol. Endocrinol. Metab.* **290**, E1048-1056, doi:10.1152/ajpendo.00340.2005 (2006).

43 Fenn, J. B., Mann, M., Meng, C. K., Wong, S. F. & Whitehouse, C. M. Electrospray ionization for mass spectrometry of large biomolecules. *Science* **246**, 64-71 (1989).

44 Karas, M., Bachmann, D., Bahr, U. & Hillenkamp, F. Matrix-assisted ultraviolet-laser desorption of nonvolatile compounds. *Int. J. Mass Spectrom. Ion Processes* **78**, 53-68, doi:10.1016/0168-1176(87)87041-6 (1987).

45 Kasumov, T. *et al.* Measuring protein synthesis using metabolic ^{2}H labeling, high-resolution mass spectrometry, and an algorithm. *Anal. Biochem.* **412**, 47-55, doi:10.1016/j.ab.2011.01.021 (2011).

46 Wang, B. *et al.* Isotopologue distributions of peptide product ions by tandem mass spectrometry: quantitation of low levels of deuterium incorporation. *Anal. Biochem.* **367**, 40-48, doi:10.1016/j.ab.2007.03.036 (2007).

47 Cabral, C. B. *et al.* Estimating glutathione synthesis with deuterated water: a model for peptide biosynthesis. *Anal. Biochem.* **379**, 40-44, doi:10.1016/j.ab.2008.04.042 (2008).

48 Papageorgopoulos, C., Caldwell, K., Shackleton, C., Schweingrubber, H. & Hellerstein, M. K. Measuring protein synthesis by mass isotopomer distribution analysis (MIDA). *Anal. Biochem.* **267**, 1-16, doi:10.1006/abio.1998.2958 (1999).

49 Papageorgopoulos, C. *et al.* Measuring synthesis rates of muscle creatine kinase and myosin with stable isotopes and mass spectrometry. *Anal. Biochem.* **309**, 1-10 (2002).

50 Doherty, M. K., Whitehead, C., McCormack, H., Gaskell, S. J. & Beynon, R. J. Proteome dynamics in complex organisms: using stable isotopes to monitor individual protein turnover rates. *Proteomics* **5**, 522-533, doi:10.1002/pmic.200400959 (2005).

51 Hellerstein, M. K. & Neese, R. A. Mass isotopomer distribution analysis at eight years: theoretical, analytic, and experimental considerations. *Am. J. Physiol.* **276**, E1146-1170 (1999).

52 Price, J. *et al.* The Effect of Long Term Calorie Restriction on in Vivo Hepatic Proteostatis: A Novel Combination of Dynamic and Quantitative Proteomics. *Mol. Cell. Proteomics* **11**, 1801-1814, doi:10.1074/mcp.M112.021204 (2012).

53 Kim, T. Y. *et al.* Metabolic labeling reveals proteome dynamics of mouse mitochondria. *Mol. Cell. Proteomics* **11**, 1586-1594, doi:10.1074/mcp.M112.021162 (2012).

54 Lau, E. *et al.* A large dataset of protein dynamics in the mammalian heart proteome. *Sci Data* **3**, 160015, doi:10.1038/sdata.2016.15 (2016).

55 Jones, P. J. & Leatherdale, S. T. Stable isotopes in clinical research: safety reaffirmed. *Clin. Sci. (Lond.)* **80**, 277-280 (1991).

56 Wang, D. *et al.* Characterization of human plasma proteome dynamics using deuterium oxide. *Proteomics Clin. Appl.* **8**, 610-619, doi:10.1002/prca.201400038 (2014).

57 Hellerstein, M. K. New stable isotope-mass spectrometric techniques for measuring fluxes through intact metabolic pathways in mammalian systems: introduction of moving pictures into functional genomics and biochemical phenotyping. *Metab. Eng.* **6**, 85-100 (2004).

58 Rachdaoui, N. *et al.* Measuring proteome dynamics in vivo: as easy as adding water? *Mol. Cell. Proteomics* **8**, 2653-2663, doi:10.1074/mcp.M900026-MCP200 (2009).

59 Wu, C. C., MacCoss, M. J., Howell, K. E., Matthews, D. E. & Yates, J. R. Metabolic labeling of mammalian organisms with stable isotopes for quantitative proteomic analysis. *Anal. Chem.* **76**, 4951-4959, doi:10.1021/ac049208j (2004).

60 Claydon, A. J., Thom, M. D., Hurst, J. L. & Beynon, R. J. Protein turnover: measurement of proteome dynamics by whole animal metabolic labelling with stable isotope labelled amino acids. *Proteomics* **12**, 1194-1206, doi:10.1002/pmic.201100556 (2012).

61 Price, J., Guan, S., Burlingame, A., Prusiner, S. & Ghaemmaghami, S. Analysis of proteome dynamics in the mouse brain. *Proc. Natl. Acad. Sci. U. S. A.* **107**, 14508-14513, doi:10.1073/pnas.1006551107 (2010).

62 Miller, B. F. *et al.* Calorie restriction does not increase short-term or long-term protein synthesis. *J. Gerontol. A Biol. Sci. Med. Sci.* **68**, 530-538, doi:10.1093/gerona/gls219 (2013).

63 Goldberg, A. L. & St John, A. C. Intracellular protein degradation in mammalian and bacterial cells: Part 2. *Annu. Rev. Biochem.* **45**, 747-803, doi:10.1146/annurev.bi.45.070176.003531 (1976).

64 Zhang, T. *et al.* Kinetics of precursor labeling in stable isotope labeling in cell cultures (SILAC) experiments. *Anal. Chem.* **86**, 11334-11341, doi:10.1021/ac503067a (2014).

65 Mathis, A. D. *et al.* Mechanisms of In Vivo Ribosome Maintenance Change in Response to Nutrient Signals. *Mol. Cell. Proteomics* **16**, 243-254, doi:10.1074/mcp.M116.063255 (2017).

66 Kasumov, T., Willard, B. & Sadygov, R. G. Current Bioinformatics Challenges in Proteome Dynamics using Heavy Water-based Metabolic Labeling. *J Data Mining Genomics Proteomics* **5**, e112, doi:10.4172/2153-0602.1000e112 (2014).

67 MacCoss, M. J., Wu, C. C., Matthews, D. E. & Yates, J. R. Measurement of the isotope enrichment of stable isotope-labeled proteins using high-resolution mass spectra of peptides. *Anal. Chem.* **77**, 7646-7653, doi:10.1021/ac0508393 (2005).

68 MacLean, B. *et al.* Skyline: an open source document editor for creating and analyzing targeted proteomics experiments. *Bioinformatics* **26**, 966-968, doi:10.1093/bioinformatics/btq054 (2010).

69 Lis, G., Wassenaar, L. I. & Hendry, M. J. High-precision laser spectroscopy D/H and 18O/16O measurements of microliter natural water samples. *Anal. Chem.* **80**, 287-293, doi:10.1021/ac701716q (2008).

70 Koizuka, I., Takeda, N., Kubo, T., Matsunaga, T. & Cha, C. I. Effects of ethyl alcohol and heavy-water administration on vestibulo-ocular reflex in rabbits. *ORL J. Otorhinolaryngol. Relat. Spec.* **51**, 151-155 (1989).

71 Zhang, J. *et al.* PEAKS DB: de novo sequencing assisted database search for sensitive and accurate peptide identification. *Mol. Cell. Proteomics* **11**, M111.010587, doi:10.1074/mcp.M111.010587 (2012).

72 Smith, G. I., Patterson, B. W. & Mittendorfer, B. Human muscle protein turnover--why is it so variable? *J Appl Physiol (1985)* **110**, 480-491, doi:10.1152/japplphysiol.00125.2010 (2011).

73 Rahman, M., Previs, S. F., Kasumov, T. & Sadygov, R. G. Gaussian Process Modeling of Protein Turnover. *J. Proteome Res.* **15**, 2115-2122, doi:10.1021/acs.jproteome.5b00990 (2016).

74 Guan, S., Price, J. C., Ghaemmaghami, S., Prusiner, S. B. & Burlingame, A. L. Compartment modeling for mammalian protein turnover studies by stable isotope metabolic labeling. *Anal. Chem.* **84**, 4014-4021, doi:10.1021/ac203330z (2012).

75 Mathis, A. *Ribosome Component Turnover Kinetics Describe a Two-Pool Kinetic Model in Dietary Restriction That Suggests RPLIO is Exchanged During Ribosome Lifespan* Master thesis, Brigham Young University, (2015).

76 Nelson, C. J., Li, L., Jacoby, R. P. & Millar, A. H. Degradation rate of mitochondrial proteins in Arabidopsis thaliana cells. *J. Proteome Res.* **12**, 3449-3459, doi:10.1021/pr400304r (2013).

77 Decaris, M. L. *et al.* Proteomic analysis of altered extracellular matrix turnover in bleomycin-induced pulmonary fibrosis. *Mol. Cell. Proteomics* **13**, 1741-1752, doi:10.1074/mcp.M113.037267 (2014).

78 Zhou, H. *et al.* Tracer-based estimates of protein flux in cases of incomplete product renewal: evidence and implications of heterogeneity in collagen turnover. *Am. J. Physiol. Endocrinol. Metab.* **309**, E115-121, doi:10.1152/ajpendo.00435.2014 (2015).

79 Vaudel, M., Barsnes, H., Berven, F. S., Sickmann, A. & Martens, L. SearchGUI: An open-source graphical user interface for simultaneous OMSSA and X!Tandem searches. *Proteomics* **11**, 996-999, doi:10.1002/pmic.201000595 (2011).

80 Vaudel, M. *et al.* PeptideShaker enables reanalysis of MS-derived proteomics data sets. *Nat. Biotechnol.* **33**, 22-24, doi:10.1038/nbt.3109 (2015).

81 Chambers, M. C. *et al.* A cross-platform toolkit for mass spectrometry and proteomics. *Nat. Biotechnol.* **30**, 918-920, doi:10.1038/nbt.2377 (2012).

82 Naylor, B. C. *et al.* DeuteRater: a tool for quantifying peptide isotope precision and kinetic proteomics. *Bioinformatics* **33**, 1514-1520, doi:10.1093/bioinformatics/btx009 (2017).

2. DeuteRater: a Tool for Quantifying Peptide Isotope Precision and Kinetic Proteomics

2.1 Chapter Summary

This chapter is the accepted manuscript introducing our DeuteRater kinetic proteomics analysis program, which was published in early 2017. The manuscript has been edited for formatting, minor error corrections, and to reflect the fact that the article has been published. This paper was published in Issue 10 of Bioinformatics doi:10.1093/bioinformatics/btx009.

2.1.1 Authors in Order of Contribution

Bradley C. Naylor, Michael T. Porter, Elise Wilson, Adam Herring, Spencer Lofthouse, Austin Hannemann, Stephen R. Piccolo, Alan L. Rockwood and John C. Price

2.1.2 Contributions of Major Authors

I performed most of the programming and was the person primarily responsible for the care of the experimental animals analyzed in this paper. The most significant contribution by another author was made by second author Michael Porter who wrote the extractor module, tested it, and prepared the samples for analysis.

2.2 Abstract

2.2.1 Motivation

Using mass spectrometry to measure the concentration and turnover of the individual proteins in a proteome enables the calculation of individual synthesis and degradation rates for

each protein. Software to analyze concentration is readily available, but software to analyze turnover is lacking. Data analysis workflows typically do not access the full breadth of information about instrument precision and accuracy that is present in each peptide isotopic envelope measurement. This method utilizes both isotope distribution and changes in neutromer spacing, which benefits the analysis of both concentration and turnover.

2.2.2 Results

We have developed a data analysis tool, DeuteRater, to measure protein turnover from metabolic D_2O labeling. DeuteRater uses theoretical predictions for label-dependent change in isotope abundance and inter-peak (neutromer) spacing within the isotope envelope to calculate protein turnover rate. We have also used these metrics to evaluate the accuracy and precision of peptide measurements, and thereby determined the optimal data acquisition parameters of different instruments, as well as the effect of data processing steps. We show that these combined measurements can be used to remove noise and increase confidence in the protein turnover measurement for each protein.

2.2.3 Availability

Source code and ReadMe for Python 2 and 3 versions of DeuteRater are available at https://github.com/JC-Price/DeuteRater. Data is at https://chorusproject.org/pages/index.html project number 1147. Software has only been tested on Windows machines. Supplemental materials are available at *Bioinformatics* online.

2.3 Introduction

Cells are dynamic, with synthesis and degradation of the cellular machinery occurring constantly throughout the life of each cell. Protein homeostasis (proteostasis) is achieved by a

careful balance of synthesis and degradation rates resulting in stable concentrations. Measuring protein concentrations over time does not characterize the changes in synthesis and degradation that occur as the cell works to maintain proteostasis. Measurement of protein turnover is required to capture this information.

Mass spectrometry can measure both protein concentration and turnover in the same sample[5,6]. Methods for measuring *in vivo* protein concentrations (quantitation) are well-developed[7,8]. Metabolic labeling with stable isotopes and mass spectrometry has been used for many years to monitor *in vivo* dynamics[1,3,4,9-12]. Only recently has it become possible to monitor individual *in vivo* protein turnover rates within complex samples. This can be done by either providing labeled amino acids[1,4,10,12] or through *in situ* labeling of nonessential amino acids. Both approaches result in permanently labeled proteins, so turnover and concentration can be measured simultaneously within complex mixtures using mass spectrometry. Metabolic labeling with deuterated water (D_2O) has several experimental advantages (Supplemental Table 2-S1), but the calculations represent a challenge for proteome scale analysis. To facilitate this analysis, we have developed DeuteRater, a user-friendly tool to quantify data accuracy and precision using previously established combinatorial statistics[16].

In order to discuss our data analysis, we will use the vocabulary proposed by Smith and coworkers[18]. Each heavy neutromer (M1, M2, etc.) within the pattern has a highly predictable relative intensity (I_x) and distance (S_x) from the monoisotopic neutromer (M0, Figure 2-1). The ratio of naturally occurring heavy isotopes create a predictable distribution of heavy neutromers. Interestingly, the exact mass of the neutromer is slightly different depending on which element holds the extra neutron. The observed mass of a neutron changes, because some mass is converted to energy to supply the necessary strong nuclear force. Larger nuclei require more

force so the carbon neutromer is lighter than the deuterium. This creates a series of isoneutromers within each neutromer (fine structure peaks with different heavy elements, ^{13}C, D, etc., Figure 2-1 A inset). The combination of I_x and S_x has been used to differentiate between distinct elemental combinations, allowing discrimination between classes of molecules based on

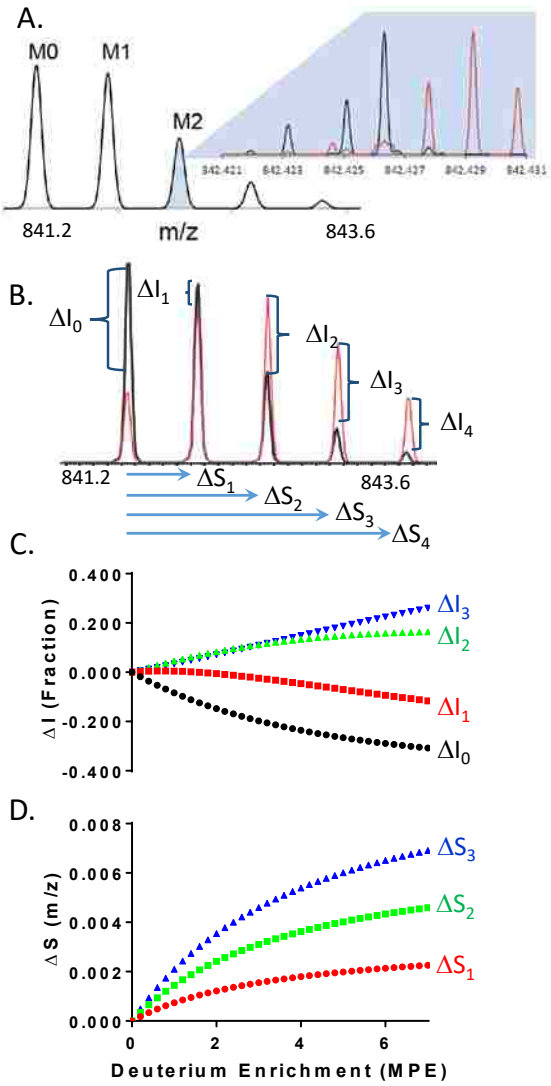

Figure 2-1 Deuterium labeling causes predictable shifts in the isotope pattern: Each molecule's isotope pattern has a series of neutromers (M0, M1, etc.) defined by the number of heavy isotopes. The position (m/z) and height of the neutromer is defined by the major isotope, ^{13}C (black line inset to A). Metabolic deuterium labeling changes the major isotope to deuterium (red line inset to A) leading to a measureable change in both neutromer intensity (ΔI_x) and spacing (ΔS_x) for each heavy neutromer peak (red spectrum B). The theoretical changes can be predicted at any molar percent excess (MPE) of added deuterium (C and D). Data and simulation for peptide LSQTFPNADFAEITK, charge state +2.

ambient isotopic ratios[10]. During metabolic deuterium labeling, we shift the major contributing isoneutromer within each neutromer of the isotopic envelope from ^{13}C to D (Figure 2-1 A inset). The change in I_x (ΔI_x) and S_x (ΔS_x) are unique depending on the number of deuterium's present, and can be predicted based on the peptide sequence and the deuterium enrichment (Figure 2-1 C and D). Therefore, during a metabolic labeling experiment, each peptide's mass spectral pattern will have multiple distinct and predictable, deuterium-dependent changes for each charge state.

The ratio of time dependent experimental change for each I_x and S_x to the theoretical maximum reports the fraction of new peptide for each detected ion in each sample. Since the fraction new ratio should be identical for each ΔI_x and ΔS_x in a given peptide, any deviation must come from instrumental or analysis related error. This means that each mass spectrum of a molecule has 2n-1 semi-independent metrics of turnover (n = number of neutromers observed for that molecule), which can be combined to analyze instrumental noise and software mistakes as well as provide turnover rates of proteins. We show here that the both ΔI_x and ΔS_x are experimentally useful for measurement of turnover, and that ΔS_x is more sensitive to noise.

2.4 Methods

2.4.1 Sample Preparation and Data Collection

For the current experiment, blood samples were collected at different time points after introduction of the metabolic label (0.4, 1, 2, 4, 8, 16, and 32 days after D_2O introduction), and analyzed by mass spectrometry. Details of animal care, sample preparation, and mass spectrometry are in the Supplemental Methods along with a graphical representation (Figure 2-S1)

2.4.2 Peptide database assembly

The open source analysis tools PeptideShaker[2] and Search GUI[1] were used for analysis of MS/MS fragmentation data as detailed in the Supplemental Methods. Peptide shaker does not utilize the FDR notation but scores every observed peptide. Peptides with a score greater than 1 based on multiple search algorithms were used for further analysis. The MS/MS fragmentation data from the unlabeled sample acquisitions were used to assemble a peptide mass and retention time database for identification of isotopic envelopes in metabolically labeled samples using DeuteRater (Figure 2-2). The DeuteRater workflow is outlined in the results (Results "DeuteRater Workflow").

2.4.3 Accuracy and Precision

In unlabeled samples, we assess accuracy relative to the unlabeled theoretical spectrum. Normalizing deviation from theory in these unlabeled samples, to the theoretical ΔS_x, ΔI_x at the same molar percent excess (MPE) deuterium of the labeled samples, allows us to quantify the deviation on an experimentally meaningful scale[15]. Accuracy is calculated using deviation from theory for the unlabeled peptide (Figures 2-S3, 2-S4, 2-S5 A-C) normalized to the experimental MPE. In this study, accuracy is only reported for unlabeled samples.

Precision—how well each of the measurements (Figure 2-1 B, ΔS_x, ΔI_x) agree with each other—can be measured in both unlabeled and labeled samples. We quantify precision by calculating the standard deviation between the fraction new peptide reported by each of the ΔI_x and ΔS_x measurements available for the individual peptide charge state. The precision is a measurement of the standard deviation between the neutromers in any isotopic distribution (Figure 2-S5 D-E). This is determined using the fraction new calculated at experimental MPE (defined by the user in Results, "DeuteRater Workflow", "Labeling Table") and is equally valid

for labeled and unlabeled samples. All data represent direct sequence-specific comparisons except Figure 2-S3.

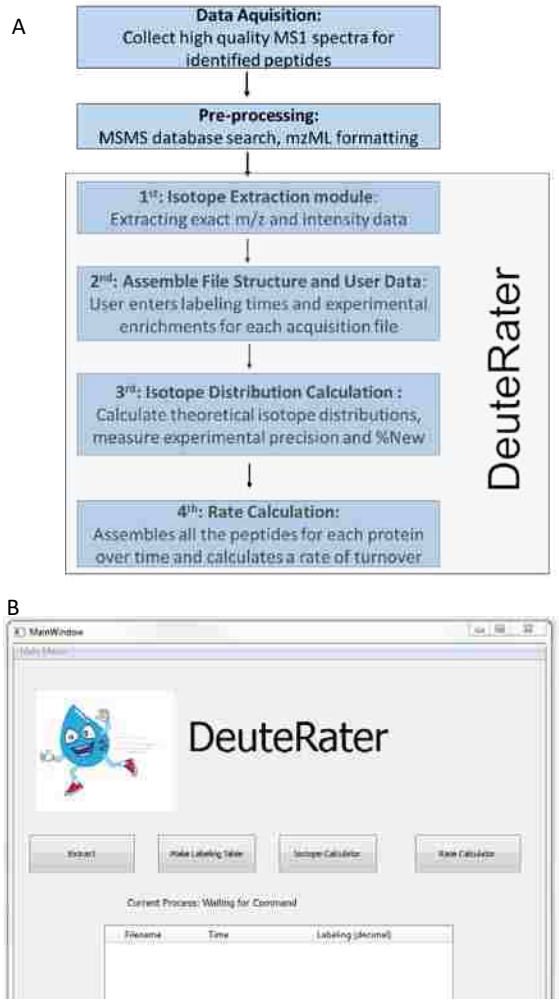

Figure 2-2 DeuteRater Workflow: DeuteRater analysis requires MS1 data where the retention time and sequences of peptides have already been established. Four sequential modules (Panel A) are presented in the graphical user interface (Panel B) of DeuteRater to conduct the analysis.

2.4.4 Comparison of Rates

We compared the results of this analysis against two published studies (Price et al 2010 and Lam et al 2014) which measured turnover of blood plasma proteins in a similar mouse model. The Price data was collected using dietary labeled amino acids while the Lam et al data

was measured using D_2O similar to this study. Analyses comparing rates between studies only considered proteins with rates between 0 and 1 day^{-1} (Figures 2-4, and 2-S6), because the time points in this experiment do not adequately constrain rates faster than 1 day^{-1}. In addition, accession numbers in the published studies often differed due to homology between proteins in the proteomic databases. To correct this, peptide sequences were matched between current and published data and the accession numbers from the current SwissProt database. The Price data[14] was refit with a median of relevant lag (t0) and protein with a rate fitting coefficient of variance (CV) of less than 0.2 were used for comparison. For the Lam et al data proteins were limited to those below one median absolute deviation for the rate (as defined by the authors[4,7,12,19]). This selected the highest confidence data from each study in order to ensure noise from different instruments did not obscure the correlations. For Figure 2-4, to prevent obvious outliers from influencing our regression analysis we used a Passing-Bablok non-parametric regression (PSI-Plot statistical package). Because we used non-parametric statistics, we report the Spearman non-parametric correlation co-efficient (JMP 12 statistical package).

2.5 Results

2.5.1 DeuteRater Workflow

The DeuteRater workflow has four modules (Figure 2-2); a comprehensive instruction manual (ReadMe) and a table of applicable filters (Table 2-S2) are provided as supplemental information.

2.5.1.1 Isotope Extraction Module

The database of peptide mass and retention time (Methods "Peptide database assembly") was used to guide extraction of MS1 data (Figure 2-2). To identify peptide isotopic

envelopes[4,7,12,19] within the MS1 spectra, the m/z values (±30 ppm) for M0-M4 of each charge state (1+ to 5+) for each observed peptide were calculated. DeuteRater then searched for these m/z values within a retention time window (±1.5 minutes) bracketing the time the peptide was fragmented and identified in the MSMS spectrum. The elution chromatogram for each isotope pattern was identified by comparing an m/z and abundance vector for each scan against the neighboring scans. We utilized the vector based comparison because it was robust and flexible, allowing simultaneous comparison of changes in m/z and intensity for all neutromers. When the vector angle changed less than $\log_{10}$ (1.2), the scan was assumed to belong to the peptide chromatogram. This vector angle criterion agreed well with our visual evaluations of the chromatogram boundaries for selected peptides.

All scans within the chromatogram were used to calculate a summed intensity and median neutromer m/z value. For each neutromer all m/z values are analyzed and the outliers removed by a Median Absolute Deviation test. The median m/z, and summed intensity of each neutromer in each peptide charge state were then annotated to that entry of a new peptide database. Ions with an incomplete neutromer series (complete series is four if the neutral mass is less than 2400 atomic mass units, or 5 if greater than that limit) were removed from the database prior to the data processing workflow. Theoretically, an incomplete neutromer series would also yield useful data, but the confidence in correctly assigning the peptide identity for the isotopic envelope is lower and the subsequent precision analysis would not be comparable. Therefore, these peptides were removed.

2.5.1.2 Labeling Table

The user enters sample specific labeling time and experimentally determined isotope enrichments.

2.5.1.3 Isotope Distribution Calculator

DeuteRater calculates the theoretical deuterium dependent change in the isotope distribution for each peptide using the EMass algorithm. To accomplish this, the elemental composition of each peptide is calculated, and the number of stable deuterium sites (X) is calculated based on the amino acid sequence. The number of isotopic labeling sites in each amino acid has been shown to be stable in mice and humans. Although DeuteRater allows the user to define the number of labels, the presets are an average of the literature values specific for mammalian tissue or cell culture.

The EMass algorithm can be used in two ways. The first method calculates ΔI_x and ΔS_x for each peptide at the user defined deuterium enrichment. This method is relatively fast, but requires recalculation if deuterium enrichment values need to be changed. Alternatively, DeuteRater can calculate the change in the isotopic envelope at multiple increments between 0 and a user defined limit. The trends in ΔI_x, and ΔS_x for each neutromer within the pattern are fit via least squares regression (Figure 2-1 C and D). Regression coefficients for each peptide, along with R^2 and error values for the fits, are then appended to the mass and retention time database to allow predictions of ΔI_x, and ΔS_x at any deuterium molar percent excess (MPE) up to a user defined maximum. This provides flexibility to quickly test the effect of different deuterium enrichments on data precision, at the cost of longer initial calculation time.

To calculate ΔI_x, the individual I_x of both the theoretical and experimental isotope patterns are normalized to the sum signal intensity of the neutromers (I_0 to I_3) in the pattern as previously described[4,20]. The M4 neutromer, with its corresponding ΔI_x and ΔS_x is only included for peptides larger than 2400 Daltons. The normalization of I_x ensures that the theoretical calculations and experimental measurements are comparable. The S_x is normalized internally

against the measured monoisotopic peak (M0, Figure 2-1 B). The experimental ΔI_x and ΔS_x are calculated versus the unlabeled theoretical baseline. Similarly, maximum theoretical deuterium dependent changes (ΔI_x^{max}, ΔS_x^{max}) are calculated by subtracting the theoretical unlabeled spectra from the theoretical spectra at the experimental deuterium enrichment (Figure 2-1 C and D, dotted line). The experimental changes are then divided by the theoretical maximum change at the experimentally determined deuterium enrichment ($\Delta I_x/\Delta I_x^{max}$, $\Delta S_x/\Delta S_x^{max}$) to calculate the time dependent ratio of change (fraction new). In an ideal spectrum, the fraction new peptide calculated for each ΔI_x and ΔS_x will be the same: deviation from this ratio between the various ΔI_x and ΔS_x measurements is a metric of the noise for that individual peptide charge state. The reported fraction new peptide can be calculated from ΔI_x or ΔS_x separately or combined into one metric. Because there are at least 7 measurements available for each peptide charge state (9 for m/z above 2400), we can apply a median absolute standard deviation correction to combined calculations to remove outliers and increase the precision. In this analysis, we observed that the ΔS_x measurements often deviated more from the median and were more sensitive to noise.

2.5.1.4 Rate Calculation Module

The user designates whether rates are calculated from ΔS_x, ΔI_x or combined data. This choice should be based on the accuracy and precision observed with an instrument (see Methods, "Comparison of Rates"). For example, we found that ΔI_x was usually best for QToF data, whereas combining ΔS_x, and ΔI_x provided improved precision with Orbitrap data. If the standard deviation of the body of measurements for each peptide were below the user defined value (0.1), the fraction new and the sample time point included in the turnover rate (***k***) calculation. The peptide fraction new measurements are fit versus time using the relationship $\mathbf{fraction\ new = a - ae^{(-kt)}}$, where ***t*** is time as previously described[21-23]. Each charge state for each peptide can

considered a separate point in the fit, or all the data points can be rolled up to a median value (Table S2). For the data presented in this paper, the asymptote value "**a**" in the equation was fixed at one. Currently, the turnover rate calculation assumes a single biological pool of unchanging concentration using each of the peptides as a replicate measure to calculate the rate constant. Protein turnover was only calculated when data at three or more (a user defined filter) time points passed the quality filters.

2.5.2 Accuracy of the isotope distribution varies with instrument data acquisition parameters

This study used three different instruments with multiple m/z resolutions, resulting in nine data sets. The number of peptide sequences identified and the identity of the sequences were significantly different between all nine data sets (Figure 2-S2). All detected peptides were compared for accuracy and precision (Figure 2-S3). Among the instrument configurations tested, we found that the Agilent 6530 QToF 10,000 m/z resolution (10k1 or 10k2) was generally the most accurate for ΔI_x measurements, but had the least accurate ΔS_x measurements. Relative to the QToF, the Orbitrap Fusion 60,000 m/z resolution (60kf) produced less accurate and precise ΔI_x measurements, but the accuracy of the ΔS_x measurements was much higher. This result was expected because the QToF has been shown to be more accurate for neutromer intensities[1] but the higher mass resolution of the Orbitrap should provide more accurate ΔS_x data.

For sequence-specific comparisons, the QToF at 10k and the Fusion at 60k were the best for ΔI (Figure 2-S5). Although the QToF collected high quality data on more total peptides (Figure 2-S3), comparison of matched peptide sequences between the QToF 10k and the Fusion 60k, revealed that accuracy (Figure 2-S5 A-C) and precision (Figure 2-S5 D-F) were comparable for the ΔI. Although the Fusion at 120k had the most accurate ΔS measurements, the loss of

accuracy in ΔI outweighed that gain. We observed that the lower resolution acquisition parameters were better for accuracy and precision in both the XL and the fusion.

2.5.3 ΔS_x is more sensitive to noise than ΔI_x

We observed that higher m/z resolutions do not necessarily increase ΔS_x accuracy. For example, the 120k Fusion data had the highest ΔS_x accuracy and precision among the tested instruments and parameters (Figure 2-S3). Although we collected data at 240k and 480k resolution, the increased m/z resolution reduced both the ΔS_x and ΔI_x accuracy and precision. This may be due to the slow scan rate for the high resolution experiments. Fewer total measurements for each peptide chromatogram would increase noise and reduce the confidence for the peptide. Noisier peptide measurements are filtered out of the data set prior to further processing, resulting in fewer usable peptide measurements for the kinetics calculations (Results, "Precision Metrics can Identify Outliers to Improve Kinetic Calculations"). Longer chromatographic times could potentially offset this effect. Although the ΔS_x is more susceptible to noise than ΔI_x, we observed increased accuracy and precision for combined (ΔI_x, ΔS_x) from the 60k data (Figure 2-S3 C, F).

2.5.4 Precision Metrics can Identify Outliers to Improve Kinetic Calculations

When we compared the peptides associated with individual proteins, we observed that the low precision peptides were often outliers when compared to the entire body of data (Figure 2-3). In Figure 2-3 A, there are a series of points near the x-axis (open circles) which seem to form a separate curve. Increasing the stringency of the precision filter in Figures 2-3 B-C removes the points. Closer inspection showed that these points were all assigned to the same peptide, suggesting a possible mistaken sequence. However, extreme precision requirements will also reduce the number of measurements (Figure 2-3 D-F). This parameter is modifiable in

DeuteRater, and for all subsequent analyses in this paper, the precision filter was set to require a deviation less than 0.1.

Turnover rates can be calculated using ΔI, ΔS, or the combination. Typically, ΔS derived rates were lower confidence, but when multiple high precision peptides were used ΔI, ΔS, and the combination provided highly consistent values (Figure 2-S6). Interestingly, although the QToF 10k data had the lowest precision for ΔS overall, we found that when multiple high precision peptides were used, the resulting turnover rates for these data were almost identical (Figure 2-S6, closest to 1 on the y axis).

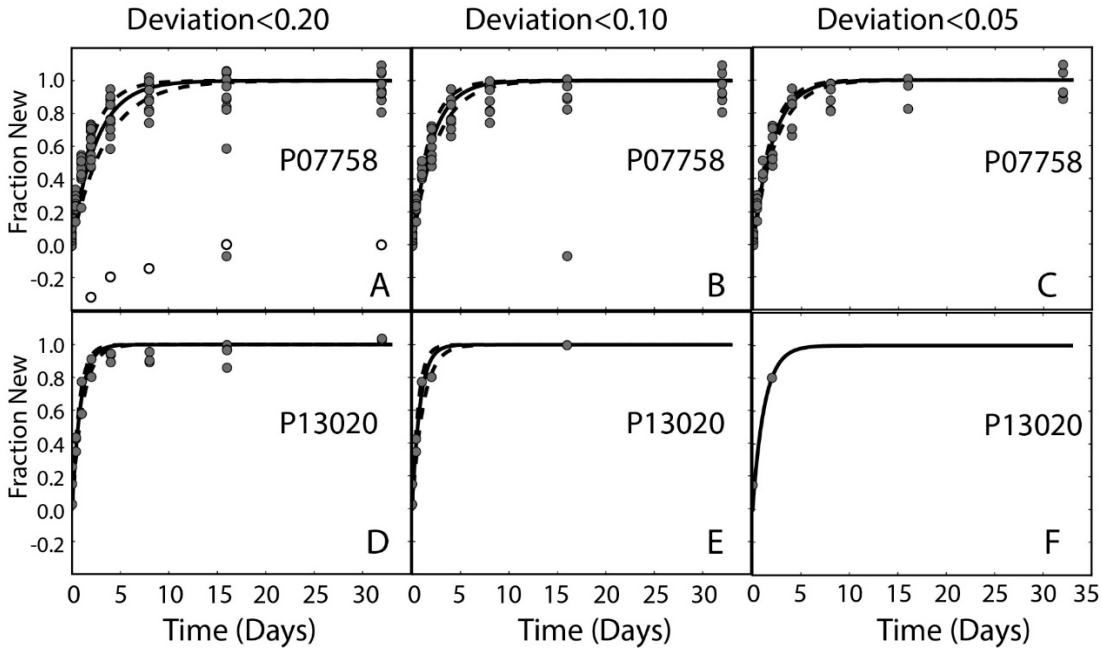

Figure 2-3 Neutromer precision provides information for outlier removal: Extracted peptide isotope patterns are subjected to a user controlled precision filter prior to calculating the turnover rate. Requiring increased precision (smaller deviation) preferentially removes results that are outside of the expected range of rates. By increasing the required precision, we remove more outliers. However some proteins, like P13020, may lose enough points that the kinetic curve is no longer well constrained. Therefore the precision filter was set at 0.1 deviation for all analyses presented here. Circles represent individual peptide charge state measurements; open circles in A are all assigned to the same peptide suggesting that it was an incorrectly identified sequence.

2.5.5 Kinetic rates are highly reproducible between studies

We tested technical variability in the turnover measurement by running two identical sample sets on the QToF at 10k and analyzing the data (Figure 2-4 A and 2-S3, 10k1 versus 10k2). Of the 53 proteins with high quality identifications, the stringent filtering criteria described above resulted in 27 proteins observed in both studies (Figure 2-4 A). This confirmed that DeuteRater analysis is consistent. We then compared our rates to published data from an independent deuterium labeling study of similar design by Lam et al.[12] (Figure 2-4 B). There were 25 proteins observed in both studies with high quality fits, evaluated as described in the

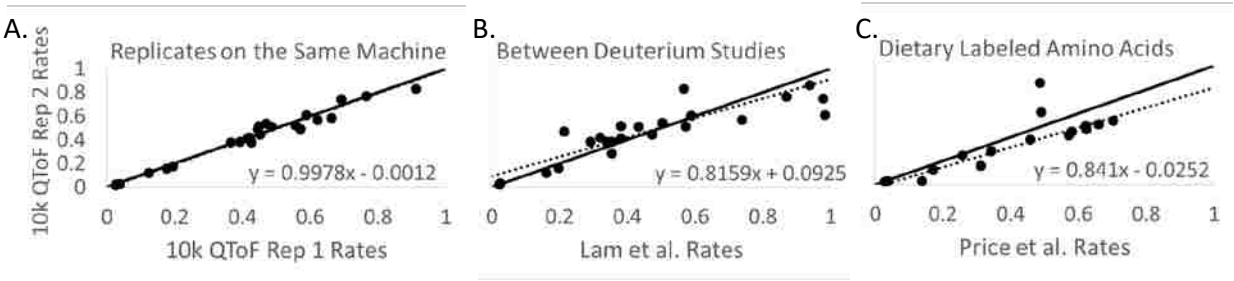

Figure 2-4 Protein turnover rates are highly reproducible between studies: Comparison of technical replicates highlights the small technical variability between analyses (A). Comparison of turnover rates in this study against similar deuterium labeling experiment by Lam et al. [1-4] (B) and dietary heavy amino acids labeling by Price et al.[5,6] show strong linear trends (C). Spearman correlation coefficients are .9777 for (A), .8962 for (B), and .8500 for (C). The unity lines represent absolute agreement between studies. All data calculated using ΔI.

methods (Methods "Comparison of Rates"). Passing-Bablok regression analysis reported that there was a strong linear correlation up to ~0.5 Day^{-1}, suggesting that the biological sampling rate differences between the studies allowed more variability in the rate calculation for fast turnover proteins. Comparison against a published dietary heavy-labeled amino acid study[24] also showed a strong linear correlation for the rates (Figure 2-4C). The rates as measured in the Price et al. study tended to be slower as the turnover increased; this could represent a real biological difference of slower trafficking of the labeled amino acids relative to deuterated water.

2.6 Discussion

Measuring turnover of individual proteins *in vivo* is a critical first step towards understanding how the cell modulates protein synthesis and/or degradation to maintain protein homeostasis (proteostasis). Metabolic D_2O labeling is an experimentally simple and inexpensive method for monitoring protein turnover (See Table 2-S1 for advantages and disadvantages). Although the data analysis is based on well understood combinatorial statistics[25], the time dependent calculations are different for each peptide. This creates an imposing data analysis challenge for a proteomics data set and has impeded widespread use of the technique. Other investigators have developed open source software for individual steps of the analysis[1,2]. Our software platform, DeuteRater, simplifies the entire data analysis workflow with a user-friendly GUI to enable proteome wide measurements of turnover. Importantly, DeuteRater is able to utilize all of the ΔS_x and ΔI_x distribution information available in the isotope pattern (Figure 2-1). This results in 2n-1 (n=number of neutromer peaks, Figure 2-1 B) measurements of turnover for each spectrum. Having multiple measurements allows precision to be quantified for each peptide charge state. This creates a continuous determination of the measurement accuracy and precision for each step of the experiment and analysis. We show here that both ΔS_x and ΔI_x can provide *in vivo* kinetic information and quantify noise in the mass spectrometer, as a robust metric to increase consistency.

As a simple example of the utility of these precision metrics, we compared the effects of the Vendor-specific versus General centroiding algorithm the ProteoWizard[1,2] application used to prepare data for DeuteRater analysis. We observed that for a single data file more isotope patterns were extracted from data centroided with the General algorithm, but that there was decreased isotope envelope accuracy. We found that even for matched peptides, both ΔI_x and

ΔS_x were less accurate in General centroiding than Vendor centroiding (Figure 2-S4). Therefore, in subsequent data analysis steps, the Vendor-specific centroiding algorithm was used.

Using the peptide accuracy and precision metrics, we can also apply rational criteria to the evaluation and optimization of instrument acquisition parameters. In our study, we tested three different instrument models and 8 different m/z resolutions (Figure 2-S3). We found that data accuracy was best when monitoring the relative neutromer intensity distribution (ΔI_x) on the QToF and the Orbitrap Fusion at low m/z resolution (60k, Figure 2-S5). The neutromer spacing (ΔS_x) was most accurate on the Orbitrap Fusion at 120k m/z resolution, but interestingly did not improve with increasing mass resolution. We attribute this to the longer scan time for each duty cycle and therefore fewer scans to average over the chromatographic elution. This suggests that ΔS_x is more sensitive to noise than ΔI_x, consistent with the much smaller theoretical range for ΔS_x relative to the range for ΔI_x (Figure 2-1). DeuteRater allows the user to decide whether to choose whether ΔS_x, ΔI_x, or the combination is used to calculate rates. This choice should be made based on the performance of the instrument. Although the matched peptide analysis showed that the combination data was better for both the QToF and Orbitrap data (Figure 2-S5), generally ΔS_x was poor for the QToF data set (Figure 2-S3). Therefore, we use the ΔI_x kinetics for QToF data and combined for Orbitrap. Even for experiments that do not use metabolic labeling, analysis of unlabeled peptide accuracy and precision is simple and fast in DeuteRater and represents a good method for monitoring instrument performance and data quality (Figure 2-S2).

We measured turnover rates for 90 proteins in blood serum, which is essentially the state of the art for the number of proteins observed in whole blood plasma with these short (25 minute) LCMS gradients[1-4]. Multiple sample preparation and data acquisition steps could be

modified to increase the breadth of proteome coverage. Although the number of proteins was sufficient for this study, DeuteRater is currently being used to analyze proteome-scale data sets consisting of thousands of proteins.

In the QToF data, which we are using as our standard of comparison, 56 of the observed proteins had turnover rates with a covariance of less than 0.2. The rates ranged from 0.02 per day, to faster than we could reliably measure with the tissue sampling intervals. Comparison of the rates between analyses in this study and with published values[1-4] showed that the turnover rates are highly consistent. For example, the reported rates for Hemoglobin Alpha (P01942) varied less than 20 percent between the studies. This suggests that the measurement of turnover kinetics is highly reproducible and that the streamlined DeuteRater analysis provides high quality results.

2.7 Acknowledgements

We are grateful to Earl Albee, Warren Bingham, and the BYU animal care facility for assistance in maintenance of the mice, and to Richard Carson for manuscript editing and logo design. We are also grateful to Takhar Kasumov and Makan Golizeh for Beta testing and identifying problems in the code.

2.8 Funding

This work was supported by BYU startup funds to JCP, Roland K. Robins Graduate Research Fellowship to BN, BYU Undergraduate Research Awards to MP, EW, AH, SL.

Conflict of Interest: none declared.

2.9 Bibliography

1 Lam, M. P. *et al.* Protein kinetic signatures of the remodeling heart following isoproterenol stimulation. *J. Clin. Invest.* **124**, 1734-1744, doi:10.1172/JCI73787 (2014).

2 Price, J. C., Guan, S., Burlingame, A., Prusiner, S. B. & Ghaemmaghami, S. Analysis of proteome dynamics in the mouse brain. *Proc. Natl. Acad. Sci. U. S. A.* **107**, 14508-14513, doi:10.1073/pnas.1006551107 (2010).

3 Karunadharma, P. P. *et al.* Subacute calorie restriction and rapamycin discordantly alter mouse liver proteome homeostasis and reverse aging effects. *Aging Cell* **14**, 547-557, doi:10.1111/acel.12317 (2015).

4 Price, J. *et al.* The Effect of Long Term Calorie Restriction on in Vivo Hepatic Proteostatis: A Novel Combination of Dynamic and Quantitative Proteomics. *Mol. Cell. Proteomics* **11**, 1801-1814, doi:10.1074/mcp.M112.021204 (2012).

5 Callister, S. J. *et al.* Normalization approaches for removing systematic biases associated with mass spectrometry and label-free proteomics. *J. Proteome Res.* **5**, 277-286, doi:10.1021/pr050300l (2006).

6 Malmstrom, J. *et al.* Proteome-wide cellular protein concentrations of the human pathogen Leptospira interrogans. *Nature* **460**, 762-765, doi:10.1038/nature08184 (2009).

7 Commerford, S. L., Carsten, A. L. & Cronkite, E. P. The distribution of tritium among the amino acids of proteins obtained from mice exposed to tritiated water. *Radiat. Res.* **94**, 151-155 (1983).

8 Schoenheimer, R., Rittenberg, D., Foster, G. L., Keston, A. S. & Ratner, S. The application of the nitrogen isotope N15 for the study of protein metabolism. *Science* **88**, 599-600, doi:10.1126/science.88.2295.599 (1938).

9 Price, J., Guan, S., Burlingame, A., Prusiner, S. & Ghaemmaghami, S. Analysis of proteome dynamics in the mouse brain. *Proc. Natl. Acad. Sci. U. S. A.* **107**, 14508-14513, doi:10.1073/pnas.1006551107 (2010).

10 Price, J. C. *et al.* Measurement of human plasma proteome dynamics with (2)H(2)O and liquid chromatography tandem mass spectrometry. *Anal. Biochem.* **420**, 73-83, doi:10.1016/j.ab.2011.09.007 (2012).

11 Doherty, M. K., Hammond, D. E., Clague, M. J., Gaskell, S. J. & Beynon, R. J. Turnover of the human proteome: determination of protein intracellular stability by dynamic SILAC. *J. Proteome Res.* **8**, 104-112, doi:10.1021/pr800641v (2009).

12 Kasumov, T. *et al.* Measuring protein synthesis using metabolic ^{2}H labeling, high-resolution mass spectrometry, and an algorithm. *Anal. Biochem.* **412**, 47-55, doi:10.1016/j.ab.2011.01.021 (2011).

13 Hellerstein, M. K. & Neese, R. A. Mass isotopomer distribution analysis at eight years: theoretical, analytic, and experimental considerations. *Am. J. Physiol.* **276**, E1146-1170 (1999).

14 Rockwood, A. L. & Haimi, P. Efficient calculation of accurate masses of isotopic peaks. *J. Am. Soc. Mass Spectrom.* **17**, 415-419, doi:10.1016/j.jasms.2005.12.001 (2006).

15 Smith, R., Taylor, R. M. & Prince, J. T. Current controlled vocabularies are insufficient to uniquely map molecular entities to mass spectrometry signal. *BMC Bioinformatics* **16 Suppl 7**, S2, doi:10.1186/1471-2105-16-S7-S2 (2015).

16 Dittwald, P. *et al.* Towards automated discrimination of lipids versus peptides from full scan mass spectra. *EuPA Open Proteom* **4**, 87-100, doi:10.1016/j.euprot.2014.05.002 (2014).

17 Vaudel, M. *et al.* PeptideShaker enables reanalysis of MS-derived proteomics data sets. *Nat. Biotechnol.* **33**, 22-24, doi:10.1038/nbt.3109 (2015).

18 Vaudel, M., Barsnes, H., Berven, F. S., Sickmann, A. & Martens, L. SearchGUI: An open-source graphical user interface for simultaneous OMSSA and X!Tandem searches. *Proteomics* **11**, 996-999, doi:10.1002/pmic.201000595 (2011).

19 Shekar, K. C. *et al.* Cardiac mitochondrial proteome dynamics with heavy water reveals stable rate of mitochondrial protein synthesis in heart failure despite decline in mitochondrial oxidative capacity. *J. Mol. Cell. Cardiol.* **75**, 88-97, doi:10.1016/j.yjmcc.2014.06.014 (2014).

20 Hsieh, E. J. *et al.* Topograph, a software platform for precursor enrichment corrected global protein turnover measurements. *Mol. Cell. Proteomics* **11**, 1468-1474, doi:10.1074/mcp.O112.017699 (2012).

21 Jiang, W. & Erve, J. C. Spectral accuracy of a new hybrid quadrupole time-of-flight mass spectrometer: application to ranking small molecule elemental compositions. *Rapid Commun. Mass Spectrom.* **26**, 1014-1022, doi:10.1002/rcm.6197 (2012).

22 MacCoss, M. J., Wu, C. C., Matthews, D. E. & Yates, J. R. Measurement of the isotope enrichment of stable isotope-labeled proteins using high-resolution mass spectra of peptides. *Anal. Chem.* **77**, 7646-7653, doi:10.1021/ac0508393 (2005).

23 Rockwood, A. L. & Erve, J. C. Mass spectral peak distortion due to Fourier transform signal processing. *J. Am. Soc. Mass Spectrom.* **25**, 2163-2176, doi:10.1007/s13361-014-0982-0 (2014).

24 Kessner, D., Chambers, M., Burke, R., Agus, D. & Mallick, P. ProteoWizard: open source software for rapid proteomics tools development. *Bioinformatics* **24**, 2534-2536, doi:10.1093/bioinformatics/btn323 (2008).

25 Geyer, P. E. *et al.* Plasma Proteome Profiling to Assess Human Health and Disease. *Cell Syst* **2**, 185-195, doi:10.1016/j.cels.2016.02.015 (2016).

3. Mechanisms of *in vivo* Ribosome Maintenance Change in Response to Nutrient Signals

3.1 Chapter Summary

As with the "DeuteRater: a Tool for Quantifying Peptide Isotope Precision and Kinetic Proteomics" Chapter, this is the accepted manuscript of a published paper. As with the "DeuteRater: a Tool for Quantifying Peptide Isotope Precision and Kinetic Proteomics" chapter, the manuscript has been edited for formatting and clarity. This paper was published in issue 16 of Molecular and Cellular Proteomics doi:10.1074/mcp.M116.063255.

3.1.1 Authors in Order of Contribution

Andrew D. Mathis[±], Bradley C. Naylor[±], Richard H. Carson, Eric Evans, Justin Harwell, Jared Knecht, Eric Hexem, Fredrick F. Peelor III, Benjamin F. Miller, Karyn L. Hamilton, Mark K. Transtrum, Benjamin T. Bikman, John C. Price

[±] These authors contributed equally to this work.

3.1.2 Contributions of Major Authors

My co-first author Andrew Mathis and I led the team responsible for animal care. I performed the analysis of "Total Pool" ribosome data, and the final round of analysis on all proteomic data. My co-first author Andrew Mathis led the "Assembled Pool" ribosome data and follow up experiments such as the qPCR. We were both involved in initial rounds of data analysis.

3.2 Abstract

Control of protein homeostasis is fundamental to the health and longevity of all organisms. Because the rate of protein synthesis by ribosomes is a central control point in this process, regulation and maintenance of ribosome function could have amplified importance in the overall regulatory circuit. Indeed, ribosomal defects are commonly associated with loss of protein homeostasis, aging and disease, whereas improved protein homeostasis, implying optimal ribosomal function, is associated with disease resistance and increased lifespan[5,6,8,9]. To maintain a high-quality ribosome population within the cell, dysfunctional ribosomes are targeted for autophagic degradation. It is not known if complete degradation is the only mechanism for eukaryotic ribosome maintenance or if they might also be repaired by replacement of defective components. We used stable-isotope feeding and protein mass-spectrometry to measure the kinetics of turnover of ribosomal RNA (rRNA) and 71 ribosomal proteins (r-proteins) in mice. The results indicate that exchange of individual proteins and whole ribosome degradation both contribute to ribosome maintenance *in vivo*. In general, peripheral r-proteins and those with more direct roles in peptide-bond formation are replaced multiple times during the lifespan of the assembled structure, presumably by exchange with a free cytoplasmic pool, whereas the majority of r-proteins are stably incorporated for the lifetime of the ribosome. Dietary signals impact the rates of both new ribosome assembly and component exchange. Signal-specific modulation of ribosomal repair and degradation could provide a mechanistic link in the frequently observed associations among diminished rates of protein synthesis, increased autophagy, and greater longevity.

3.3 Introduction

Cells achieve protein homeostasis (proteostasis) by carefully balancing the synthesis and folding of each protein against the protein degradation and cellular proliferation rates. Controlled shifts in proteostasis occur during cell differentiation, and in response to stimuli[10-13], while uncontrolled changes promote neurodegenerative disease, cancer[1,5,17-19], and aging. This suggests that each cell coordinately regulates the ribosome, proteasome, and other key structures of protein metabolism to achieve proteostasis. However, the regulatory mechanisms for coordination, and how the proteome is remodeled to achieve a new proteostasis, are poorly understood.

Diets restricting calories or amino acids (DR) protect against aging and the diseases of aging, in model organisms[5,6,19]. Low calorie diets have been shown to reduce rates of protein synthesis and degradation for much of the observed proteome[2]. Recent reports suggest that high protein synthesis demand is associated with reduced ribosomal accuracy[23] and efficiency[24]. This suggests that maintaining ribosome quality is an intricate task that requires constant cellular effort.

Translation rate is a metric of ribosome quality[25]. Ribosomes that stall during protein production are immediately tested by the Ribosome Quality Control (RQC) complex[26]. The RQC specifically tests the large subunit for activity[27], and presumably sequesters inactive ribosomes. Degradation of unnecessary or damaged ribosomes often occurs through directed autophagy (ribophagy)[28]. Ribophagy is presumably one of the primary roles for autophagy, indeed the earliest descriptions of autophagic vesicles show ribosomes in the interior[29]. An important open question though is: Can dysfunctional ribosomes be repaired, or is ribophagy the only option?

Exchange of damaged ribosomal components could allow the cell to repair faulty ribosomes instead of degrading the entire structure. The formation of new ribosomes is extremely costly and has been estimated to account for 15% of the protein synthesis budget[5,6,9,19]. In yeast protein synthesis accounts for at least 90% of the energy usage[5,6,9,19]. Damaged ribosomes in *E. coli* have been shown to regain activity after exchange of ribosomal proteins (r-proteins) for undamaged copies. Although it has never been demonstrated in eukaryotes, exchange of damaged protein components could reduce the total energy expenditure to maintain active ribosomes.

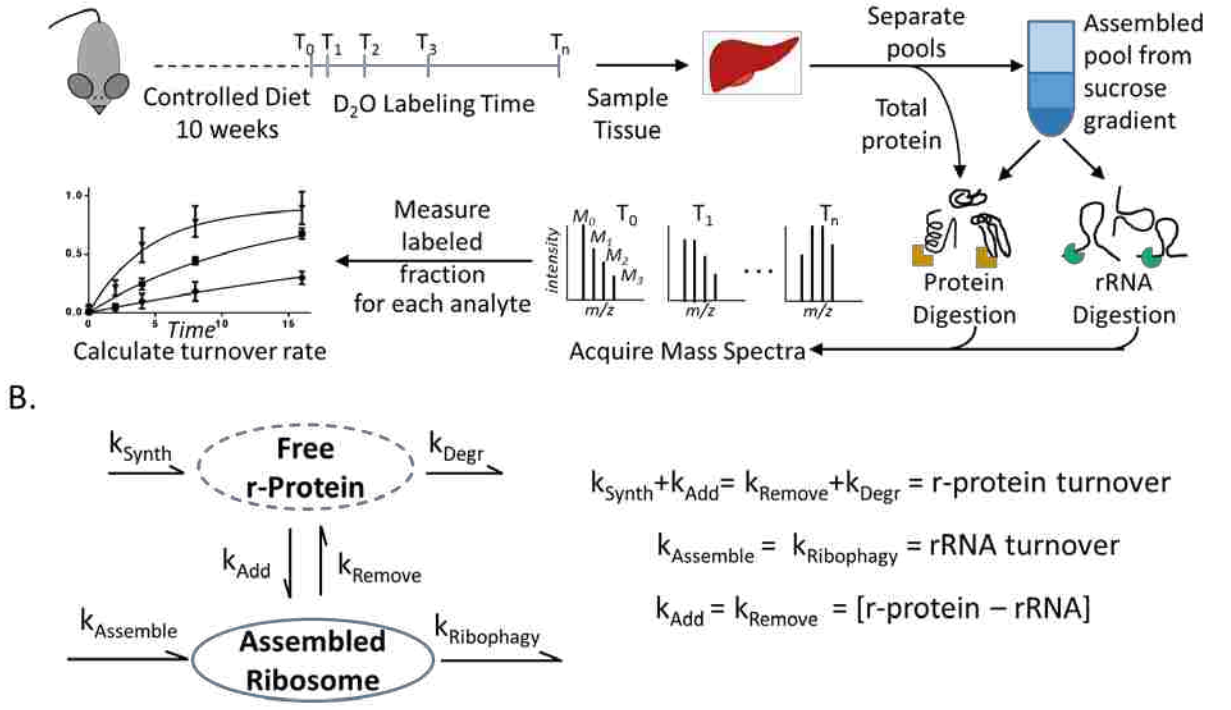

Figure 3-1 Experimental Overview: Workflow for heavy isotope labeling, analyte isolation, and measurement of turnover rates (A). Kinetic model for utilizing turnover measurements to describe ribosome maintenance and turnover (B). Under these experimental conditions, opposing rates are equal maintaining homeostasis.

Here we show that exchange of r-proteins is occurring *in vivo*. Using metabolic labeling (Figure 3-1 A) and a kinetic model, we calculate exchange rates between assembled and free

pools (Figure 3-1 B). Further, we show that r-protein exchange and ribophagy rates change with dietary signals. We compare mice fed an *ad libitum* (AL) versus a restricted diet (dietary restriction, DR), and observe that kinetically there are three groups of proteins in the assembled ribosome. One group is never exchanged and is degraded via ribophagy with the rRNA. The second group is exchanged multiple times with cytosolic copies and has members with either fast or slow cytosolic turnover. A third group of proteins alternates between the first two groups. We find that both ribophagy and r-protein exchange are modulated by dietary signaling. Our observations offer insight into the connection between reduced protein synthesis, and increased autophagy[6] with increased health and longevity.

3.4 Methods

3.4.1 Mouse handling

Mice were housed, diet restricted, and metabolically labeled according to protocols approved by the Brigham Young University Institutional Animal Care and Use Committee (IACUC). Ten-week-old male C57BL/6 mice were obtained from Charles River Laboratories. For the duration of the experiment, mice were housed in a specific-pathogen-free (SPF) facility with 12-hour light/dark cycles. All mice were fed an *ad libitum* (AL) diet for 1 week with 3–4 mice per cage. AL consumption amounts were monitored during the first week. After one week mice were separated and assigned to a dietary restricted (DR, n=20) or ad libitum (AL, n=19) fed diet on Harlan 8604 chow. The DR cohort then received a metered 65% daily ration for the rest of the study. The low-calorie diet used in this study restricted every component of the diet equally, which classically is termed dietary restriction (DR). Mouse weights were recorded each week. After 10 weeks of treatment, mice received an intraperitoneal sterile D_2O saline injection (35µL/g body weight) to immediately bring body water to 5% D2O as previously described [35].

Drinking water was supplemented to 8% molar percent excess (MPE) D_2O to maintain 5% body water throughout the experiment. Mice (n=17) were sacrificed in duplicate (n=2) at time points 0 days (no D_2O injection), 0.4 days, 1 day, 2 days, 4 days, 8 days, 16 days, and triplicate at 32 days. Mice were immediately dissected, blood was extracted by cardiac puncture for % D_2O analysis, and organs were either used fresh for mitochondrial respiration measurements or flash frozen on blocks of solid CO_2. Tissues were stored at -80 °C.

3.4.2 Mitochondrial respiration

Fresh liver tissue was quickly removed from exsanguinated mice and immediately placed in ice-cold mitochondrial respiration buffer 05 (MiR: 0.5 mM EGTA, 10 mM KH2PO4, 3 mM $MgCl_2$-6 H_2O, 60 mM K-lactobionate, 20 mM HEPES, 110 mM Sucrose, 1 mg/ml fatty acid free BSA, pH 7.1) and trimmed of connective tissue. Tissue was gently separated and homogenized under a surgical scope (Olympus, ST) to particles of around 1 mg. Homogenate was then transferred to a tube with chilled MiR05 and 50 µg/ml saponin and rocked at 4˚C for 30 min, then washed in MiR05 at 4˚C for at least 15 min before use. High-resolution O_2 consumption was determined at 37˚C using the Oroboros O_2K Oxygraph. Before addition of sample into respiration chambers, a baseline respiration rate was determined. After addition of sample, the chambers were hyperoxygenated to ~350 nmol/ml. Following this, respiration was determined as indicated. Lastly, residual oxygen consumption was measured by adding antimycin A (2.5 µM) to block complex III action, effectively stopping any electron flow and providing a baseline respiration rate.

3.4.3 Isolating assembled ribosomes

Separation of free ribosomal proteins and assembled ribosomes was performed using a sucrose gradient as follows. Frozen liver, 62–215mg, from time points 0, 1 day, 4 days, 8 days,

and 16 days was homogenized in polysome buffer (20mM Tris/HCl, 150 mM NaCl, 5 mM $MgCl_2$, 1 mM Dithiothreitol, 1:100 dilution protease inhibitor cocktail (Sigma), and 1% Triton X-100) using a bead homogenizer: 30 seconds, 4 m/s, repeated 1–3 times depending on need. Lysate was placed into a new Eppendorf tube and clarified by centrifugation at 20,000g for 20 minutes at 4 °C. After clarification, sample was decanted then ~300 µL was passed through a 2.2mL sucrose cushion (1M sucrose, 20mM Tris/HCl, 150 mM NaCl, 5 mM $MgCl_2$, and 1 mM Dithiothreitol) for 12 hours at ~200,000g (40,600rpm) 4 °C using a Ti-55 rotor on the Optima L-100XP Ultracentrifuge (Beckman Coulter). After centrifugation, sucrose was decanted and the ribosome pellet was suspended in 6M Guanidine/HCl, 100mM Tris/HCl pH 8.5.

3.4.4 Polysome analysis

The polysome analysis was patterned on the method of Zhao et al[36]. Sucrose density gradients were prepared using 5 layers of buffered sucrose (50 mM Tris, 50 mM Ammonium Acetate, 12 mM $MgCl_2$, pH 7.0, and either 7%, 21%, 33%, 47% or 60% sucrose). 1 mL of each mixture was placed in a centrifuge tube from high density (60%) at the bottom to low density (7%) at the top. This step gradient was stored at 4° C overnight to allow formation of a continuous gradient. The next morning flash frozen liver tissue was homogenized in lysis buffer (15 mM $MgCl_2$, 200 mM KCl, 1 % Triton x-100, 100 ug/mL cycloheximide, 2 mM DTT, .1% diethyl pyrocarbonate, pH 7.4) at 6 m/s for 60 s in a MP-Biomedicals FastPrep®-24. The homogenate was centrifuged to clarify (14,000 g, 5 min, 4° C). Approximately 1.2 mg of total protein loaded onto each gradient. The sample was then separated within the sucrose gradient using high speed centrifugation (99526 g, 4 hrs, 4° C) in a Beckman Coulter Optima™ L-100 XP. Polysomes analyzed using an Isco UA-6 Absorbance Detector at 254 nm. Six mice from AL and six from DR were run in duplicate for assessment of polysome profiles.

3.4.5 Mass spectrometry sample preparation

New DNA was measured as the isotope incorporation into the ribose moiety of the nucleoside bases, as previously described[6,37]. New rRNA was also measured as the isotope incorporation into the ribose moiety of the nucleoside bases, by adapting the GC-MS method to follow the heavier ribose instead of the deoxy-ribose. DNA was isolated from tissue homogenates using the DNEasy kit (Qiagen). RNA was extracted from the assembled ribosomes using the Purlink RNA minikit (Life Technologies). rRNA was isolated by homogenizing liver tissue in 20mM Tris pH=7.2, 0.2M sucrose, 2mM $MgCl_2$, 150 mM KCl, 1mM dithiothretol with protease inhibitor cocktail (Sigma), Cycloheximide (Sigma). This homogenate was clarified by brief centrifugation (10 minutes at 14,000 G). Clarified homogenate was spun at 100,000xG through a 1M sucrose cushion in the same buffer for 16 hours. The supernatant was discarded and the pellet containing assembled ribosomes were resuspended using 100 µL 6M guanidine HCL pH=8. Isolated RNA/DNA was hydrolyzed overnight at 37 °C with nuclease S1 and potato acid phosphatase. Hydrolysates were reacted with pentafluorobenzyl hydroxylamine and acetic acid and then acetylated with acetic anhydride and 1-methylimidazole. Dichloromethane extracts were dried, resuspended in ethyl acetate, to be analyzed by GC-MS.

Assembled pool protein samples were prepared for protein mass spectrometry using modified filter-aided sample preparation[6,37]. Briefly, protein was denatured in 6 M Guanidine/HCl 100 mM Tris/HCl (pH 8.5), cysteines were reduced using dithiothreitol and alkylated using iodoacetamide. Samples were placed on 500 µL 30kD filters and washed 2–3 times on the filters using 6 M Guanidine/HCl 100mM Tris/HCl pH 8.5. The guanidine solution was removed by two to three 25 mM ammonium bicarbonate washes. Proteins were resuspended in 25 mM ammonium bicarbonate and digested overnight using Pierce MS-Grade

Trypsin in a 1:50 (w:w) ratio or minimum 0.1 µg or 0.5 µg of trypsin per sample. Trypsin digest was quenched using phenylmethane-sulfonylfluoride (PMSF) or centrifuging through above mentioned filters to remove trypsin. Samples were spun through filters, placed in mass spec vials, speed vacuumed to dry, and then suspended at ~1 µg/µL in 3% acetonitrile 0.1% formic acid.

Total pool samples were prepared from whole liver lysates protocols similar to ribosomal samples. Liver was homogenized in a 100 mM ammonium bicarbonate solution with the protease inhibitor cocktail (Sigma) aiming for a final concentration of approximately 10 mg/ml protein concentration. Approximately 500 µg of protein was lysed in 6M Guanidine/HCl 100mM Tris/HCl and subject to similar filter-aided preparations and trypsin digestion as described above. After digestion, samples were spun through filters, speed vacuumed to dry, and resuspended in 10 mM LC-MS grade ammonium formate pH 9.5. Samples were fractionated using high pH C18 high performance liquid chromatography (HPLC), which is orthogonal to low pH C18 chromatography[38]. Fractionation was performed using the 1260 HPLC Infinity (Agilent) and the Gemini 50 x 2.00 mm C18 column with 3 µm beads and 110 angstrom pore size. Peptides were eluted using a 10 mM ammonium formate pH 9.5 H_2O/acetonitrile gradient from 3% B to 60% B over 40 minutes flowing at 1 mL/min. Gradient A is 97% H_2O, 3% acetonitrile, 10mM ammonium formate pH 9.5. Gradient B is 10% H_2O, 90% acetonitrile, 10mM ammonium formate pH 9.5. 1 mL fractions were collected. 1 mL fractions were pooled into 8 fractions by pooling every 8th fraction. For instance, fractions 1, 9, 17, and 25 would be pooled into one fraction. Pooled fractions were speed vacuumed to dryness then suspended in 200 µL of 80% acetonitrile (to extract peptides but leave some salts) and decanted into a mass

spectrometry vial. Samples were again speed vacuumed to dry and then suspended in 40 µL of 3% acetonitrile 0.1% formic acid for LC-MS analysis.

3.4.6 LC-MS proteomics acquisition

As described previously, protein identification and kinetic acquisition were performed on the Agilent 6530 Q-ToF mass spectrometer coupled to capillary and nanoflow Agilent 1260 HPLC using the chipcube nano-spray source[6,37]. Peptides were eluted from the Agilent C18 Polaris chip at 300 nL/min using an H_2O-Acetonitrile gradient acidified to pH 4 by use of Pierce LC-MS grade formic acid. Buffer A was 3% acetonitrile, 0.1% formic acid. Buffer B was 97% acetonitrile, 0.1% formic acid. The elution gradient is as follows: 0 minutes, 100% A; 0.1 minutes, 95% A; 27 minutes, 40% A; followed by high percentage B column washing and low percentage B equilibration. The Agilent 6530 Q-ToF mass spectrometer was run in 2 Ghz high dynamic range mode. Protein identification runs were performed in MS/MS mode using collision induced dissociation with nitrogen gas. MS1 and MS2 data were collected at a maximum rate of 4 spectra/second with CID fragmentation on the top 10 most abundant precursors. Dynamic exclusion was set to 0.2 minutes. Kinetic acquisitions were performed in MS-only mode and collected at 1 spectra/second. MS only mode increases signal intensity, improves signal-to-noise, and gives more scan points per elution chromatogram greatly enhancing isotopomer analysis accuracy. Raw data is available for download at the Chorus Project (ID# 1148).

3.4.7 Peptide identification

Peptide identifications were made using SpectrumMill B.06 then overlaid onto kinetic acquisitions. SpectrumMill searches were performed against the Uniprot Mouse database (12-2015, with 16,802/51,418 entries searched) with MS1 tolerance ±20ppm and a MS2 tolerance

±50 ppm, cabomidomethylation (C) as a static modification, and pyroglutamic acid (n-term) and oxidation (M) as dynamic modifications.

Searches were performed using trypsin as a digestion enzyme allowing 2 missed cleavages at lysine or arginine. A second search with no specific enzyme was performed against a restricted library of identified proteins. Following general recommendations from Agilent, peptides with a score greater than 7 and greater than 60% scored peptide intensity were used for further analysis. False discovery rate was calculated by the built-in algorithms of the Spectrum Mill software, and was set at 1% for peptides and proteins. Identified peptides were exported and used to calculate mass isotopomer distributions and extract peptide isotope patterns from MS-only acquisitions (supplemental information).

3.4.8 Mass isotopomer and kinetic analysis

MS-only isotopomer data was extracted based on peptide identification from MS/MS acquisition using m/z (± 12 ppm) and retention time alignment (± 0.8 minutes). Data extraction and analysis was conducted using our DeuteRater[39] software tool based on previous publications [40]. Briefly, isotope peaks M0–M4 were normalized against the sum of the signal intensity, then compared to theoretical calculations based on percentage D_2O enrichment to determine fraction deuterium enriched (new) peptide (as previously described[37,39]). Theoretical calculations were determined using the EMass algorithm and based on the number of possible deuterium incorporation sites per amino acid. The theoretical changes in abundance of each isotope peak M0–M4 were compared against experimental changes at each time point in order to determine a time dependent percentage of newly synthesized peptide reported for each isotope peak. Thus, for each peptide there are up to 5 (M0-M3 for peptides below and M0-M4 for peptides above m/z=2400) semi-independent measurements of the peptide turnover, as previously described[6].

We used the standard deviation between these measurements as a metric of the measurement precision for that peptide. If peptide precision was low (i.e. standard deviation exceeded 0.1) the data point was removed from downstream analysis (Figure 3-S2). Additional filters were also applied to remove peptides with total relevant intensity below 20,000 counts and a retention time deviation greater than 0.5 minutes.

The median percent new was calculated at each point and outliers (defined as greater than 1.4X the median absolute standard deviation) were removed from the calculation of the protein percent new. All peptide measurements for an individual time point that passed these filters were weighted equally in the calculation of the fraction new protein at that time point. As described previously, the combined fraction new measurements were fit using a non-linear least squares regression based on first-order kinetic rate equations[34]. The proteins with high precision data at 3 or more time points were fit according to first-order rate kinetics. We required 3 or more labeled time points in order to increase the confidence of the rate constant (Figure 3-S2). For the regression fit, time point zero is set to 0% new, and is given a standard deviation of 0.05 based on the accuracy during long term performance of this instrument. The standard deviation and confidence interval from these fits were used to compare protein and rRNA in subsequent analysis. Coefficients of variance (standard deviation of the fit over the turnover rate) above 0.2 are considered high confidence fits.

3.4.9 rRNA turnover analysis

After running in scan mode, peaks were identified at m/z 212 and 433. From these it was determined that the 212 had better peak shape, accurately predicted natural abundance in an unlabeled sample, and was therefore used for subsequent analyses. Based on accurate mass and isotope distribution we identified the fragment. Mass isotopomer calculations were performed

on the fragment using EMass software based on 3 incorporated deuteriums. The monoisotopic M+1, and M+2 were used was used for % new RNA analysis and errors. Two mice were measured in triplicate at each time point. Rates and confidence intervals are solely based on standard deviations from least squared fits to first-order rate kinetics. Data was fit using a single-phase association curve in GraphPad Prism. Rates and confidence intervals are solely based on standard deviations from least squared fits to first-order rate kinetics. Data was fit using a single-phase association curve in GraphPad Prism.

3.4.10 Quantitative polymerase chain reaction

Quantitative polymerase chain reaction (qPCR) was performed using SYBR green on an Applied Biosystems 7500 instrument. Reverse transcription was performed with the iScript cDNA synthesis kit (Bio Rad) and SYBR green master mix (Bio-Rad). Primers: 18s rRNA forward(CTTAGAGGGACAAGTGGCG) reverse(ACGCTGAGCCAGTCAGTGTA); 16s Mitochondrial rRNA forward(CGAGGGTCCAACTGTCTCTT) reverse(GGTCACCCCAACC GAAATTT); vRNA forward(GCTGAGCGGTTACTTTGACA) reverse(GTCTCGAACCAA ACACTCATG); TATA forward(ACAGCCTTCCACCTTATGCT) reverse (GATTGCTGTA CTGAGGCTGC). qPCR instrument parameters were as follows: Stage 1 (1 cycle) 50 °C for 2 minutes; Stage 2 (1 cycle) 95 °C for 15 seconds; Stage 3 (30–45 cycles depending on need), 95 °C for 15 seconds, 59 °C for 1 minute. Melt curves to determine product purity and efficiency calculations were performed on all primer sets (supplemental data). qPCR primer efficiency was calculated using Real-time PCR Miner 4.1[42,43]. Relative concentrations were calculated using method by Pfaffl, which corrects for differences in primer efficiency[42,43].

3.4.11 Calculation of exchange rate:

Using the kinetic model (Figure 3-1B), the rate of change for each protein in each pool can be described mathematically as:

Free Pool: $$\frac{d[P_{i\,free}]}{dt} = k_{synth} - k_{deg} - k_{add} + k_{remove} = 0 \quad (3\text{-}1)$$

Where P_i is an individual protein concentration, k_{synth} is the synthesis rate, k_{deg} is the degradation rate, k_{add} is the rate of proteins adding to the assembled ribosome, while k_{remove} is the rate of proteins leaving the assembled ribosome and reentering the free pool.

Assembled Pool: $$\frac{d[P_{i\,assembled}]}{dt} = k_{assemble} - k_{ribophagy} + k_{add} - k_{remove} = 0 \quad (3\text{-}2)$$

Where in addition to the terms above, $k_{assemble}$ is the apparent rate of formation and export of the intact active ribosome from the nucleolus to the cytosol. $k_{ribophagy}$ is the rate of whole ribosome degradation; this includes both protein and rRNA.

Ribosome pool: $$\frac{d[rRNA]}{dt} = k_{assemble} - k_{ribophagy} = 0 \quad (3\text{-}3)$$

Total protein pool: $$\frac{d[P_{i\,total}]}{dt} = \frac{\frac{d[P_{i\,free}]}{dt} + \frac{d[P_{i\,assembled}]}{dt}}{2} = 0 \quad (3\text{-}4)$$

Exchange rate: $$\frac{d[Pi]}{dt} = \left[\frac{d[Pi\,assembled]}{dt} - \frac{d[rRNA]}{dt}\right] = k_{add} - k_{remove} = 0 \quad (3\text{-}5)$$

3.4.12 Experimental Design and Statistical Rational

There were 2 biological replicates for each time point in each kinetic pool measurement (assembled/total) of each diet (AL vs DR). Each kinetic rate was determined by up to 10 biological replicates, so no technical replicates were included. A minimum of three time points were required to fit a rate constant, because with three time points the rates are well constrained (Figure 3-S2). As described above, peptide measurements were included if they met the retention time and precision filters. Statistical analysis and graphing was performed using

GraphPad Prism and the Numpy software package. GraphPad Prism was used to fit the DNA to a first order kinetic[38] and rRNA to a second-order kinetic[6] as previously described, and to calculate 95% confidence intervals. An in house Python tool termed DeuteRater[45] was used to calculate the fraction new peptide, fit the protein turnover rates to a single pool model using first-order rate kinetics, and calculate 95% confidence intervals. If rates were outside of the 95% confidence interval of rRNA or another protein they were considered significantly different.

3.5 Results

3.5.1 Short term dietary restriction (DR) elicits the canonical physiological changes associated with lifespan extension

Restricted mice (n= 18) lost weight relative to AL controls (n=18) for the first two weeks of the restricted diet, after which they gained weight at a rate similar to controls (Figure 3-2 A). In order to ensure that both the AL and the DR mice were at homeostasis, the dietary treatment

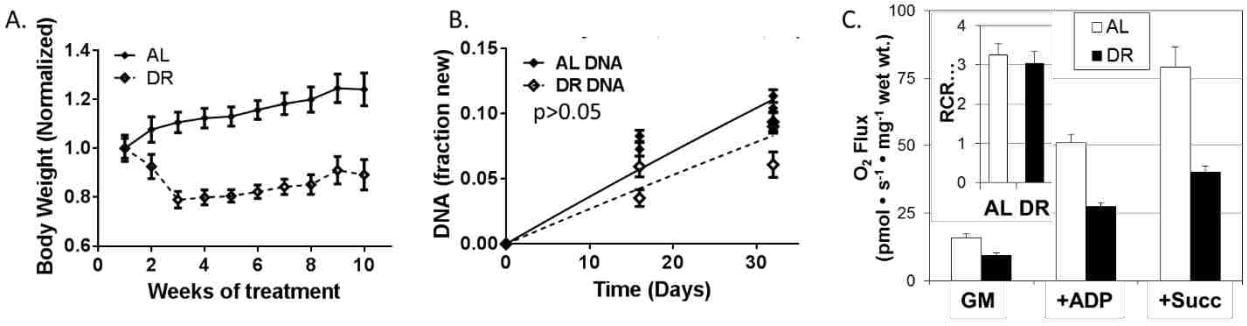

Figure 3-2 Short-term DR elicits the classic physiological and biochemical adaptations associated with lifespan extension: After an initial weight loss, DR mice continued to gain weight at a reduced rate (A). Liver cell proliferation was reduced ($p<0.01$) from 0.04% per day to 0.03% per day (B). DR reduces mitochondrial respiration, samples were treated with: GM: Glutamate (10 mM) + Malate (2 mM); + ADP (2.5 mM Adenosine diphosphate); +Succ: (Succinate 10 mM). Respiratory control ratio (RCR; inset) was unchanged (C).

was continued for 10 weeks prior to initiating the metabolic labeling experiment (Figure 3-1). Using previously described methods[5], we found that the cell proliferation rate was reduced 25%

($p<0.05$) in DR (Figure 3-2 B). Consistent with previous reports, we observed liver tissue respiration capacity was decreased by DR[5,6], for both complex 1 and complex 2 driven electron transport (Figure 3-2 C). Respiratory efficiency, which is the ratio of the ADP dependent O_2 usage (+ADP) versus non-specific oxygen usage (Glutamate+Malate), was not changed (inset to Figure 3-2 C).

3.5.2 Ribosome activity is reduced during DR

Similar to published protocols[5,6], we used a sucrose gradient to separate out the various ribosome states within the liver tissue of AL and DR animals (Figure 3-1). Polysome analysis (Figure 3-3 A) was conducted twice on 6 animals from each diet group, and the normalized area under the curve of each ribosomal species was quantified. The number of ribosomes actively transcribing mRNA (polysomes) was significantly lower ($p<0.05$) in DR tissue (Figure 3-3 B). Interestingly, the total number of ribosomes, as measured by qPCR, was not significantly changed by DR (Figure 3-S1). These combined results suggest that during DR a lower percentage of available ribosomes are actively producing protein, similar to previous reports[34].

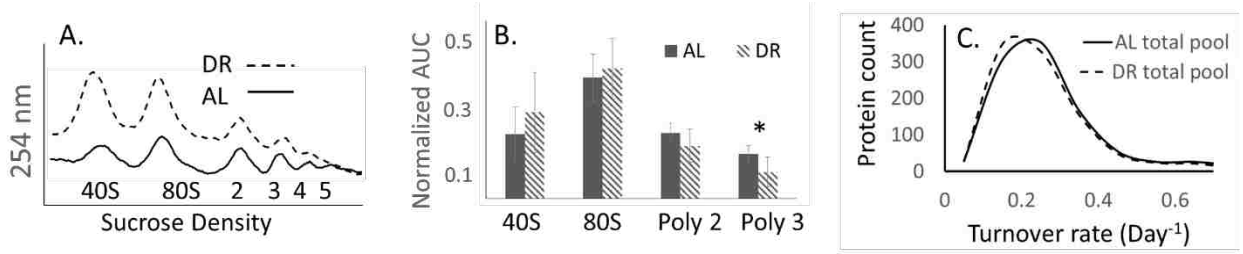

Figure 3-3 Short-term DR reduces percentage of active ribosomes: Representative data from polysome analysis in which a density gradient separates individual subunits from active ribosomes in both AL and DR tissue (A). Quantitation of the populations suggests that DR increases the free 40S state by significantly decreasing the number of active polysomes (Poly 3 in panel B) Comparison of turnover rates for 1050 matched proteins showed a statistically non-significant general reduction of protein turnover rates in DR. (C)

We also compared ribosome activity by measuring turnover (synthesis + degradation) rates for 1050 proteins observed in both AL and DR (Figure 3-3 C). Consistent with previous

investigations of changes in protein turnover during low calorie diets, we observed that during DR the median protein turnover rate was 5% slower (Figure 3-3 C). This decrease is smaller than in previously reported studies[42,43,46], and not statistically significant. We are currently investigating how specific components of the diet may have modified regulation of global protein homeostasis during lower calorie intake. Together these results suggest that the overall ribosome pool has slightly reduced activity with more ribosomes in the cell as dissociated subunits in DR tissue.

3.5.3 Turnover rate of the rRNA backbone is slightly faster in DR tissue

Assembled ribosomes were isolated from the liver tissue of 2 animals at each of the 8 time points and separated into two samples for analysis of rRNA and r-protein turnover (Figure 3-1 A). New rRNA was measured as the isotope incorporation into the ribose moiety of the nucleoside bases, similar to the accepted method for measuring DNA synthesis. The fraction new rRNA increased exponentially with time (Figure 3-4). Previously, rRNA modeling has shown that in rapidly dividing cultures incorporation of a precursor pool improved model accuracy[47]. We compared both the single pool and the precursor model for fitting the rRNA data. Incorporating the precursor pool as described in the literature resulted in precursor pool

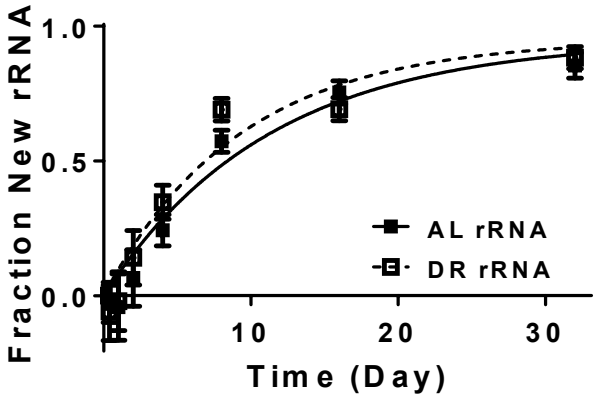

Figure 3-4 rRNA turnover measures eukaryotic ribophagy: Deuterium incorporation into the ribose of the rRNA bases is not significantly slower in AL (10.1±1.2% Day^{-1}) than the DR (11.1±1.7% Day^{-1}).

sized of 13% and 6% for AL and DR tissue respectively. We observed a non-significant increase in rRNA turnover in the DR tissue (11.1±1.7% Day^{-1}) relative to AL tissue (10.1±1.2% Day^{-1}).

We checked whether mitochondrial ribosomes are a potential source of contaminating rRNA (Figure 3-S1). Protein mass spectrometry of the isolated ribosomes confirmed that minor amounts of mitochondrial r-proteins were present. Mitochondrial r-proteins share little or no homology with the eukaryotic ribosomes and therefore cannot confound the measurement of protein kinetics. As measured by our assay, mitochondrial rRNA cannot be differentiated from eukaryotic rRNA. Therefore, in order to determine the effect of mitochondrial rRNA on measured ribophagy rates, we isolated ribosomes both with and without non-ionic detergent. With detergent, we measured a relative 5-fold higher concentration of eukaryotic ribosomal rRNA. Without detergent, the total ribosomal isolation was less efficient, but the amount of eukaryotic 18S to mitochondrial 16S rRNA as measured by qPCR increased 50 percent (Figure 3-S1). The large relative change in the mitochondrial content did not change our rates of rRNA turnover in these samples (Figure 3-S1), indicating that the absolute contamination from the mitochondrial ribosome rRNA is relatively minor, and does not bias our results for cellular rRNA and ribophagy rates.

Simple stoichiometry of the rRNA within the cell supports the conclusion that mitochondrial contamination will not bias rRNA rates. Based on studies in yeast, there are approximately 14 times more eukaryotic than mitochondrial ribosomes[6,37,49]. The eukaryotic ribosome contains approximately 3 times the number of rRNA bases. Therefore, the rRNA bases from eukaryotic ribosomes are about 42-fold more abundant than mitochondrial, which suggests that the rRNA turnover rate will dominated by the eukaryotic ribosomes. Our sample

preparation also removed many of the mitochondria prior to ribosome isolation and should further bias the sample towards eukaryotic ribosomes.

3.5.4 Dietary Restriction significantly changes the turnover rates of proteins in the assembled ribosome

Similar to our previous studies, isotope incorporation into multiple tryptic peptides was measured for each protein in multiple samples along the time-course[42]. We isolated assembled ribosomes for analysis of r-protein turnover (Figure 3-1 A). Turnover rates were significantly different between the individual r-proteins (Figure 3-6 A); we measured turnover rates for 71 of the 80 integral r-proteins with turnover rates ranging from 4-25% per day (Supplemental Table 3-S1). Interestingly, the median turnover rate for the entire group of r-proteins in the assembled ribosome is the same as the rRNA turnover rate (0.10 Day^{-1} in AL, 0.11 Day^{-1} in DR). Comparison of the individual protein turnover rates to the rRNA rate shows that many (approximately 80%) of the proteins turnover within two standard deviations of the rRNA rate (Figure 3-5 B, C, and D, grey symbols). This suggests that the rRNA and these proteins may all be synthesized and degraded together as a unit, as occurs during ribophagy. In addition, the large number of individual protein measurements makes the DR-dependent increase in ribophagy statistically significant (Figure 3-5 D, $p<0.0005$).

DR also increased the observed range of rates within the assembled ribosome, but the rRNA turnover confidence interval (CI, defined as 2 standard deviations) was also wider so the percentage of non-exchanging proteins stayed around 80%. The proteins at the 60S/40S interface (L10, L36A, L24, L34, and L19) were still among the fastest turnover proteins within the assembled ribosome, and were replaced faster than the rRNA CI (Figure 3-3 D). Although there were several proteins slower than the rRNA CI in both AL and DR, these proteins were not

the same in both groups (Figure 3-5 D). Importantly, each of these protein turnover rates was calculated from multiple measurements of multiple peptides.

3.5.5 Turnover for most r-proteins is not different between the Assembled and Total Pools

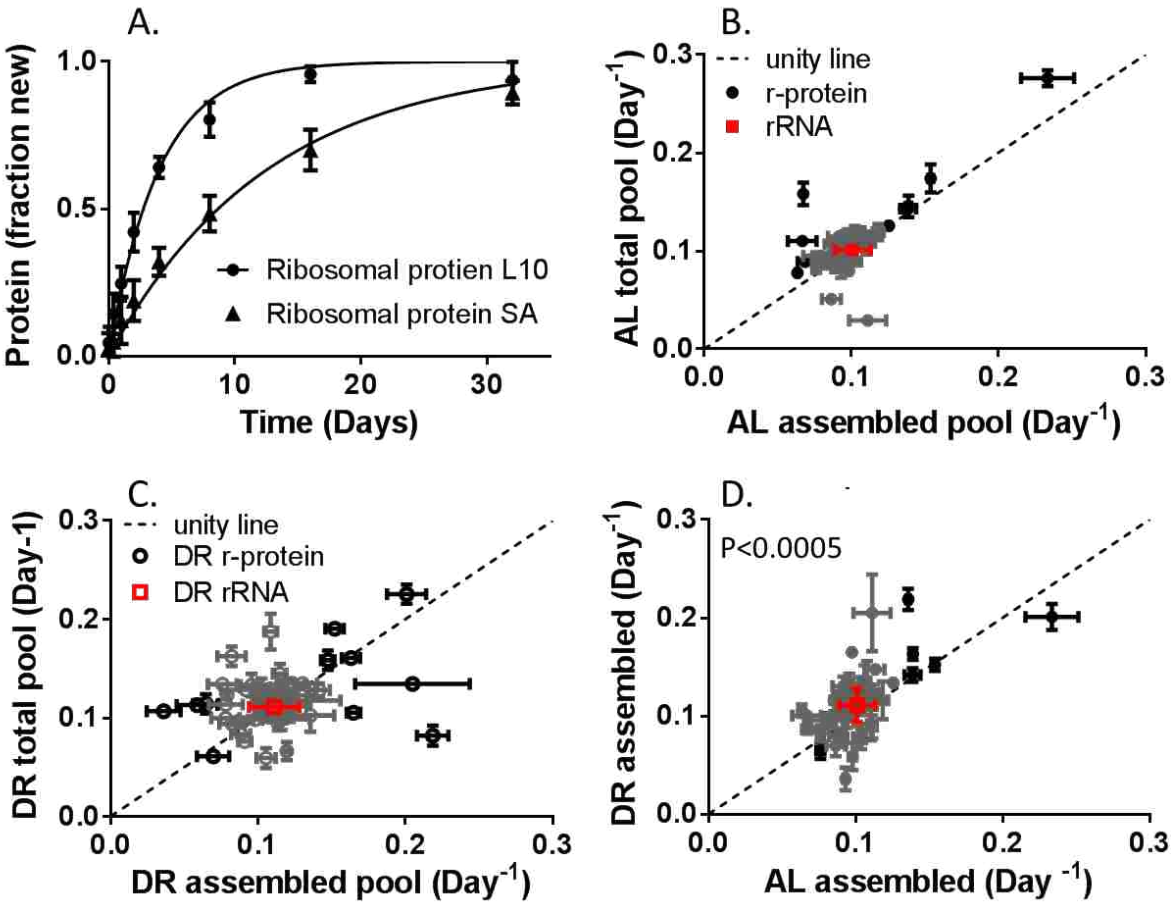

Figure 3-5 Turnover rates of r-protein are equivalent between pools, but not between dietary groups: Individual ribosomal proteins turnover at different rates within the assembled ribosome (A), but have the same rate in both assembled and total pools (B, C). Approximately 80% of r-protein turnover rates (gray circles) are within the confidence interval of the rRNA (red). R-Proteins with unusually fast or slow turnover (black circles) were observed in both AL (B) and DR (C) tissue. Comparison of assembled AL and DR (D) showed that some of the outlier proteins are the same in both conditions.

We were not confident that we could keep assembled and free pools separate during tissue homogenization. Therefore, we measured the total pool (free + assembled) and assembled pool turnover. The turnover rate within the total cellular lysate represents the average of the free

and assembled protein pools (Equation 3-4). A deviation between assembled and total pool turnover rates could indicate that exchange is a rate limiting process. Generally, we observed that there was no statistically significant change in turnover between assembled and total protein pools regardless of dietary intervention (Figure 3-3 A and B). Individual proteins had altered turnover in either AL or DR mice, but not in both. Experiments in *E. coli* suggest that greater than 95% of the r-proteins in the cell are bound in the ribosome structure[51]. A mass averaged turnover measurement would suggest that the total pool rate should reflect the assembled pool similar in these measurements.

3.5.6 Calculation of r-protein exchange rates

A kinetic model for ribosome biogenesis and maintenance was used to compare the turnover of the assembled and total r-proteins and to calculate the exchange between pools (Figure 3-1 B). We measured the relative concentration of the rRNA by qPCR between experimental cohorts and did not see a significant change. The unchanged rRNA concentration and the steady rate of weight increase (Figure 3-2) after the 10 weeks of dietary acclimation reinforces the conclusion that these proteins are at a condition of homeostasis. Therefore, under these conditions, the total concentrations are constant and the opposing rates of synthesis and degradation are balanced (i.e. k_{add} is equal to k_{remove}).

Using the kinetic model, the rate of change for each protein in each pool can be described mathematically as shown in supplemental methods. We have directly measured the turnover of the rRNA, which represents the turnover of the ribosome as a unit (Equation 3-3). We also measured the protein turnover rate within the assembled ribosome (Equation 3-2, $k_{assemble} + k_{add}$, note that $k_{assemble} = k_{ribophagy}$ and $k_{add} = k_{remove}$ due to homestasis) and the total pool (Equation 3-4, $k_{synth} + k_{add}$, noting that $k_{synth} = k_{deg}$ and $k_{add} = k_{remove}$). We therefore calculate the exchange rate

(k_{add} *and* k_{remove}) as the absolute value of the difference in turnover rates of the assembled pool and the rRNA (Equation 3-5: Figure 3-1 B).

This calculation suggests that the greater the difference between r-protein and rRNA the faster the exchange rate. We therefore define all proteins more than two standard deviations from the rRNA rate (outside the confidence interval or CI, black symbols, Figures 3-5 B, and C) as fast exchange with the cytosolic pool (Figure 3-6 A). This separates the r-proteins into essentially three groups: 1-Static, 2-rapid exchange-fast turnover, as well as rapid exchange-slow turnover proteins, and 3-proteins that switch between groups 1 and 2. Static proteins are integrated into the ribosome during initial assembly and are degraded with the assembled unit by ribophagy (Figure 3-5 A gray circles within the square, ~80% of the r-proteins are in this group). The fast exchange proteins (triangles in Figure 3-5 A) can be divided into two groups, fast exchange - fast turnover proteins (12%), and fast exchange - slow turnover proteins (8%).

In DR tissue, there were slight differences in the identity of the individual r-proteins, but a similar percentage distribution of proteins. Proteins L3, L10, L38, L24, and S27-like were still fast exchange. This suggests that these proteins are rarely degraded by ribophagy and exchange is intrinsic to the operation of the ribosome. Proteins L19 and L34 are still at the fast end of the range, but fail to exceed the confidence interval of the rRNA. This suggests that L19 and L34 are not exchanged as frequently during DR, but that ribophagy plays a larger role in defining their lifetime.

Of the fourteen fast exchange proteins observed in the AL ribosome, twelve either were at the interface between subunits or have significant surface exposed to the cytosol. Seven of these proteins were fast exchange in both DR and AL ribosomes. Rapid exchange proteins with fast turnover tend to be located at the interface between the 60S and 40S subunits, and are

involved with the structural motions of catalysis[22]. For example, L24, L34, and L19 bridge the interface between the 60S and 40S ribosome (Figure 3-6). They hold the subunits together and participate in the rotation between subunits during peptide bond synthesis[2]. Other fast turnover proteins L10 and L36 also have an active role in the formation of new peptide bonds, and are close to the interface between the subunits (Figure 3-6 B). Protein L38 is also part of this group, but its function is less well understood and may play a role in mRNA substrate selection[29]. Although there were a variety of rapid exchange proteins with slow turnover in either AL, or DR, only L3 was rapid exchange under both conditions.

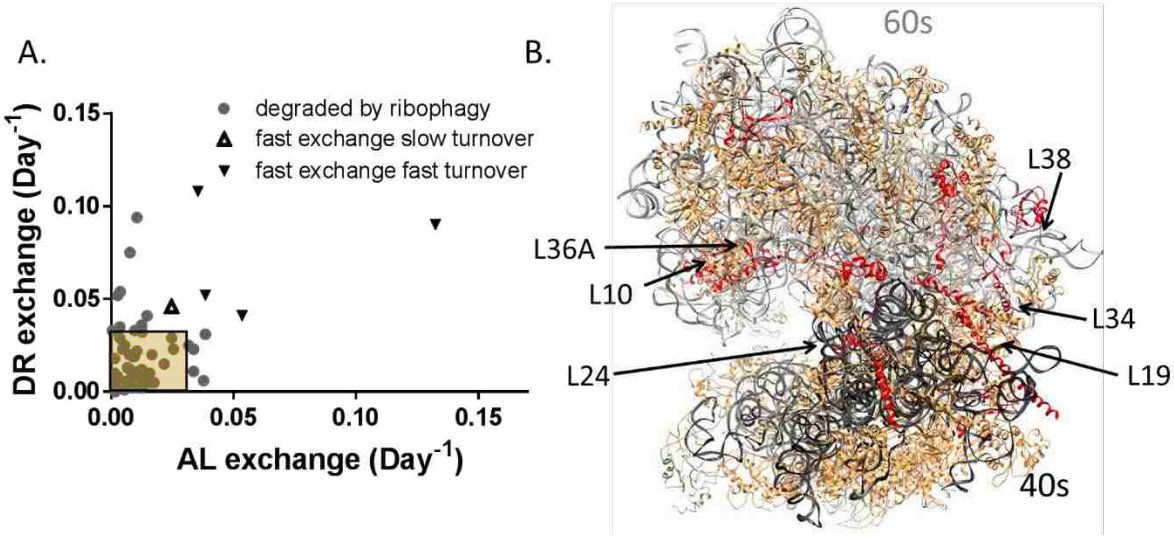

Figure 3-6 In vivo exchange of r-proteins: Most r-proteins exchange slowly (gray circles) and are within the expected range for ribophagy (yellow box in A). Exchange rates for some r-proteins is outside of the expected ribophagy rate in one condition (gray circles outside in white field for AL or DR). Some exchange rates are rapid enough that these proteins are rarely degraded by ribophagy and instead are degraded in the free pool (triangles). Some members of this group have slow cytosolic turnover (A, open triangles), others have fast cytosolic turnover (A, closed triangles). (Panel B) Slow exchange proteins (tan) cover the majority of the ribosome structure. Fast turnover/fast exchange r-proteins (closed triangles) are primarily at the interface between 60S (gray rRNA) and 40S (black rRNA) subunits (red proteins, model PDB: 4UG0).

In AL ribosomes, L35a and slow turnover L7 were fast exchange but do not follow the structural trend of surface exposure. In the ribosome crystal structure (PDB: 4UGO), they both seem to be buried underneath large rRNA loops and slow exchange proteins. Interestingly, they

are next to each other in the structure, suggesting that the rRNA may be displaced to allow exchange of these proteins simultaneously.

3.6 Discussion

The ribosome is a multi-megadalton complex of RNA and protein that synthesizes most proteins in the cell. High demand for protein synthesis reduces ribosome efficiency[4] and accuracy[2,52]. In bacteria, damaged ribosomes can regain activity by replacement of damaged r-proteins in the assembled structure with undamaged cytosolic copies[2,52]. Exchange of r-proteins may also be important to the functional integrity of the ribosome in eukaryotes[5,6], although this idea is controversial. Metabolic labeling affords a means to evaluate this hypothesis by testing directly for the replacement (turnover) of ribosomal components *in vivo*. We used metabolic deuterium incorporation rates to compare turnover of ribosomal RNA (rRNA) and the individual r-proteins in the assembled ribosome in mice (Figure 3-1 A). We also tested whether dietary restriction (DR), which has previously been shown to modulate rates of ribosome biogenesis, assembly, and activity in cells[5,6] and mice[42,43], can impact r-protein exchange rates.

Components of the ribosome reside in two kinetically distinct pools (Figure 3-1 B), with different synthesis and degradation rates for the assembled complex and its individual constituents[5,6]. At homeostasis, the rates of opposing steps in the model (e.g., assembly and ribophagy) should be equal (Figure 3-1 B). Physiological and biochemical metrics of the DR effect verified that the mice used in these experiments were at homeostasis (Figure 3-2) prior to metabolic labeling, similar to previous studies[53,54]. The model also assumes that free rRNA, without r-proteins, is degraded rapidly relative to the turnover of the assembled structure, as observed previously[6,37,49]. Under this assumption, turnover of rRNA reflects only turnover of the

assembled ribosomes (Equation 3-3). Turnover of r-proteins in the assembled pool would depend on the kinetics of both assembly and exchange (Equation 3-2, $k_{assemble} + k_{add}$, note that $k_{assemble} = k_{ribophagy}$ and $k_{add} = k_{remove}$ due to homeostasis). We therefore calculated the exchange rate (k_{add} *and* k_{remove}) as the absolute value of the difference in turnover rates of individual r-proteins (P_i) in the assembled pool and the rRNA (Equation 3-5: Figure 3-1 B).

Assembled ribosomes isolated from the liver tissue of two animals at each of eight time points after introduction of the metabolic label were separated into two samples for analysis of rRNA and r-protein turnover (Figure 3-1 A). The amount of new rRNA increased exponentially with time (Figure 3-4) and could be modeled by assumption of a single pool. There was a statistically insignificant increase in rRNA turnover increased in the DR tissue [(11.1 ± 1.7) %•Day^{-1}] relative to control with no dietary restriction (Ad libitum or AL) tissue [(10.1 ± 1.2) %•Day^{-1}]. In DR, although fewer ribosomes were actively translating protein (Figure 3-3), the total number was not different between AL and DR tissue (via qPCR, Figure 3-S1 B). The results imply that, on average, ribosomes were less active and had a slightly shorter lifetime (6 Days) in tissues of DR animals than in those from the AL animals (7 Days). The measurements of protein turnover within the assembled ribosome and the observed proteome support these results.

Turnover rates of the individual ribosomal proteins (r-proteins) were resolved by monitoring incorporation of deuterium into multiple tryptic peptides for each protein along the labeling time-course (Figure 3-5A), as previously described[55]. Within the set of 71 (out of 80 total) integral r-proteins monitored, a range of 4-28% per day was observed (Supplemental Table 3-S1). Most r-proteins turn over at rates that are similar to (within two standard deviations of) that of the rRNA (Figures 3-5 B, C, D grey symbols), implying that this large group of r-proteins

and the rRNA are replaced together as a unit (i.e., complete degradation of the complex). Indeed, the average rate for the r-proteins (10.2% in AL and 11.3% in DR) matched the ribophagy rate (10.1% in AL and 11.1% in DR) remarkably well. Comparison of resolved turnover rates of the individual r-protein components (Figure 3-5 D) makes it apparent that the small DR-dependent increase in rRNA turnover (Figure 3-4) is significant ($p<0.0005$). Overall, ~80% of r-proteins, had individual turnover rates which match the ribophagy rate (within 2 standard deviations of the rRNA). This agrees with earlier studies of average rRNA and r-protein turnover.

The increased rate of ribophagy in DR tissues was surprising. In agreement with previous studies we observed that DR slows cell proliferation (Figure 3-2B) and protein synthesis (Figure 3-3). Interestingly, the cellular half-life (169 days in AL) is 25 times greater that the ribosome half-life in AL. In DR, the ribosome turnover is accelerated relative to cell proliferations, becoming 37 times greater. The two-dimensional comparison suggests that the rate of ribophagy, specifically, doubles relative to the rate of other processes like mitochondria specific degradation or cell division. The up-regulation of ribophagy during DR, may explain the previous observation that increased autophagy and lower protein synthesis rates work together to improve cellular fitness and whole organism lifespan.

Although the turnover rate of r-proteins averaged over the entire set reflects the ribophagy rate (as previously reported), a small but intriguing set of r-proteins have significantly different turnover rates (Figures 3-5 B, C, and D, black symbols). Importantly, some of the proteins with unusually fast or slow turnover are the same in both AL and DR tissues (Figure 3-2 D). The parallel behavior of these proteins in both dietary cohorts suggests that the difference in their turnover rates might be intrinsic and functionally relevant. The difference in turnover may be due to the free pool r-protein turnover rate (Figure 3-1 B), which is independent of the

ribophagy rate. The free pool turnover rate is difficult to measure directly, since it is very low concentration for each r-protein[4,50], and homogenizing the tissue is likely to break assembled ribosomes, contaminating the free pool. However, as shown in equation 3-5, the exchange rate of each protein can be calculated without direct measurement of the free pool. The proteins that are exchanged rapidly out of the assembled structure would have turnover rates defined by the free pool. Therefore, fast exchange between the assembled and free pool could explain outliers at both the fast and slow end of the turnover range (Figure 3-5).

When we compared the calculated exchange rates (Figure 3-6 A) against the ribosome structure, we saw that the fast exchange and fast turnover r-proteins are predominately located at the interface between the 60S and 40S subunits (Figure 3-6 B). This region is known to undergo significant movement during the catalytic activity of the ribosome[4,50]. There are at least two possible hypotheses to explain why ribosomal maintenance would include fast exchange of these proteins. First: proteins at this location may be more prone to damage and therefore exchange more rapidly. Second: damage of these proteins dramatically reduces formation of the 80S ribosome and ensures that there is a longer exchange period. Three of these proteins (L19, L24 and L34) are structurally important, acting like long fingers to secure the 40S to the 60S subunit (Figure 3-6). The other members of this subgroup (L10, L36A, and L38) are also localized in the interface, either on the beak or directly across from it. Breaking the 80S down to the 40S and 60S could facilitate exchange of these proteins due to lost surface interactions and greater access to the cytosol.

Cytosolic RPL36a and L10 are critical to formation of the P-site during assembly, and guide the structural rotation necessary to form each peptide bond[6,18]. Dysfunction of these and other fast exchange proteins is associated with disease[6,18]; therefore, exchange may represent an

important method to maintain ribosomal quality. Greater exchange of these proteins in AL tissue relative to the ribophagy rate may indicate that damage to these specific proteins occurs prior to ribophagy.

One interpretation of these results is that ribophagy and r-protein exchange are both used to maintain the active pool of ribosomes (Figure 3-7). Simplistically, the high synthetic demand and longer lifespan for individual ribosomes observed in AL tissue might result in accumulation of damaged ribosomes, as only a few selected proteins can be repaired. Slower cell proliferation in DR suggests that, because there is less dilution into new cells, protein degradation is up regulated to match synthesis[22]. Lower synthetic demand with an accompanying increase in ribophagy, would allow for more extensive turnover of the assembled ribosome pool. Better maintenance of the ribosome might lead to higher quality nascent peptides and improved

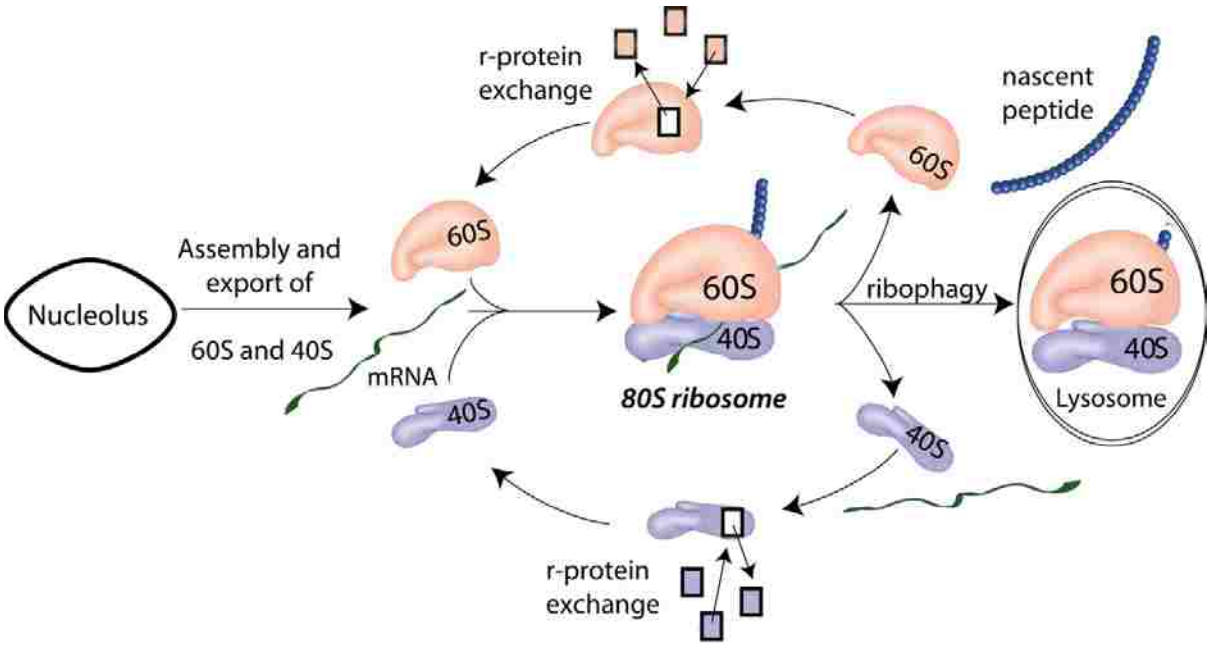

Figure 3-7 In vivo ribosome maintenance requires ribophagy and r-protein exchange: Each day, approximately 10% of the ribosomal pool is replaced via assembly of new ribosomes and ribophagy. During the lifetime of the assembled ribosomal structure, ribosome protein exchange occurs primarily when the ribosome disassociates to its individual subunits. This exchange may be a fast, low cost, method to repair and modify ribosomes. Cellular energetics and demand for protein synthesis may modulate the relative contribution of ribophagy, versus exchange in response to stalled or damaged ribosomes.

accuracy[5,6,8,9] and efficiency relative to AL tissue. This provides an attractive interpretation for the frequently observed connection between lower rates of protein synthesis, increased autophagy, and improved protein homeostasis and longevity.

It has been observed that the ribosome quality control (RQC) complex is required to dissociate stalled 80S ribosomes[2]. Our data suggests that ribosomes exchange components most rapidly when dissociated into subunits, potentially after the RQC has dissociated the complex. These results raise several interesting questions about mechanisms for maintenance. Is there cross talk between RQC activity and ribosome component turnover? What factors control ribosome component exchange? We assume a passive model, but could the RQC coordinate active exchange? Proteins L35a and L7 are fast exchange in AL tissue, but are buried within the rRNA. These proteins may require outside assistance to facilitate exchange. Finally, does r-protein exchange improve the quality of nascent peptides? Initial results suggest that reducing global protein synthesis may improve protein quality[3]. Further investigation is needed to confirm whether ribosomal maintenance is a mechanistic link explaining how lower protein synthesis burdens are connected to improved protein homeostasis and lifespan.

In conclusion, this work uses a generally applicable strategy for investigating cellular maintenance of the proteome, including multi-protein and ribonuclear structures. Here we show that exchange of protein components and degradation of the entire ribosome are important maintenance strategies. Our results suggest a mechanism wherein dissociation of 60S and 40S subunits promotes *in vivo* r-protein exchange. We find that dietary signals can change both ribophagy and r-protein exchange rates. Future work testing biological models which modulate the RQC activity and/or mTOR signaling will test whether this is mechanism is generally

applicable. In addition, linking changes in longevity to the rates of protein synthesis and autophagy as we have done may help identify mechanisms of aging.

3.7 Acknowledgments

We are grateful to J. Martin Bollinger Jr., Alan Buskirk, Barry Willardson, and Natalie Blades for constructive insights and helpful conversations. Earl Albee, Warren Bingham, and the BYU animal care facility for assistance in maintenance of the mice. Nathan Keyes and Ryne Peters for assistance with Ribosome Supplemental Figure 1. This work was supported by BYU startup funds to JCP, Roland K. Robins Graduate Research Fellowship to BCN and RHC, BYU Undergraduate Research Awards to EE, JH, JK, EH.

Competing Interests: None

3.8 Bibliography

1 Ben-Zvi, A., Miller, E. A. & Morimoto, R. I. Collapse of proteostasis represents an early molecular event in Caenorhabditis elegans aging. *Proc. Natl. Acad. Sci. U. S. A.* **106**, 14914-14919, doi:10.1073/pnas.0902882106 (2009).

2 Conn, C. S. & Qian, S. B. Nutrient signaling in protein homeostasis: an increase in quantity at the expense of quality. *Sci Signal* **6**, ra24, doi:10.1126/scisignal.2003520 (2013).

3 Choesmel, V. *et al.* Impaired ribosome biogenesis in Diamond-Blackfan anemia. *Blood* **109**, 1275-1283, doi:10.1182/blood-2006-07-038372 (2007).

4 Xue, S. & Barna, M. Specialized ribosomes: a new frontier in gene regulation and organismal biology. *Nat. Rev. Mol. Cell Biol.* **13**, 355-369, doi:10.1038/nrm3359 (2012).

5 Karunadharma, P. P. *et al.* Subacute calorie restriction and rapamycin discordantly alter mouse liver proteome homeostasis and reverse aging effects. *Aging Cell* **14**, 547-557, doi:10.1111/acel.12317 (2015).

6 Price, J. *et al.* The Effect of Long Term Calorie Restriction on in Vivo Hepatic Proteostatis: A Novel Combination of Dynamic and Quantitative Proteomics. *Mol. Cell. Proteomics* **11**, 1801-1814, doi:10.1074/mcp.M112.021204 (2012).

7 van der Goot, A. T. *et al.* Delaying aging and the aging-associated decline in protein homeostasis by inhibition of tryptophan degradation. *Proc. Natl. Acad. Sci. U. S. A.* **109**, 14912-14917, doi:10.1073/pnas.1203083109 (2012).

8 Houtkooper, R. H. *et al.* Mitonuclear protein imbalance as a conserved longevity mechanism. *Nature* **497**, 451-457, doi:10.1038/nature12188 (2013).

9 Selman, C. *et al.* Ribosomal protein S6 kinase 1 signaling regulates mammalian life span. *Science* **326**, 140-144, doi:10.1126/science.1177221 (2009).

10 Kristiansen, M. *et al.* Disease-associated prion protein oligomers inhibit the 26S proteasome. *Mol. Cell* **26**, 175-188, doi:10.1016/j.molcel.2007.04.001 (2007).

11 Repetto, E., Yoon, I. S., Zheng, H. & Kang, D. E. Presenilin 1 regulates epidermal growth factor receptor turnover and signaling in the endosomal-lysosomal pathway. *J. Biol. Chem.* **282**, 31504-31516, doi:10.1074/jbc.M704273200 (2007).

12 Safar, J. G. *et al.* Prion clearance in bigenic mice. *J. Gen. Virol.* **86**, 2913-2923, doi:10.1099/vir.0.80947-0 (2005).

13 Lee, S. & Notterpek, L. Dietary restriction supports peripheral nerve health by enhancing endogenous protein quality control mechanisms. *Exp. Gerontol.* **48**, 1085-1090, doi:10.1016/j.exger.2012.12.008 (2013).

14 Leprivier, G., Rotblat, B., Khan, D., Jan, E. & Sorensen, P. H. Stress-mediated translational control in cancer cells. *Biochim. Biophys. Acta* **1849**, 845-860, doi:10.1016/j.bbagrm.2014.11.002 (2015).

15 Montanaro, L., Trere, D. & Derenzini, M. Nucleolus, ribosomes, and cancer. *Am. J. Pathol.* **173**, 301-310, doi:10.2353/ajpath.2008.070752 (2008).

16 Kolch, W. & Pitt, A. Functional proteomics to dissect tyrosine kinase signalling pathways in cancer. *Nat. Rev. Cancer* **10**, 618-629, doi:10.1038/nrc2900 (2010).

17 de Groot, M. J. *et al.* Quantitative proteomics and transcriptomics of anaerobic and aerobic yeast cultures reveals post-transcriptional regulation of key cellular processes. *Microbiology* **153**, 3864-3878, doi:10.1099/mic.0.2007/009969-0 (2007).

18 Miller, B. F., Drake, J. C., Naylor, B., Price, J. C. & Hamilton, K. L. The measurement of protein synthesis for assessing proteostasis in studies of slowed aging. *Ageing Res Rev* **18**, 106-111, doi:10.1016/j.arr.2014.09.005 (2014).

19 Dai, D. F. *et al.* Altered proteome turnover and remodeling by short-term caloric restriction or rapamycin rejuvenate the aging heart. *Aging Cell* **13**, 529-539, doi:10.1111/acel.12203 (2014).

20 McCay, C. M., Crowell, M. F. & Maynard, L. A. The effect of retarded growth upon the length of life span and upon the ultimate body size. *Nutrition* **5**, 155-171; discussion 172 (1935).

21 Anderson, R. M., Shanmuganayagam, D. & Weindruch, R. Caloric restriction and aging: studies in mice and monkeys. *Toxicol. Pathol.* **37**, 47-51, doi:10.1177/0192623308329476 (2009).

22 Borkowski, O. *et al.* Translation elicits a growth rate-dependent, genome-wide, differential protein production in Bacillus subtilis. *Mol. Syst. Biol.* **12**, 870, doi:10.15252/msb.20156608 (2016).

23 Brandman, O. *et al.* A ribosome-bound quality control complex triggers degradation of nascent peptides and signals translation stress. *Cell* **151**, 1042-1054, doi:10.1016/j.cell.2012.10.044 (2012).

24 Shen, P. S. *et al.* Protein synthesis. Rqc2p and 60S ribosomal subunits mediate mRNA-independent elongation of nascent chains. *Science* **347**, 75-78, doi:10.1126/science.1259724 (2015).

25 Ossareh-Nazari, B. *et al.* Ubiquitylation by the Ltn1 E3 ligase protects 60S ribosomes from starvation-induced selective autophagy. *J. Cell Biol.* **204**, 909-917, doi:10.1083/jcb.201308139 (2014).

26 Ashford, T. P. & Porter, K. R. Cytoplasmic components in hepatic cell lysosomes. *J. Cell Biol.* **12**, 198-202 (1962).

27 Schleif, R. Control of production of ribosomal protein. *J. Mol. Biol.* **27**, 41-55 (1967).

28 Warner, J. R. The economics of ribosome biosynthesis in yeast. *Trends Biochem. Sci.* **24**, 437-440 (1999).

29 Pulk, A. *et al.* Ribosome reactivation by replacement of damaged proteins. *Mol. Microbiol.* **75**, 801-814, doi:10.1111/j.1365-2958.2009.07002.x (2010).

30 Edwards, C. *et al.* Mechanisms of amino acid-mediated lifespan extension in Caenorhabditis elegans. *BMC Genet.* **16**, 8, doi:10.1186/s12863-015-0167-2 (2015).

31 Eisenberg, T. *et al.* Nucleocytosolic depletion of the energy metabolite acetyl-coenzyme a stimulates autophagy and prolongs lifespan. *Cell Metab.* **19**, 431-444, doi:10.1016/j.cmet.2014.02.010 (2014).

32 Salminen, A. & Kaarniranta, K. Regulation of the aging process by autophagy. *Trends Mol. Med.* **15**, 217-224, doi:10.1016/j.molmed.2009.03.004 (2009).

33 Zhao, S. & Fernald, R. D. Comprehensive algorithm for quantitative real-time polymerase chain reaction. *J. Comput. Biol.* **12**, 1047-1064, doi:10.1089/cmb.2005.12.1047 (2005).

34 Neese, R. A. *et al.* Measurement in vivo of proliferation rates of slow turnover cells by 2H2O labeling of the deoxyribose moiety of DNA. *Proc. Natl. Acad. Sci. U. S. A.* **99**, 15345-15350, doi:10.1073/pnas.232551499 (2002).

35 Wisniewski, J. R., Zougman, A., Nagaraj, N. & Mann, M. Universal sample preparation method for proteome analysis. *Nat. Methods* **6**, 359-362, doi:10.1038/nmeth.1322 (2009).

36 Wang, Y. *et al.* Reversed-phase chromatography with multiple fraction concatenation strategy for proteome profiling of human MCF10A cells. *Proteomics* **11**, 2019-2026, doi:10.1002/pmic.201000722 (2011).

37 Price, J. C. *et al.* Measurement of human plasma proteome dynamics with (2)H(2)O and liquid chromatography tandem mass spectrometry. *Anal. Biochem.* **420**, 73-83, doi:10.1016/j.ab.2011.09.007 (2012).

38 Naylor, B. C. *et al.* DeuteRater: a tool for quantifying peptide isotope precision and kinetic proteomics. *Bioinformatics* **33**, 1514-1520, doi:10.1093/bioinformatics/btx009 (2017).

39 Hellerstein, M. K. & Neese, R. A. Mass isotopomer distribution analysis at eight years: theoretical, analytic, and experimental considerations. *Am. J. Physiol.* **276**, E1146-1170 (1999).

40 Rockwood, A. L. & Haimi, P. Efficient calculation of accurate masses of isotopic peaks. *J. Am. Soc. Mass Spectrom.* **17**, 415-419, doi:10.1016/j.jasms.2005.12.001 (2006).

41 Pfaffl, M. W. A new mathematical model for relative quantification in real-time RT-PCR. *Nucleic Acids Res.* **29**, e45 (2001).

42 Chen, S. S., Sperling, E., Silverman, J. M., Davis, J. H. & Williamson, J. R. Measuring the dynamics of E. coli ribosome biogenesis using pulse-labeling and quantitative mass spectrometry. *Mol. Biosyst.* **8**, 3325-3334, doi:10.1039/c2mb25310k (2012).

43 Leick, V. & Andersen, S. B. Pools and Turnover Rates of Nuclear Ribosomal Rna in Tetrahymena-Pyriformis. *Eur. J. Biochem.* **14**, 460-&, doi:DOI 10.1111/j.1432-1033.1970.tb00311.x (1970).

44 Martin-Montalvo, A. & de Cabo, R. Mitochondrial metabolic reprogramming induced by calorie restriction. *Antioxid. Redox Signal.* **19**, 310-320, doi:10.1089/ars.2012.4866 (2013).

45 Zhao, N. *et al.* Low intracellular iron increases the stability of matriptase-2. *J. Biol. Chem.* **290**, 4432-4446, doi:10.1074/jbc.M114.611913 (2015).

46 Schilling, B. *et al.* Platform-independent and label-free quantitation of proteomic data using MS1 extracted ion chromatograms in skyline: application to protein acetylation and phosphorylation. *Mol. Cell. Proteomics* **11**, 202-214, doi:10.1074/mcp.M112.017707 (2012).

47 Ghaemmaghami, S. *et al.* Global analysis of protein expression in yeast. *Nature* **425**, 737-741, doi:10.1038/nature02046 (2003).

48 O'Brien, T. W. Properties of human mitochondrial ribosomes. *IUBMB life* **55**, 505-513, doi:10.1080/15216540310001626610 (2003).

49 Price, J., Guan, S., Burlingame, A., Prusiner, S. & Ghaemmaghami, S. Analysis of proteome dynamics in the mouse brain. *Proc. Natl. Acad. Sci. U. S. A.* **107**, 14508-14513, doi:10.1073/pnas.1006551107 (2010).

50 Khatter, H., Myasnikov, A. G., Natchiar, S. K. & Klaholz, B. P. Structure of the human 80S ribosome. *Nature* **520**, 640-645, doi:10.1038/nature14427 (2015).

51 Kondrashov, N. *et al.* Ribosome-mediated specificity in Hox mRNA translation and vertebrate tissue patterning. *Cell* **145**, 383-397, doi:10.1016/j.cell.2011.03.028 (2011).

52 Molin, S., Von Meyenburg, K., Maaloe, O., Hansen, M. T. & Pato, M. L. Control of ribosome synthesis in Escherichia coli: analysis of an energy source shift-down. *J. Bacteriol.* **131**, 7-17 (1977).

53 Fujii, K., Kitabatake, M., Sakata, T. & Ohno, M. 40S subunit dissociation and proteasome-dependent RNA degradation in nonfunctional 25S rRNA decay. *EMBO J.* **31**, 2579-2589, doi:10.1038/emboj.2012.85 (2012).

54 Williamson, R., Lanyon, G. & Paul, J. Preferential degradation of "messenger RNA" in reticulocytes by ribonuclease treatment and sonication of polysomes. *Nature* **223**, 628-630 (1969).

55 Nikolov, E. N., Dineva, B. B., Dabeva, M. D. & Nikolov, T. K. Turnover of ribosomal proteins in regenerating rat liver after partial hepatectomy. *Int. J. Biochem.* **19**, 159-163 (1987).

56 Bruss, M. D., Thompson, A. C., Aggarwal, I., Khambatta, C. F. & Hellerstein, M. K. The effects of physiological adaptations to calorie restriction on global cell proliferation rates. *Am. J. Physiol. Endocrinol. Metab.* **300**, E735-745, doi:10.1152/ajpendo.00661.2010 (2011).

57 Thompson, A. C. *et al.* Reduced in vivo hepatic proteome replacement rates but not cell proliferation rates predict maximum lifespan extension in mice. *Aging Cell* **15**, 118-127, doi:10.1111/acel.12414 (2016).

58 Sulima, S. O. *et al.* Eukaryotic rpL10 drives ribosomal rotation. *Nucleic Acids Res.* **42**, 2049-2063, doi:10.1093/nar/gkt1107 (2014).

4. Creation of Software Tools and Methods for Measurement of Kinetic Proteomics in Humans

4.1 Chapter Summary

Unlike the previous two chapters, this work has not been published. I have written this work in the form of a paper for consistency. The Future Directions section at the end of the chapter indicates how the work is proceeding to bring the software and data to publication quality. The basis of this work is modifications of the DeuteRater program required to analyze data from kinetic proteomic experiments using humans as subjects.

4.1.1 Authors in Order of Contribution

Bradley C. Naylor, Marcus Hadfield, David Parkinson, Austin Ahlstrom, Austin Hannemann, Paul Hafen, John Dallon, Rob Hyldahl, and John C. Price.

4.1.2 Contributions of Major Authors

I led making the adjustments of DeuteRater, led the human experiment, and prepared and analyzed the samples by mass spectrometry. Other authors assisted in the human experiment design, collecting samples from the subjects, wrote parts of the updated program, and providing insight into differential equations to model the data.

4.2 Abstract

Turnover for 1000's individual proteins can be measured simultaneously using kinetic proteomics methods, which monitor metabolic incorporation of an isotopic label over time. Metabolic labeling using ^2H_2O has several experimental advantages for kinetic proteomics and has been used in a variety of organisms from cells to humans. We previously published a software tool, DeuteRater, that facilitates analysis of ^2H_2O-based kinetic proteomics experiments. However, large animals such as humans often require experimental changes from metabolic labeling methods for small animals or cell culture. Although DeuteRater offered several improvements upon available software tools, it could not utilize data from these large animal experiments. Therefore, we have developed a new software tool called DeuteRater-H, which improves upon current calculation techniques for human kinetic proteomics and is an open source software tool to perform kinetic proteomic analysis on human subjects.

4.3 Introduction

Living cells are dynamic systems. They constantly create new proteins and destroy old proteins based on protein damage[4,5], circadian rhythms[6], changing environmental conditions[7], and normal maintenance[1,3,8-11]. The proteome scale study of protein turnover rates is called kinetic proteomics. Kinetic proteomics measurements of normal conditions can reveal interesting maintenance programs, such as differential replacement rates of proteins in a large protein complex[11]. Kinetic proteomic analysis of different biological conditions can yield information about how diseases affect cells, or even discover changes in protein turnover that can function as biomarkers[12,13]. Due to the amount of information provided by the technique, there is a need to provide easy-to-use, open source software for kinetic proteomics in clinical settings[2,3].

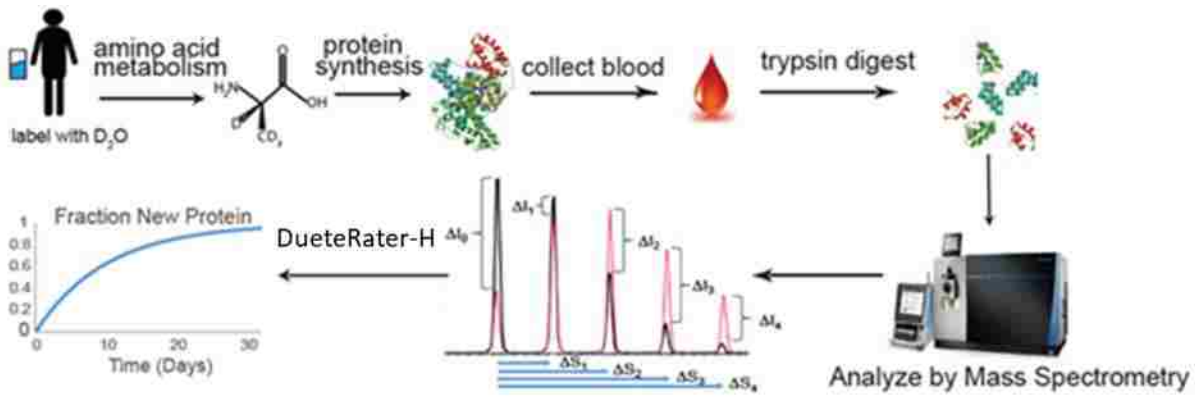

Figure 4-1: Experimental Workflow. Basic kinetic proteomics experimental workflow used in this study. Humans are provided with D2O, which is incorporated into amino acids and proteins. Biological samples can then be taken, and proteins digested into peptides. The peptides are analyzed by mass spectrometry and DeuteRater-H can then be used to turn the measured isotopic differences into a protein turnover rate.

Kinetic proteomics has several advantages that make it ideal for human studies. Important metabolic insights can be gained from proteins that are relatively abundant and easily accessible[10,12,13], and the workflow is relatively simple (Figure 4-1). A heavy isotope label, generally deuterium in the form of deuterated water (D_2O), is provided to the subject. The heavy label is incorporated into bio-synthesized molecules in the organism, such as non-essential amino acids. The labeled amino acids are used to synthesize proteins, resulting in new proteins containing extra heavy isotopes. The shift in signal intensity and mass spacing between the different isotopic populations of a peptide, called neutromers, is easily measurable by mass spectrometry and the percent protein replacement or turnover can be calculated[1,3].

The basic idea of kinetic proteomics has been around since the early 1990s[14,15] and deuterated water labeling has been used for proteomics since 2011[16]. However, while studies have been performed in humans, there are no open source software tools available to perform the analysis. Although we[1], and others[16,17] have made software and algorithms to analyze kinetic proteomics data in experimental animals, the requirements for working with human subjects

complicate the analysis. Most methods of heavy labeling other than D_2O require complete dietary control[8,18] or intra-venous infusion[19], which are often impractical in humans. However, rapidly changing D_2O enrichments can cause vertigo[20,21], therefore humans studies cannot follow the protocol of rapid enrichment used for animal studies. Low deuterium enrichments (below 1 molar percent excess) can be used to limit vertigo, but low isotopic enrichment reduces signal to noise, making turnover rates difficult to measure. To avoid the deuterium-dependent vertigo while still obtaining acceptable signal, a steadily increasing enrichment is administered over several days (Figure 4-2 A-B). This introduces a problem. The deuterium enrichment is used to determine the maximum theoretical change in the neutromer peaks of each peptide. Knowing the maximum theoretical change allows the experimental change to be expressed as a percentage (Figure 4-2 C). If the enrichment is changing, the calculations become much more complex because the maximum theoretical change in the neutromer peaks shift with each additional protein replaced in the population (Figure 4-2 D).

In order to handle this problem, it is necessary to use a differential equation to combine the equation for fitting the subject's deuterium enrichment with the equation for the change in isotopic abundance or spacing from the unlabeled baseline (Figure 4-3). Previously the equations were limited to a rise to plateau enrichment curve and only using the mono-isotopic peak for rate determination[2,3]. Now we need to allow for the increased complexity in enrichment and isotopic measurement.

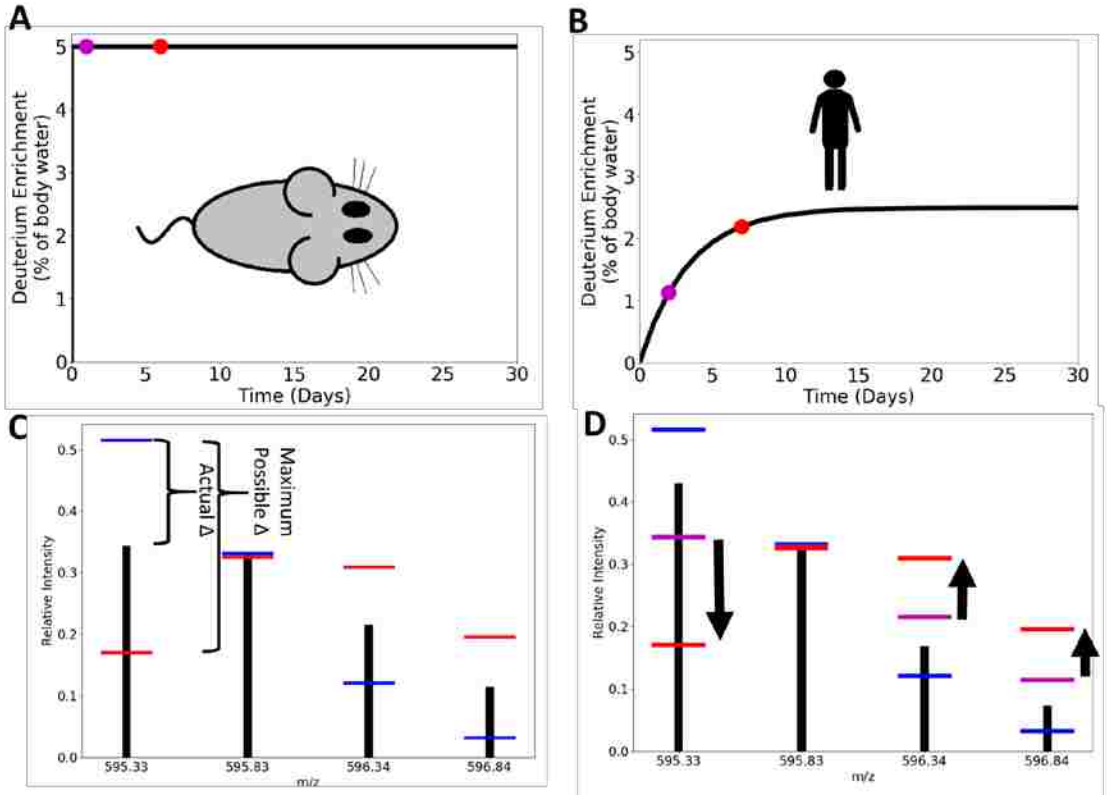

Figure 4-2 Differences in Analysis between Animal Models and Humans: In a small animal, such as a mouse, a Constant Enrichment model can be used with a greater percent of body water being replaced with deuterium (Panel A). A large intraperitoneal bolus injection is used to bring the animal instantly to the desired level of deuterium, where they are maintained for the duration of the experiment. In humans, due to issues of vertigo from deuterium and the impracticality of large intraperitoneal injections in human subjects, the deuterium label is applied over time, creating an increasing enrichment, generally in the form of a rise to plateau kinetic (Panel B). The enriched percent of body water is also lower in a human due to the larger amount of water in a human. The calculation for Fraction new protein for a constant enrichment experiment is relatively simple (Panel C). The distance between the isotopic height at no labeling (blue line) to the isotopic height measured at a certain time (black lines) is compared to the distance between the isotopic height at no labeling and the isotopic height when all proteins are labeled (red lines). Since all points are constant (red and purple points in panel A), this calculation is the same at all time points, save for the experimentally measured component. If the enrichment is changing, the enrichment at an earlier time is less than the enrichment at a later time (purple and red dots on Panel B), the enrichment for proteins produced at those times is different (purple and red lines on panel D). Thus, the black lines in panel D are a combination not just of unlabeled and labeled populations, but unlabeled and many different labeled populations. Since only the average of all these populations is observed in the mass spectrometer, a method of deconvolution is necessary for the data to be interpreted.

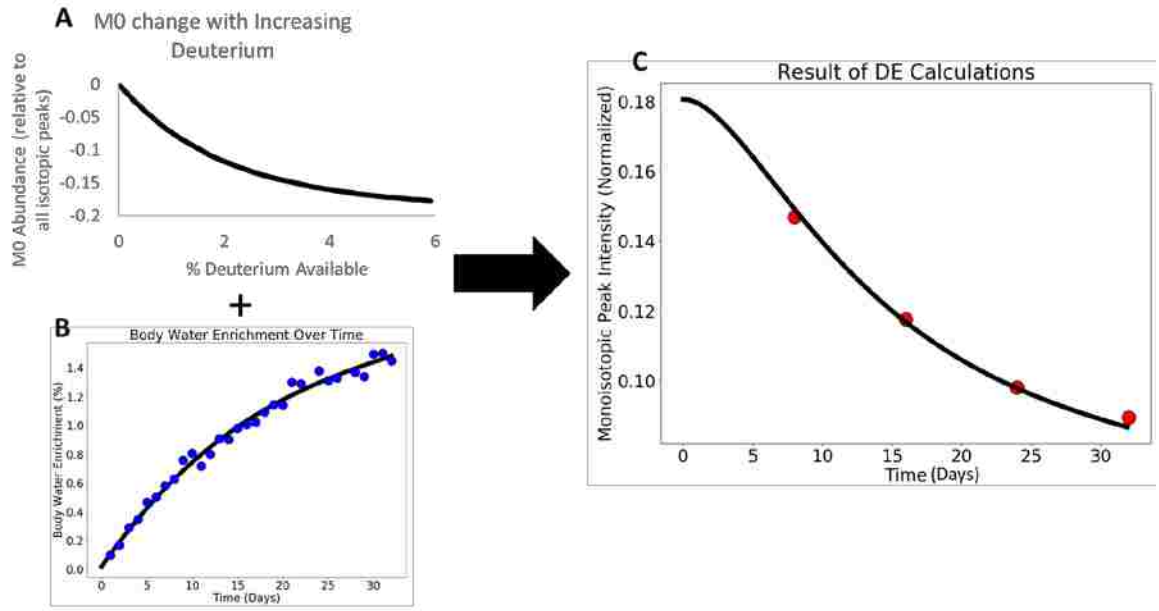

D

$$Fractional\ Enrichment = enrichment\ function(t)$$

$$\Delta\ Isotope\ = Isotope\ Function\ (Fractional\ Enrichment)$$

$$dSignal/dt = (baseline + \Delta\ Isotope\ - Signal) * k$$

Figure 4-3 Differential Equation Analysis. This represents the basic principle of the analysis. Dots are actual data, and the black lines are lines fit to the data, or theoretical models. Panel A shows a theoretical model of abundance of M0 changes with increasing Deuterium available for the synthesis of this protein. 0 represents M0 with no extra deuterium. Panel B shows how the amount of deuterium present in the body changes over time. The equations of Panel A and Panel B are combined in such a way that the resulting equation's only unknown variable is the protein turnover rate. The actual changes in M0 are fit to this equation in Panel C, and the turnover rate can be calculated from a variable in the fit line. The equation is represented in Panel D. The amount of body water enrichment is calculated from the time based on whatever function is used to fit the water in panel B (first equation). This enrichment is then used to determine the maximal change in the neutromer peak (middle equation). This can be m0 as in Panel A, though any neutromer abundance or spacing model will work. The change in Signal (abundance or spacing) is then represented by the lowest equation, with the k in the equation represents the peptide turnover rate (bottom equation). This can be solved as an ordinary differential equation in a least squares curve fit to solve for k.

In this study, we build upon DeuteRater[1], our data analysis tool for performing kinetic proteomics on the simpler labeling scheme, and previous software that uses differential equations for human kinetic proteomics[2] to create DeuteRater-H, an open source software tool to perform human kinetic proteomic calculations. We show that even in these cases where isotopic

enrichment is changing neutromer intensity and spacing can be used together to monitor isotope incorporation and that by incorporating the information from these peptide specific measurements for each peptide we improve signal to noise in the calculation of protein turnover kinetics.

4.4 Methods

4.4.1 Metabolic Labeling and Sample Collection

All experiments were performed under the approval of the Institutional Review Board of Brigham Young University. Three males and three females above the age of 20 years were recruited. Subjects were randomly assigned numbers from 1-6. Subjects had no serious health conditions and were not taking regular medication known to cause biases in blood biochemistry, such as blood thinners. The study lasted for 32 days, divided into 8 day pieces. Each day subjects consumed 3 doses (morning, noon, and night) of 99.8% deuterated water. The deuterated water volume was increased following this schedule: 22 mL per dose for the first 24 doses (Day 1-8), 26 mL per dose for the next 24 doses (Days 9-16), 30 mL per dose for the next 24 doses (Day 9-24), and 34 mL per dose for the final 24 doses (Day 25-32). Saliva was collected daily to allow for measurement of the body water deuterium enrichment. Every 8 days, subjects were provided with enough doses of deuterated water and saliva sampling swabs (salivettes) for 3 doses of deuterated water per day and one salivette per day. Subjects kept a diary to record compliance. Subjects were generally compliant with one or two missed doses occurring occasionally.

At days 0, 8, 16, 24 and 32, approximately 20 mLs of blood were collected from each subject. On days 16 and 32 one muscle biopsy from each of the subjects' legs were collected.

Biopsies removed approximately 50 mg of tissue per leg. Muscle biopsies were performed by Dr. Robert Hyldahl at Brigham Young University.

4.4.2 Deviations from the Schedule

Aside from minor non-compliance with a salivette, or deuterium dose, or variations in amount tissue collected, there were some significant changes to the protocol described above. Subject 5 started the experiment on schedule but the first blood draw occurred on the day after deuterium dosing started. Subject 1 had a similar situation, though the first blood draw was 3 days after deuterium was provided. Both of those changes presented minimal issues. More serious was that Subject 2 started a day after the other subjects, and had an infection at a biopsy site after the first muscle biopsy. We immediately excluded Subject 2 from further participation after discovery of the infection.

4.4.3 Measurement of Deuterium Enrichment

Saliva was collected by the subjects and stored frozen until given to researchers. Saliva was stored by researchers at -20°C until deuterium enrichment could be measured. For processing, 100 µL aliquots, or less if there were less than 100 µL of saliva, were distilled overnight at 95° C to purify the water in the sample. 5 µL aliquots of saliva distillates were diluted 1:300 and deuterium molar percent excess (MPE) was measured. MPE was measured in the samples against an accompanying standard curve using a cavity ring-down water isotope analyzer (Los Gatos Research [LGR], Los Gatos, CA, USA) according to the published method[22]. Serum was also distilled using the same method (with 50 µL instead of 100) for some subjects.

4.4.4 Preparation of Biological Samples

After collection, blood was stored on ice until it could be separated into its components. First, blood was centrifuged at 200 x g for 20 minutes at 4°C. Serum was removed from red blood cells and the serum was further centrifuged at 2000 x g for 10 minutes at 4°C. Serum was removed from buffy coat pellet. The pellet was re-suspended in Phosphate Buffered Saline (PBS), moved to a storage vial and centrifuged again using the same centrifuge settings. PBS was decanted. Red blood cells, serum, and buffy coat were stored at -80°C until they could be processed further. Muscle biopsies were immediately frozen in dry ice. Samples were stored at -0°C.

4.4.5 Preparation for Mass Spectrometry Analysis

Serum protein concentrations were measured using a bicinchoninic acid (BCA) protein assay (Thermo Fisher). 50 µg of each sample from each subject was placed on 30 kDa mass cutoff Amicon Ultracel centrifugal filters. 100 µL of guanidine (6 M, 100 mM Tris-HCl pH 8.5) was added to the sample and centrifuged at 14,000g for 15 minutes. Another wash with guanidine (same volume and centrifuge settings) was performed. Flow-through was discarded. 100 µL of guanidine was added to the filter, and was brought to 10 mM dithiothreitol. The filter was placed in a sand bath at 60 °C for 60 minutes. After 5 minutes of cooling, the sample was brought to 20 mM iodoacetamide. Samples were incubated in the dark for 60 minutes. Samples were centrifuged at 14,000g for 15 minutes. 200 µL Ammonium Bicarbonate (ABC, 25 mM, pH 8.5) was added to the filters, which were spun at 14,000g for 15 minutes. After a second ABC wash (same volume and centrifuge settings), ABC was added to the filter until the volume was 300 µL. The collection vial was replaced with a clean vial. 1 µg Trypsin Pierce MS grade was added to each sample, which were incubated at 37°C overnight. Samples were centrifuged at

14,000 g for 30 minutes. 100 µL of ABC were added to the filter, which was centrifuged again for 30 minutes at 14,000 g. Filters were discarded and the filtrate was dried using a SpeedVac (Sorval) vacuum centrifuge. The dried samples were stored at 4°C until use.

4.4.6 Mass Spectrometry Analysis

All experimental subjects provided five blood samples, all of which were analyzed with a Fusion Lumos Tribrid (Orbitrap) mass spectrometer from ThermoFisher Scientific. Samples were resuspended in 0.1% Formic Acid (Pierce LC-MS grade) in H_2O (Optima grade Thermo Fischer). Tryptic peptides were separated using a reverse phase C18 column (Acclaim PepMap™ 100) and a Thermo Easy-Spray source. Mobile phase for the Liquid Chromatography was 0.1% Formic Acid in H_2O (Buffer A) and 0.1% Formic Acid in 80% Acetonitrile (Optima grade Thermo Fischer) with 20% H_2O (Buffer B) on an Easy-nLC 1200 HPLC system. Samples were eluted using a gradient of 5% B to 22% B over 85 minutes, 22% to 32% B over 15 minutes, with a wash of 32% to 95% B over 10 minutes, which was held at 95% B for 10 minutes. Sample loading and equilibration were performed using the HPLC's built in methods. MS only runs were performed using 2400 V in the ion source 60000 Resolution with a scan range of 375-1700 m/z, 30% RF Lens, Quadrupole Isolation, 8 *10^5 AGC Target and a maximum injection time of 50 ms. MS/MS scans were performed using same settings as MS only scans with 3 seconds allowed per MS/MS after each MS scan using the following filters: peptide monoisotopic peak determination, an intensity threshold of 5*10^3, only fragmenting charge states +2 to +6, a dynamic exclusion that excluded a peak after being chosen once within 60 seconds, with an error tolerance of 10 ppm high and low, and isotopes excluded. The fragmentation scan used an isolation window of 1.6 m/z, CID fragmentation with an energy of 30%, detection in the linear ion trap in Rapid scan mode with a AGC target of 1*10^4, a

maximum injection time of 35 milliseconds and used the "Inject Ions for All Available Parallelizable Time" option.

Data is available upon request.

4.4.7 Identification of Peptides and Using DeuteRater-H

Peptides were identified from MS/MS spectra of early time point samples using the software platform PEAKS 8[23]. PEAKS settings were as follows: mass only correct precursor refinement, trypsin as the digestion enzyme, 3 missed cleavages and 1 non-specific cleavage allowed. Carbamidomethylation was set as a fixed modification and pyro-glutamic acid from Q and Oxidation of M were allowed variable modifications with 3 variable modifications allowed per peptide. Identification database was SwissProt validated database downloaded August 2017, restricted to *Homo sapiens* protein entries. PEAKS PTM, which searches for PTMs not specified in the search, and SPIDER, which searches for point mutations, were also examined. Data from the Orbitrap instrument was analyzed with settings specifying CID fragmentation, precursor data was collected in an Orbitrap with an allowed error tolerance of 4.0 ppms, and fragmentation data was collected in a linear ion trap with an allowed error of 0.2 Daltons. QToF data was analyzed with settings specifying CID fragmentation, precursor data was collected in a ToF with an error tolerance of 10.0 ppms , and fragmentation data was collected in a ToF with an allowed error of 0.05 daltons.

Those identifications under a 1% False Discovery Rate cutoff were exported and used to create a peptide accurate mass and retention time database for DeuteRater. All post-translational modifications except carbamidomethylation, pyroglutamic acid from Q and oxidation of M were discarded. High confidence peptide identifications that incorporated point mutations from SPIDER were kept. Data was then analyzed by DeuteRater-H. Details of DeuteRater-H

calculation are in the Results section under “Changes made to DeuteRater for Human Calculations”.

4.4.8 Filtering Turnover Rate Results

All protein turnover rates were calculated by averaging the rates of peptide measurements (abundance and spacing of all neutromers) from peptides belonging to that protein that had rate fits with an R^2 value greater than or equal to 0.9 and a coefficient of variance (standard deviation / rate value) (cv) of 0.5 or less. Several filters were applied to protein rates: to ensure that these average rates were within the reliable range defined by our sampling, all rates below 0 or above 2 (fractional turnover per day) were removed, all protein rates coming from a single measurement were removed. The cv filter was designed to ensure that when filtering by error, the measurement was not biased against faster rates whose 95% confidence intervals have higher numerical values even if the relative error is quite small.

4.4.9 Comparison of Kinetic Rates to Kinetic Rates from Previous Studies

For comparison between subjects, all proteins present in all 6 subjects that made it through the filter described in “Filtering Turnover Rate Results” were transformed (log base 2) and subjected to a Tukey Kramer comparison of multiple means by the JMP 12 statistical software package.

For comparison between our data and published data, we averaged all proteins that made it through the filter described in “Filtering Turnover Rate Results” were averaged across all experimental subjects. Rates reported from the literature were averaged across all subjects in the study they appeared in and those rates not between 0 and 2 (fractional turnover per day) were removed.

4.5 Results

4.5.1 Changes made to DeuteRater for Human Calculations

Starting from the framework of DeuteRater[1], we made two major changes. First, we required the user to provide data on heavy isotope enrichment at various time-points for each experimental subject. After collecting this data, we created a fit line for that data with an equation chosen by the user (rise to plateau by default). Second, differential rate calculations (Figure 4-3) were performed on a peptide by peptide basis, unlike in DeuteRater. Rates with an R^2 of greater than 0.9 and a coefficient of variance (cv) (calculated as standard deviation / rate value) of less than 0.5 were kept (by default, filters can be altered), other rates were discarded. Rates for peptides belonging to the same protein were weighted by cv and averaged together to obtain a turnover rate for the protein. Peptides and proteins were calculated independently for each experimental subject.

4.5.2 Improved Flexibility of DeuteRater-H

In previous studies of human kinetic proteomics, a rise to plateau model has been used for the deuterium enrichment of experimental subjects[2,3]. This was a reasonable way to start the method as it most closely models the small animal calculations, and it is experimentally easier, requiring the experimental subjects to consume the same volume of deuterium on the same schedule for the entire experiment. Since DeuteRater-H uses a differential equation and should be able to use any shape of enrichment profile (Figure 4-3 D), we provided subjects with increasing amount of deuterium throughout the experiment as detailed under "Metabolic Labeling and Sample Collection" in the Methods section. We did this to provide flexibility to the calculations, and to test whether the increasing amount of deuterium would allow measurements of fast turnover proteins at late time points to be useful in calculating the turnover

rate, as observed previously[3]. The increasing deuterium amounts do not cause any noticeable negative results to the subjects or the data analysis.

Previous work also focused on the abundance change of the mono-isotopic peak[2]. The mono-isotopic peak is often the best peak for kinetic calculations because its intensity change is usually relatively large and is easily predictable. However, we established with DeuteRater[1] that multiple changes in the isotope pattern, including the spacing between neutromers, can be used to improve the quality of the kinetic calculations. In DeuteRater-H we have demonstrated that all measurements can also be utilized in a situation where isotopic enrichment is changing over time (Figure 4-4). However, not all measurements are useful for every peptide. Some metrics, especially spacing, have low signal to noise. As a result, DeuteRater-H applies filters to the peptide rate calculated from each metric. Only those calculated curves with an R^2 greater than 0.9, and a coefficient of variation less than 0.5 were rolled into protein rates.

4.5.3 Comparison of Experimental Subjects to Each Other

Experimental subjects were compared to each other to ensure that analysis of healthy subjects yields similar results. If the subjects were vastly different from each other, it could indicate a problem with the software performing the calculations. A Tukey-Kramer multiple comparison test was used to compare all turnover rates from all proteins in the filtered data that were present in all 6 experimental subjects with at least two peptide calculations, either two or more peptides for a single protein or two or more abundance or spacing metrics passing the filters for a single peptide (Table 4-1). Turnover rates underwent a Logarithmic transformation (base 2) prior to statistical testing to create a normal distribution. Turnover rates represented in Table 4-1 are not transformed. Logarithmic transformation of data and the Tukey-Kramer test, which compares all possible combinations of subjects, were performed using the JMP 12

statistical package. The result showed four significant differences, between Subject 2 and Subject 1, Subject 2 and Subject 4, Subject 2 and Subject 5, and Subject 2 and Subject 6 with p-values of .0390, .0452, .0473, and .0476 respectively.

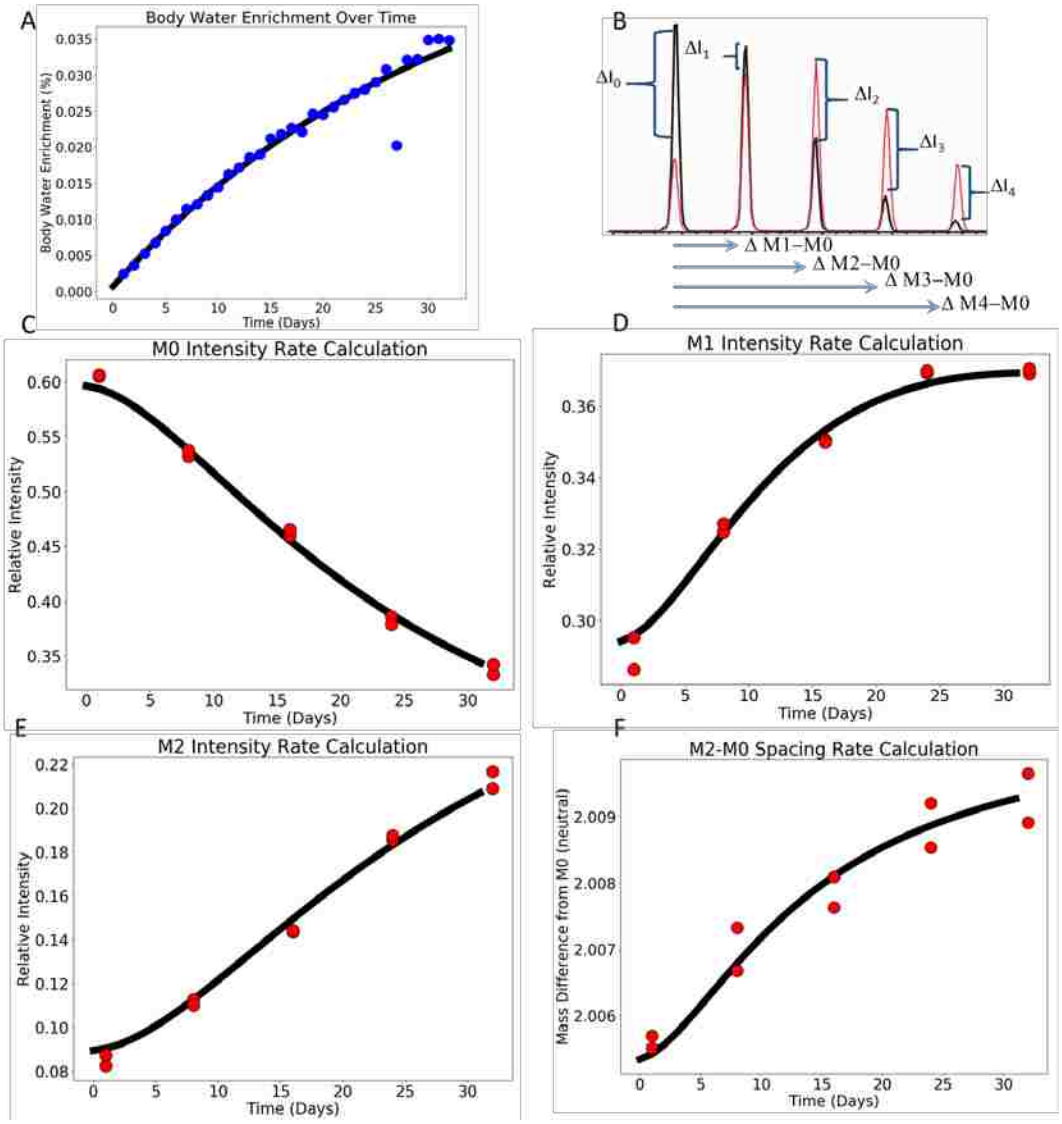

Figure 4-4 Improved Calculations using DeuteRater-H. Panel A shows a deuterium enrichment curve for Subject 5 in this study. Panel B shows the metrics used in fitting, the ΔI values indicating abundance changes, and the Δ M –M0 measurements indicating differences in spacing which were discussed in depth in Figure 4-3 and our previous work. DeuteRater-H allows calculation of human turnover rates by combining multiple metrics including the traditional M0 peak (no heavy isotopes panel C), other isotopic peaks (D-E) and the spacing between peaks (F). Panels C-F are for peptide ADLSGITGAR from subject 5. All time-points have two measurements at each time point (representing charge states +2 and +3)

All significant differences are between Subject 2 and other subjects. Subject 2 had health problems due to a leg infection as a result of the muscle biopsy, and had a drop in enrichment around week 3 due to strenuous exercise. Therefore, the significantly decreased rates in for Subject 2 may be due to exertion changing water consumption and reducing deuterium enrichment, or may be some biological effect from the exertion or infection.

Table 4-1 Data from Proteins in All Six Experimental Subjects. This table shows the accession numbers and turnover rates of proteins observed in all 6 subjects with more than one measurement (peptide, abundance measurement, or spacing measurement). The turnover units are fractional turnover per day with error being 2 standard deviations to approximate a 95% confidence interval.

Protein Accession Number	Protein Name	S1 Rate	S2 Rate	S3 Rate	S4 Rate	S5 Rate	S6 Rate
P0DOY3	Immunoglobulin lambda constant 3	0.04 ± 0.002	0.03 ± 0.004	0.03 ± 0.027	0.09 ± 0.044	0.04 ± 0.065	0.04 ± 0.006
P0DOX8	Immunoglobulin lambda-1 light chain	0.05 ± 0.043	0.1 ± 0.06	0.03 ± 0.019	0.07 ± 0.048	0.02 ± 0.004	0.04 ± 0.013
A0A075B6P5	Immunoglobulin kappa variable 2-28	0.13 ± 0.107	0.03 ± 0.03	0.03 ± 0.008	0.06 ± 0.051	0.01 ± 0.005	0.04 ± 0.015
P02746	Complement C1q subcomponent subunit B	0.13 ± 0.046	0.15 ± 0.085	0.1 ± 0.163	0.23 ± 0.193	0.18 ± 0.167	0.2 ± 0.017
P35542	Serum amyloid A-4 protein	0.12 ± 0.026	0.11 ± 0.189	0.16 ± 0.006	0.07 ± 0.223	0.14 ± 0.122	0.16 ± 0.023
P01619	Immunoglobulin kappa variable 3-20	0.08 ± 0.095	0.08 ± 0.028	0.04 ± 0.142	0.06 ± 0.072	0.02 ± 0.03	0.04 ± 0.023
P0DOX7	Immunoglobulin kappa light chain	0.08 ± 0.088	0.03 ± 0.047	0.03 ± 0.115	0.04 ± 0.041	0.02 ± 0.107	0.04 ± 0.027
P01871	Immunoglobulin heavy constant mu	0.15 ± 0.113	0.08 ± 0.039	0.05 ± 0.048	0.07 ± 0.051	0.06 ± 0.072	0.05 ± 0.027
A0A0C4DH31	Immunoglobulin heavy variable 1-18	0.12 ± 0.062	0.03 ± 0.021	0.03 ± 0.025	0.08 ± 0.044	0.05 ± 0.141	0.03 ± 0.036
O14791	Apolipoprotein L1	0.13 ± 0.021	0.08 ± 0.066	0.1 ± 0.071	0.15 ± 0.124	0.14 ± 0.136	0.1 ± 0.036

Protein Accession Number	Protein Name	S1 Rate	S2 Rate	S3 Rate	S4 Rate	S5 Rate	S6 Rate
P0DOX2	Immunoglobulin alpha-2 heavy chain	0.11 ± 0.257	0.07 ± 0.046	0.08 ± 0.126	0.09 ± 0.068	0.03 ± 0.062	0.05 ± 0.039
P00739	Haptoglobin-related protein	0.14 ± 0.031	0.07 ± 0.012	0.08 ± 0.014	0.1 ± 0.057	0.1 ± 0.029	0.1 ± 0.039
P05090	Apolipoprotein D	0.1 ± 0.043	0.04 ± 0.004	0.09 ± 0.078	0.09 ± 0.057	0.11 ± 0.155	0.09 ± 0.043
P02768	Serum albumin	0.04 ± 0.078	0.03 ± 0.026	0.03 ± 0.045	0.07 ± 0.049	0.03 ± 0.049	0.03 ± 0.048
P01701	Immunoglobulin lambda variable 1-51	0.03 ± 0.002	0.03 ± 0.014	0.04 ± 0.019	0.07 ± 0.088	0.03 ± 0.002	0.06 ± 0.05
P01023	Alpha-2-macroglobulin	0.07 ± 0.05	0.07 ± 0.025	0.05 ± 0.084	0.15 ± 0.063	0.06 ± 0.067	0.06 ± 0.051
P01876	Immunoglobulin heavy constant alpha 1	0.06 ± 0.062	0.05 ± 0.044	0.08 ± 0.154	0.21 ± 0.092	0.08 ± 0.086	0.08 ± 0.054
P0DOX5	Immunoglobulin gamma-1 heavy chain	0.1 ± 0.073	0.03 ± 0.025	0.03 ± 0.08	0.07 ± 0.052	0.02 ± 0.045	0.03 ± 0.056
P02790	Hemopexin	0.11 ± 0.203	0.08 ± 0.034	0.07 ± 0.114	0.21 ± 0.117	0.07 ± 0.073	0.07 ± 0.062
P02787	Serotransferrin	0.1 ± 0.074	0.09 ± 0.088	0.08 ± 0.098	0.13 ± 0.101	0.09 ± 0.078	0.07 ± 0.073
P08185	Corticosteroid-binding globulin	0.1 ± 0.052	0.06 ± 0.039	0.08 ± 0.096	0.07 ± 0.162	0.15 ± 0.102	0.08 ± 0.076
P43652	Afamin	0.12 ± 0.085	0.07 ± 0.115	0.15 ± 0.29	0.11 ± 0.146	0.16 ± 0.108	0.15 ± 0.084
P00450	Ceruloplasmin	0.13 ± 0.141	0.07 ± 0.108	0.11 ± 0.117	0.11 ± 0.166	0.12 ± 0.084	0.12 ± 0.086
P02652	Apolipoprotein A-II	0.2 ± 0.059	0.12 ± 0.16	0.16 ± 0.205	0.22 ± 0.239	0.17 ± 0.252	0.14 ± 0.09
P27169	Serum paraoxonase/arylesterase 1	0.29 ± 0.143	0.1 ± 0.061	0.09 ± 0.065	0.19 ± 0.161	0.15 ± 0.112	0.1 ± 0.099

Protein Accession Number	Protein Name	S1 Rate	S2 Rate	S3 Rate	S4 Rate	S5 Rate	S6 Rate
P02763	Alpha-1-acid glycoprotein 1	0.31 ± 0.25	0.12 ± 0.089	0.13 ± 0.165	0.38 ± 0.223	0.14 ± 0.125	0.14 ± 0.101
P01009	Alpha-1-antitrypsin	0.11 ± 0.148	0.07 ± 0.076	0.13 ± 0.162	0.12 ± 0.145	0.15 ± 0.13	0.13 ± 0.121
P02766	Transthyretin	0.09 ± 0.031	0.2 ± 0.273	0.2 ± 0.255	0.18 ± 0.331	0.3 ± 0.351	0.27 ± 0.122
P02765	Alpha-2-HS-glycoprotein	0.09 ± 0.134	0.11 ± 0.062	0.14 ± 0.135	0.05 ± 0.178	0.17 ± 0.163	0.15 ± 0.13
P02647	Apolipoprotein A-I	0.14 ± 0.071	0.07 ± 0.057	0.13 ± 0.102	0.13 ± 0.196	0.17 ± 0.112	0.12 ± 0.133
P02760	Protein AMBP	0.12 ± 0.239	0.08 ± 0.18	0.15 ± 0.198	0.32 ± 0.279	0.17 ± 0.285	0.26 ± 0.134
P01011	Alpha-1-antichymotrypsin	0.18 ± 0.185	0.09 ± 0.198	0.16 ± 0.281	0.19 ± 0.283	0.16 ± 0.165	0.11 ± 0.136
P15169	Carboxypeptidase N catalytic chain	0.2 ± 0.145	0.08 ± 0.013	0.11 ± 0.077	0.17 ± 0.116	0.14 ± 0.111	0.16 ± 0.139
P06396	Gelsolin	0.12 ± 0.188	0.19 ± 0.138	0.13 ± 0.182	0.15 ± 0.259	0.17 ± 0.162	0.14 ± 0.147
P00734	Prothrombin	0.23 ± 0.216	0.13 ± 0.136	0.18 ± 0.199	0.18 ± 0.16	0.24 ± 0.159	0.18 ± 0.15
P02679	Fibrinogen gamma chain	0.17 ± 0.237	0.08 ± 0.185	0.13 ± 0.134	0.21 ± 0.178	0.16 ± 0.148	0.18 ± 0.156
P19827	Inter-alpha-trypsin inhibitor heavy chain H1	0.16 ± 0.169	0.17 ± 0.157	0.2 ± 0.237	0.21 ± 0.237	0.22 ± 0.193	0.23 ± 0.156
P02675	Fibrinogen beta chain	0.15 ± 0.182	0.08 ± 0.089	1.34 ± 0.218	0.45 ± 0.175	0.18 ± 0.175	0.19 ± 0.158
P06727	Apolipoprotein A-IV	0.1 ± 0.13	0.16 ± 0.25	0.11 ± 0.082	0.1 ± 0.13	0.17 ± 0.129	0.12 ± 0.169
P04003	C4b-binding protein alpha chain	0.13 ± 0.286	0.08 ± 0.09	0.13 ± 0.135	0.14 ± 0.162	0.19 ± 0.14	0.13 ± 0.178

Protein Accession Number	Protein Name	S1 Rate	S2 Rate	S3 Rate	S4 Rate	S5 Rate	S6 Rate
P01042	Kininogen-1	0.17 ± 0.248	0.14 ± 0.123	0.18 ± 0.181	0.26 ± 0.235	0.21 ± 0.2	0.17 ± 0.181
P02748	Complement component C9	0.11 ± 0.141	0.38 ± 0.429	0.15 ± 0.14	0.19 ± 0.147	0.3 ± 0.296	0.25 ± 0.184
P08603	Complement factor H	0.13 ± 0.112	0.08 ± 0.079	0.13 ± 0.146	0.3 ± 0.142	0.17 ± 0.147	0.14 ± 0.185
P10643	Complement component C7	0.12 ± 0.095	0.09 ± 0.038	0.15 ± 0.134	0.15 ± 0.092	0.1 ± 0.225	0.14 ± 0.187
P04217	Alpha-1B-glycoprotein	0.25 ± 0.246	0.17 ± 0.149	0.16 ± 0.161	0.23 ± 0.282	0.23 ± 0.176	0.2 ± 0.189
P08697	Alpha-2-antiplasmin	0.21 ± 0.351	0.17 ± 0.331	0.22 ± 0.432	0.14 ± 0.19	0.27 ± 0.368	0.31 ± 0.192
P01024	Complement C3	0.15 ± 0.257	0.17 ± 0.21	0.2 ± 0.247	0.22 ± 0.238	0.23 ± 0.193	0.2 ± 0.199
P02774	Vitamin D-binding protein	0.16 ± 0.246	0.38 ± 0.246	0.25 ± 0.308	0.05 ± 0.277	0.24 ± 0.243	0.24 ± 0.222
P36955	Pigment epithelium-derived factor	0.14 ± 0.087	0.14 ± 0.06	0.19 ± 0.258	0.09 ± 0.153	0.37 ± 0.169	0.22 ± 0.235
P01019	Angiotensinogen	0.08 ± 0.154	0.31 ± 0.247	0.21 ± 0.523	0.23 ± 0.258	0.27 ± 0.207	0.23 ± 0.24
Q14624	Inter-alpha-trypsin inhibitor heavy chain H4	0.18 ± 0.166	0.33 ± 0.238	0.22 ± 0.332	0.2 ± 0.205	0.28 ± 0.218	0.22 ± 0.258
P01008	Antithrombin-III	0.33 ± 0.288	0.18 ± 0.158	0.21 ± 0.301	0.18 ± 0.299	0.27 ± 0.273	0.22 ± 0.268
P04196	Histidine-rich glycoprotein	0.38 ± 0.271	0.3 ± 0.234	0.21 ± 0.369	0.22 ± 0.262	0.23 ± 0.213	0.35 ± 0.282
P02671	Fibrinogen alpha chain	0.16 ± 0.245	0.09 ± 0.172	0.17 ± 0.217	0.23 ± 0.239	0.21 ± 0.212	0.45 ± 0.287
P00747	Plasminogen	0.46 ± 0.325	0.38 ± 0.214	0.23 ± 0.291	0.13 ± 0.265	0.26 ± 0.273	0.24 ± 0.289

Protein Accession Number	Protein Name	S1 Rate	S2 Rate	S3 Rate	S4 Rate	S5 Rate	S6 Rate
P01031	Complement C5	0.12 ± 0.115	0.08 ± 0.031	0.18 ± 0.229	0.08 ± 0.176	0.21 ± 0.2	0.23 ± 0.297
P05543	Thyroxine-binding globulin	0.2 ± 0.241	0.06 ± 0.043	0.13 ± 0.082	0.23 ± 0.136	0.16 ± 0.119	0.14 ± 0.297
P06312	Immunoglobulin kappa variable 4-1	0.6 ± 0.347	0.03 ± 0.011	0.16 ± 0.49	0.04 ± 0.064	0.03 ± 0.008	0.07 ± 0.305
P19823	Inter-alpha-trypsin inhibitor heavy chain H2	0.12 ± 0.23	0.29 ± 0.211	0.21 ± 0.236	0.18 ± 0.229	0.26 ± 0.21	0.21 ± 0.308
P05155	Plasma protease C1 inhibitor	0.15 ± 0.047	0.07 ± 0.011	0.3 ± 0.463	0.1 ± 0.035	0.36 ± 0.36	0.27 ± 0.327
P00738	Haptoglobin	0.14 ± 0.27	0.07 ± 0.244	0.34 ± 0.469	0.14 ± 0.162	0.27 ± 0.239	0.31 ± 0.334
P02751	Fibronectin	0.19 ± 0.086	0.1 ± 0.331	0.28 ± 0.352	0.2 ± 0.242	0.23 ± 0.292	0.32 ± 0.334
P00751	Complement factor B	0.24 ± 0.239	0.06 ± 0.296	0.25 ± 0.313	0.16 ± 0.218	0.26 ± 0.309	0.27 ± 0.335
P04004	Vitronectin	0.37 ± 0.264	0.13 ± 0.201	0.27 ± 0.297	0.27 ± 0.26	0.32 ± 0.295	0.3 ± 0.375
P04114	Apolipoprotein B-100	0.08 ± 0.285	0.17 ± 0.311	0.22 ± 0.286	0.1 ± 0.226	0.24 ± 0.321	0.25 ± 0.387
P02749	Beta-2-glycoprotein 1	0.15 ± 0.24	0.08 ± 0.22	0.42 ± 0.547	0.23 ± 0.288	0.46 ± 0.382	0.39 ± 0.393
P07225	Vitamin K-dependent protein S	0.12 ± 0.047	0.11 ± 0.069	0.14 ± 0.135	0.14 ± 0.253	0.14 ± 0.149	0.14 ± 0.401
P13671	Complement component C6	0.46 ± 0.061	0.15 ± 0.169	0.2 ± 0.509	0.15 ± 0.163	0.28 ± 0.275	0.26 ± 0.407
P10909	Clusterin	0.38 ± 0.229	0.4 ± 0.28	0.24 ± 0.301	0.21 ± 0.322	0.39 ± 0.617	0.29 ± 0.441
P02649	Apolipoprotein E	0.19 ± 0.279	0.22 ± 0.307	0.39 ± 0.506	0.38 ± 0.306	0.57 ± 0.508	0.41 ± 0.445

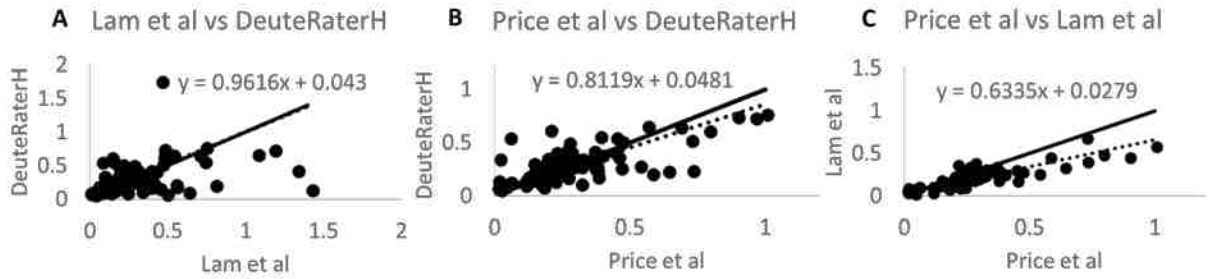

Figure 4-5 Comparison of DeuteRater-H to Previous Human Kinetic Proteomics Experiments. This figure compares turnover rates of proteins observed in humans. Points are turnover rates of the same protein in the different studies. The solid black lines represent the unity line, where all points should be assuming no error. The dotted black line and equations represent the best fit line of the comparison. Panel A shows a comparison to Lam et al upon which we based our differential calculations[1-4], while panel B shows a comparison to a study that used SAAM II compartmental models[5,6]. Panel C shows comparison of Price et al and Lam et al to determine the expected amount of error due to biological noise. Fits are Passing-Bablok regressions to prevent problems due to outliers.

4.5.4 Comparison to Previous Work

The final test of new software is validation of turnover rates using previously published datasets. Since all previous studies and the current study contained multiple non-genetically identical subjects, we averaged all calculated protein rates across all subjects for which it was observed in both our dataset, previous explicit differential calculations[2] or SAAM II compartmental models[3]. All data points used in this comparison are shown in Table 4-2. We then compared all proteins calculated by the current study to the other studies (Figure 4-5). Agreement is sufficiently good to justify publication.

Table 4-2 Data points used in Figure 4-5. If a cell contains "N.O." it was not observed in that study, and so not graphed. Values are rates average rates between all samples ± std. dev. A std. dev. of 0 indicates a rate was only observed for one subject in that study, so no std. dev. could be calculated.

Protein Accession Number	Protein Number	DeuteRater-H Rate	Lam et al[2] Rate	Price et al[3] Rate
P01834	Immunoglobulin kappa constant	0.05±0.015	0.03±0.015	0.02±0.001

Protein Accession Number	Protein Number	DeuteRater-H Rate	Lam et al[2] Rate	Price et al[3] Rate
P01859	Immunoglobulin heavy constant gamma 2	0.05±0.020	0.04±0.006	0.02±0.005
P0DOX5	Immunoglobulin gamma-1 heavy chain	0.06±0.018	N.O.	0.01±0.004
P0DOY3	Immunoglobulin lambda constant 3	0.06±0.030	N.O.	0.02±0.001
P0DOX7	Immunoglobulin kappa light chain	0.06±0.027	N.O.	0.03±0.006
P0DOX8	Immunoglobulin lambda-1 light chain	0.06±0.022	N.O.	0.03±0.002
P01861	Immunoglobulin heavy constant gamma 4	0.07±0	0.04±0.015	0.01±0.003
P04433	Immunoglobulin kappa variable 3-11	0.07±0.008	0.02±0	0.02±0.007
P02745	Complement C1q subcomponent subunit A	0.07±0.026	0.13±0.030	0.18±0.025
P02768	Serum albumin	0.07±0.021	0.03±0.019	0.03±0.030
P01023	Alpha-2-macroglobulin	0.08±0.012	0.04±0.008	0.04±0.011
P80748	Immunoglobulin lambda variable 3-21	0.08±0.005	0.00±0	0.02±0
P01871	Immunoglobulin heavy constant mu	0.09±0.031	0.04±0.026	0.11±0.090
A0A075B6P5	Immunoglobulin kappa variable 2-28	0.09±0.033	N.O.	0.03±0.003
P01619	Immunoglobulin kappa variable 3-20	0.09±0.023	N.O.	0.03±0
P00739	Haptoglobin-related protein	0.10±0.014	2.84±2.610	0.32±0.046

Protein Accession Number	Protein Number	DeuteRater-H Rate	Lam et al[2] Rate	Price et al[3] Rate
P02787	Serotransferrin	0.10±0.012	0.08±0.026	0.05±0.024
P02747	Complement C1q subcomponent subunit C	0.10±0.015	0.10±0.007	0.17±0.092
P02790	Hemopexin	0.11±0.032	0.06±0.000	0.11±0.068
P01876	Immunoglobulin heavy constant alpha 1	0.12±0.024	0.08±0.019	0.06±0.011
P08185	Corticosteroid-binding globulin	0.12±0.047	0.08±0.003	0.22±0.179
P01860	Immunoglobulin heavy constant gamma 3	0.13±0.016	0.08±0.023	0.01±0
P00450	Ceruloplasmin	0.13±0.012	0.10±0.026	0.11±0.055
P19652	Alpha-1-acid glycoprotein 2	0.14±0.014	0.17±0.027	0.14±0.056
P02746	Complement C1q subcomponent subunit B	0.14±0.049	0.09±0.019	0.18±0
P02750	Leucine-rich alpha-2-glycoprotein	0.15±0.050	0.18±0.040	0.19±0.049
O75636	Ficolin-3	0.15±0.038	0.15±0.035	0.18±0
P00748	Coagulation factor XII	0.16±0.066	0.21±0.031	0.27±0.091
P29622	Kallistatin	0.16±0.056	0.23±0.077	0.38±0.138
P01009	Alpha-1-antitrypsin	0.17±0.019	0.09±0.019	0.12±0.054
P08603	Complement factor H	0.18±0.028	0.14±0.036	0.16±0.056

Protein Accession Number	Protein Number	DeuteRater-H Rate	Lam et al[2] Rate	Price et al[3] Rate
P49908	Selenoprotein P	0.19±0	0.81±0.429	0.58±0
P02652	Apolipoprotein A-II	0.20±0.045	0.15±0.058	0.21±0.102
P02679	Fibrinogen gamma chain	0.20±0.027	0.13±0.041	0.16±0.078
P02765	Alpha-2-HS-glycoprotein	0.21±0.101	0.15±0.031	0.19±0.070
P02675	Fibrinogen beta chain	0.21±0.022	0.09±0.030	0.14±0.058
P05546	Heparin cofactor 2	0.21±0.088	0.26±0.048	0.23±0.055
P06727	Apolipoprotein A-IV	0.22±0.081	0.31±0.072	0.64±0.315
Q9NZP8	Complement C1r subcomponent-like protein	0.22±0	0.32±0.062	0.73±0
P01011	Alpha-1-antichymotrypsin	0.23±0.082	0.14±0.019	0.19±0.169
Q96PD5	N-acetylmuramoyl-L-alanine amidase	0.23±0.039	0.20±0.046	0.20±0.035
P02760	Protein AMBP	0.23±0.072	0.40±0.222	0.38±0.120
P04217	Alpha-1B-glycoprotein	0.24±0.025	0.18±0.022	0.24±0.102
P19827	Inter-alpha-trypsin inhibitor heavy chain H1	0.24±0.034	0.19±0.022	0.37±0.224
P00734	Prothrombin	0.25±0.058	0.22±0.034	0.24±0.098
P00742	Coagulation factor X	0.25±0.158	0.29±0.035	0.46±0

Protein Accession Number	Protein Number	DeuteRater-H Rate	Lam et al[2] Rate	Price et al[3] Rate
P02671	Fibrinogen alpha chain	0.26±0.033	0.16±0.028	0.17±0.074
P07360	Complement component C8 gamma chain	0.26±0.066	0.20±0.025	0.26±0
P19823	Inter-alpha-trypsin inhibitor heavy chain H2	0.26±0.032	0.20±0.046	0.29±0.109
P01019	Angiotensinogen	0.26±0.113	0.26±0.061	0.32±0.148
P01042	Kininogen-1	0.27±0.039	0.33±0.129	0.26±0.093
P35858	Insulin-like growth factor-binding protein complex acid labile subunit	0.27±0.146	0.24±0.031	0.54±0.246
P06681	Complement C2	0.27±0.078	0.33±0.069	0.38±0
P25311	Zinc-alpha-2-glycoprotein	0.27±0.105	0.25±0.082	0.37±0.087
P05543	Thyroxine-binding globulin	0.28±0.152	0.10±0.022	0.24±0
P01031	Complement C5	0.28±0.111	0.19±0.031	0.29±0.148
P22792	Carboxypeptidase N subunit 2	0.28±0.245	0.20±0.049	0.28±0
P02763	Alpha-1-acid glycoprotein 1	0.29±0.204	0.19±0.100	0.14±0.051
P01024	Complement C3	0.30±0.083	0.17±0.027	0.27±0.099
P02774	Vitamin D-binding protein	0.31±0.051	0.36±0.126	0.34±0.153
P05156	Complement factor I	0.31±0.026	0.32±0.071	0.21±0

Protein Accession Number	Protein Number	DeuteRater-H Rate	Lam et al[2] Rate	Price et al[3] Rate
P00751	Complement factor B	0.32±0.071	0.26±0.030	0.33±0.156
P02766	Transthyretin	0.33±0.257	0.25±0.043	0.31±0.267
P07358	Complement component C8 beta chain	0.33±0.175	0.23±0.028	0.25±0.149
P02748	Complement component C9	0.33±0.250	0.25±0.017	0.30±0.088
P06312	Immunoglobulin kappa variable 4-1	0.33±0.213	N.O.	0.02±0.008
P0C0L5	Complement C4-B	0.33±0.070	0.30±0.060	0.32±0.123
P08697	Alpha-2-antiplasmin	0.34±0.089	0.21±0.073	0.19±0.103
P04196	Histidine-rich glycoprotein	0.35±0.128	0.26±0.055	0.37±0.049
P00738	Haptoglobin	0.35±0.126	0.35±0.122	0.46±0.552
P01008	Antithrombin-III	0.37±0.094	0.23±0.054	0.40±0.156
Q14624	Inter-alpha-trypsin inhibitor heavy chain H4	0.39±0.291	0.22±0.040	0.44±0.161
P06396	Gelsolin	0.40±0.397	0.19±0.024	0.23±0.029
P0C0L4	Complement C4-A	0.40±0.170	0.43±0.035	0.28±0.085
P00747	Plasminogen	0.41±0.119	0.30±0.056	0.36±0.131
P13671	Complement component C6	0.41±0.100	0.39±0.061	0.26±0.092

Protein Accession Number	Protein Number	DeuteRater-H Rate	Lam et al[2] Rate	Price et al[3] Rate
P05155	Plasma protease C1 inhibitor	0.48±0.289	0.28±0.067	0.27±0.068
P36955	Pigment epithelium-derived factor	0.50±0.562	0.21±0.033	0.47±0.015
P04004	Vitronectin	0.51±0.261	0.47±0.120	0.73±0.162
P27169	Serum paraoxonase/arylesterase 1	0.53±0.627	0.08±0.028	0.05±0
P02751	Fibronectin	0.53±0.349	0.15±0.053	0.45±0.171
P09871	Complement C1s subcomponent	0.54±0.376	0.74±0.258	0.39±0.142
P02656	Apolipoprotein C-III	0.60±0.334	0.47±0.093	0.79±0.120
P43652	Afamin	0.60±0.506	0.14±0.036	0.21±0.067
P00736	Complement C1r subcomponent	0.63±0.747	0.71±0.244	0.69±0.248
P02749	Beta-2-glycoprotein 1	0.64±0.325	0.54±0.125	0.56±0.221
P02753	Retinol-binding protein 4	0.72±0.690	1.19±0.161	0.96±0
P10909	Clusterin	0.73±0.762	0.48±0.089	0.90±0.475
P02649	Apolipoprotein E	0.76±0.489	0.75±0.162	1.00±0.525
P13645	Keratin type I cytoskeletal 10	0.06±0	0.00±0.006	N.O.
P20742	Pregnancy zone protein	0.08±0	0.01±0.01	N.O.

Protein Accession Number	Protein Number	DeuteRater-H Rate	Lam et al[2] Rate	Price et al[3] Rate
P05090	Apolipoprotein D	0.11±0.047	0.04±0.002	N.O.
O75882	Attractin	0.07±0.046	0.04±0.014	N.O.
P04180	Phosphatidylcholine-sterol acyltransferase	0.10±0.003	0.05±0	N.O.
Q15582	Transforming growth factor-beta-induced protein ig-h3	0.10±0	0.05±0.002	N.O.
Q15848	Adiponectin	0.07±0	0.05±0.012	N.O.
P06276	Cholinesterase	0.17±0	0.05±0.010	N.O.
P20851	C4b-binding protein beta chain	0.16±0.049	0.08±0	N.O.
P14151	L-selectin	0.08±0	0.08±0.010	N.O.
P22352	Glutathione peroxidase 3	0.10±0.028	0.08±0.034	N.O.
O43866	CD5 antigen-like	0.11±0.029	0.09±0.052	N.O.
P08519	Apolipoprotein(a)	0.33±0.200	0.09±0	N.O.
P15169	Carboxypeptidase N catalytic chain	0.16±0.036	0.09±0.009	N.O.
P05452	Tetranectin	0.10±0.006	0.10±0.016	N.O.
P01591	Immunoglobulin J chain	0.15±0.126	0.11±0	N.O.
Q16610	Extracellular matrix protein 1	0.16±0.049	0.12±0.032	N.O.

Protein Accession Number	Protein Number	DeuteRater-H Rate	Lam et al[2] Rate	Price et al[3] Rate
P43251	Biotinidase	0.09±0	0.13±0.024	N.O.
P02647	Apolipoprotein A-I	0.16±0.029	0.14±0.061	N.O.
P04003	C4b-binding protein alpha chain	0.18±0.033	0.14±0.031	N.O.
P23142	Fibulin-1	0.12±0.018	0.16±0.032	N.O.
P03952	Plasma kallikrein	0.23±0.067	0.16±0.052	N.O.
P35542	Serum amyloid A-4 protein	0.16±0.026	0.16±0.052	N.O.
P07225	Vitamin K-dependent protein S	0.26±0.131	0.17±0.025	N.O.
P10643	Complement component C7	0.20±0.087	0.19±0.029	N.O.
Q04756	Hepatocyte growth factor activator	0.24±0.076	0.19±0.032	N.O.
P05160	Coagulation factor XIII B chain	0.27±0.071	0.23±0.086	N.O.
Q13790	Apolipoprotein F	0.16±0	0.23±0.037	N.O.
Q96KN2	Beta-Ala-His dipeptidase	0.08±0	0.24±0.038	N.O.
Q03591	Complement factor H-related protein 1	0.34±0.105	0.26±0	N.O.
P48740	Mannan-binding lectin serine protease 1	0.28±0	0.27±0.065	N.O.
P07357	Complement component C8 alpha chain	0.46±0.443	0.28±0.062	N.O.

Protein Accession Number	Protein Number	DeuteRater-H Rate	Lam et al[2] Rate	Price et al[3] Rate
P04114	Apolipoprotein B-100	0.48±0.268	0.28±0.064	N.O.
Q9UGM5	Fetuin-B	0.27±0.159	0.31±0.110	N.O.
Q06033	Inter-alpha-trypsin inhibitor heavy chain H3	0.36±0.130	0.32±0.053	N.O.
P18428	Lipopolysaccharide-binding protein	0.33±0	0.33±0.107	N.O.
Q96IY4	Carboxypeptidase B2	0.19±0	0.33±0.047	N.O.
P17936	Insulin-like growth factor-binding protein 3	0.10±0	0.34±0.100	N.O.
P02743	Serum amyloid P-component	0.29±0.099	0.39±0.156	N.O.
P55056	Apolipoprotein C-IV	0.16±0	0.39±0.053	N.O.
Q08380	Galectin-3-binding protein	0.15±0.083	0.45±0.233	N.O.
Q14520	Hyaluronan-binding protein 2	1.74±2.668	0.46±0.116	N.O.
P02654	Apolipoprotein C-I	0.68±0.176	0.48±0.226	N.O.
Q9UK55	Protein Z-dependent protease inhibitor	0.05±0	0.49±0.117	N.O.
P02655	Apolipoprotein C-II	0.20±0	0.55±0.179	N.O.
P00740	Coagulation factor IX	0.17±0.032	0.56±0.172	N.O.
Q5D862	Filaggrin-2	0.08±0	0.64±0	N.O.

Protein Accession Number	Protein Number	DeuteRater-H Rate	Lam et al[2] Rate	Price et al[3] Rate
P36980	Complement factor H-related protein 2	0.64±0.682	1.08±1.025	N.O.
O95445	Apolipoprotein M	0.41±0.330	1.33±0	N.O.
O14791	Apolipoprotein L1	0.13±0.026	1.42±1.277	N.O.

4.6 Discussion

We created DeuteRater-H, a version of DeuteRater adjusted for human kinetic proteomics. The program calculates protein turnover rates on a proteome scale. We have enabled the use of multiple equations for deuterium enrichment fits, and have enabled the calculation of protein turnover rates from multiple metrics in humans, as we have previously done for our DeuteRater software tool[1]. The program is free to use, user-friendly and can calculate large numbers of protein turnover rates at a time.

However, there are still problems to address before DeuteRater-H is ready for release. The main problem is justifying then novel nature of DeuteRater-H as an improvement on previously published methods. Work is ongoing to demonstrate that the use of multiple metrics are useful in kinetic calculations.

4.7 Future Directions

4.7.1 Computational Development

The main changes that need to be made to DeuteRater-H are more comparisons to confirm that multiple metrics are useful. I will also create an executable file to make it easier for

other labs to use DeuteRater-H. As soon as these steps are accomplished, DeuteRater-H will be ready for distribution.

4.7.2 Biology

Once the DeuteRater-H program is complete and confirmed to function, the data from the experimental subjects must be analyzed in more detail. Muscle, buffy coat and red blood cell samples from the experimental subjects must be analyzed to calculate protein turnover rates. Once we have a database of healthy protein turnover rates, we will design experiments with subjects who have diseases so turnover rates may be compared between healthy and sick conditions. Such a comparison could provide a turnover rate based biomarker or an improved understanding of the disease state. These diseases include mitochondrial dysfunction or age relating wasting of muscle tissue.

An area of exploration is the difference observed between the male and female subjects. Previous studies have reported that males and females have significant differences in protein turnover rates[10]. It will be an important test to see if we observe the same effect.

4.8 Acknowledgements

This work was supported by a grant from the Fritz B. Burns Foundation, BYU startup funds to JCP, Graduate Research Fellowship to BCN, and BYU Undergraduate Research Awards to MH and DP.

4.9 Bibliography

1 Naylor, B. C. *et al.* DeuteRater: a tool for quantifying peptide isotope precision and kinetic proteomics. *Bioinformatics* **33**, 1514-1520, doi:10.1093/bioinformatics/btx009 (2017).

2 Lam, M. P. *et al.* Protein kinetic signatures of the remodeling heart following isoproterenol stimulation. *J. Clin. Invest.* **124**, 1734-1744, doi:10.1172/JCI73787 (2014).

3 Price, J. C. *et al.* Measurement of human plasma proteome dynamics with (2)H(2)O and liquid chromatography tandem mass spectrometry. *Anal. Biochem.* **420**, 73-83, doi:10.1016/j.ab.2011.09.007 (2012).

4 Pulk, A. *et al.* Ribosome reactivation by replacement of damaged proteins. *Mol. Microbiol.* **75**, 801-814, doi:10.1111/j.1365-2958.2009.07002.x (2010).

5 Kim, Y. E., Hipp, M. S., Bracher, A., Hayer-Hartl, M. & Hartl, F. U. Molecular chaperone functions in protein folding and proteostasis. *Annu. Rev. Biochem.* **82**, 323-355, doi:10.1146/annurev-biochem-060208-092442 (2013).

6 Sinturel, F. *et al.* Diurnal Oscillations in Liver Mass and Cell Size Accompany Ribosome Assembly Cycles. *Cell* **169**, 651-663.e614, doi:10.1016/j.cell.2017.04.015 (2017).

7 Ma, X. M. & Blenis, J. Molecular mechanisms of mTOR-mediated translational control. *Nat. Rev. Mol. Cell Biol.* **10**, 307-318, doi:10.1038/nrm2672 (2009).

8 Price, J., Guan, S., Burlingame, A., Prusiner, S. & Ghaemmaghami, S. Analysis of proteome dynamics in the mouse brain. *Proc. Natl. Acad. Sci. U. S. A.* **107**, 14508-14513, doi:10.1073/pnas.1006551107 (2010).

9 Price, J. *et al.* The Effect of Long Term Calorie Restriction on in Vivo Hepatic Proteostatis: A Novel Combination of Dynamic and Quantitative Proteomics. *Mol. Cell. Proteomics* **11**, 1801-1814, doi:10.1074/mcp.M112.021204 (2012).

10 Shankaran, M. *et al.* Circulating protein synthesis rates reveal skeletal muscle proteome dynamics. *J. Clin. Invest.* **126**, 288-302, doi:10.1172/JCI79639 (2016).

11 Mathis, A. D. *et al.* Mechanisms of In Vivo Ribosome Maintenance Change in Response to Nutrient Signals. *Mol. Cell. Proteomics* **16**, 243-254, doi:10.1074/mcp.M116.063255 (2017).

12 Decaris, M. L. *et al.* Turnover rates of hepatic collagen and circulating collagen-associated proteins in humans with chronic liver disease. *PLoS One* **10**, e0123311, doi:10.1371/journal.pone.0123311 (2015).

13 Decaris, M. L. *et al.* Identifying nonalcoholic fatty liver disease patients with active fibrosis by measuring extracellular matrix remodeling rates in tissue and blood. *Hepatology* **65**, 78-88, doi:10.1002/hep.28860 (2017).

14 Hellerstein, M. K. Relationship between precursor enrichment and ratio of excess M2/excess M1 isotopomer frequencies in a secreted polymer. *J. Biol. Chem.* **266**, 10920-10924 (1991).

15 Hellerstein, M. K. & Neese, R. A. Mass isotopomer distribution analysis: a technique for measuring biosynthesis and turnover of polymers. *Am. J. Physiol.* **263**, E988-1001 (1992).

16 Kasumov, T. *et al.* Measuring protein synthesis using metabolic ^{2}H labeling, high-resolution mass spectrometry, and an algorithm. *Anal. Biochem.* **412**, 47-55, doi:10.1016/j.ab.2011.01.021 (2011).

17 MacCoss, M. J., Wu, C. C., Matthews, D. E. & Yates, J. R. Measurement of the isotope enrichment of stable isotope-labeled proteins using high-resolution mass spectra of peptides. *Anal. Chem.* **77**, 7646-7653, doi:10.1021/ac0508393 (2005).

18 Hsieh, E. J. *et al.* Topograph, a software platform for precursor enrichment corrected global protein turnover measurements. *Mol. Cell. Proteomics* **11**, 1468-1474, doi:10.1074/mcp.O112.017699 (2012).

19 Basak, J. M. *et al.* Measurement of apolipoprotein E and amyloid beta clearance rates in the mouse brain using bolus stable isotope labeling. *Mol. Neurodegener.* **7**, 14, doi:10.1186/1750-1326-7-14 (2012).

20 Jones, P. J. & Leatherdale, S. T. Stable isotopes in clinical research: safety reaffirmed. *Clin. Sci. (Lond.)* **80**, 277-280 (1991).

21 Koizuka, I., Takeda, N., Kubo, T., Matsunaga, T. & Cha, C. I. Effects of ethyl alcohol and heavy-water administration on vestibulo-ocular reflex in rabbits. *ORL J. Otorhinolaryngol. Relat. Spec.* **51**, 151-155 (1989).

22 Lis, G., Wassenaar, L. I. & Hendry, M. J. High-precision laser spectroscopy D/H and 18O/16O measurements of microliter natural water samples. *Anal. Chem.* **80**, 287-293, doi:10.1021/ac701716q (2008).

23 Zhang, J. *et al.* PEAKS DB: de novo sequencing assisted database search for sensitive and accurate peptide identification. *Mol. Cell. Proteomics* **11**, M111.010587, doi:10.1074/mcp.M111.010587 (2012).

5. Short-Term Calorie Restriction Elicits Nutrient-Specific Post-Transcriptional Regulation of Proteostasis

5.1 Chapter Summary

Like the previous chapter, this work has not been published, though some of the mice from these experiments were used for the papers presented in the chapters "DeuteRater: a Tool for Quantifying Peptide Isotope Precision and Kinetic Proteomics" and "Mechanisms of *in vivo* Ribosome Maintenance Change in Response to Nutrient Signals". The goal of this work was to combine kinetic proteomics with other methods to create a workflow that can solve biological questions.

5.1.1 Authors in Order of Contribution

Bradley C. Naylor*, Richard Carson*, Monique Speirs, Nathan Keyes, Ryne Peters, Brittany Johnson, Stephen Ames, Benjamin T. Bikman, Jonathan T. Hill, John C. Price

* These authors contributed equally to this work

5.1.2 Contributions of Major Authors

For this work, I led the mouse work on the high protein diet, the kinetic proteomic analysis, and the quantitative proteomics analysis. My co-first author, Richard Carson, led the mouse work on the low protein diet, the RNA-Seq work, and the combination of the datasets.

5.2 Abstract

Biological aging seems to be primarily driven by a loss of protein homeostasis [1,2]. For over 100 years it has been known that dietary signals can change the rate of aging[3,4]. We, and others, therefore have concluded that the rate of protein homeostasis loss can be slowed by dietary interventions. Several very insightful investigations into protein homeostasis have utilized luciferase or similar reporters as genetic reporters to identify important differences between long lived and short lived animals[1,2]. Further insight into the regulation of protein homeostasis would benefit from measuring individual synthesis and degradation rates for each protein in the proteome systems wide measurement to identify how protein specific regulation of these processes contributes to the maintenance or loss of protein homeostasis.

5.3 Introduction

Cells are not simple nor static. They constantly change in response to their needs and various external stimuli. Healthy cells monitor and modify these changes with exquisitely fine control. Loss of control is the basis for many of the untreatable diseases plaguing society today. Control of protein quality and concentration in the cell is termed proteostasis. Synthesis, folding, and degradation of each protein in the cell need to be controlled in order for protein homeostasis to be maintained. Loss of proteostasis is the root cause of aging[1,5-8], cancer[9-11], and neurodegeneration[12-15]. Loss of proteostasis is often observed by dramatically changing protein concentrations. Concentration control occurs through the careful balance of synthesis and degradation. In fact, the classic model for change in protein concentration includes the rates of synthesis and degradation (Equation 5-1).

$$\frac{d[Protein]}{dt} = k_{\substack{Protein \\ synthesis}}[mRNA] - k_{\substack{Protein \\ degradation}}[Protein] - k_{\substack{Cell \\ division}}[volume] \quad (5\text{-}1)$$

In terminally differentiated cells as found in the majority of human tissues we can assume the $k_{division}$ is essentially zero. Which means that changes in concentration are due to the difference in synthesis rate versus the degradation rate. Methods for measuring protein concentration *in vivo* are well developed[16,17] using mass spectrometry relative and absolute concentrations can be measured for thousands of individual proteins in a biological sample. Measuring concentration changes over time though is not sufficient to be able to know what is happening with synthesis and degradation. For example, concentration may go up in a condition but that increased concentration may be the result of an increase in protein synthesis or a decrease in degradation rates.

The replacement (turnover) rates of each protein are also controlled by the individual synthesis and degradation rates. We and others have recently developed methods to monitor protein turnover rates for thousands of individual proteins *in vivo*[18-22]. Canonically, turnover can be described as the average of synthesis and degradation rates (Equation 5-2)

$$Protein\ Turnover\ (Day^{-1}) = (k_{\substack{Protein \\ synthesis}}([mRNA]) + k_{\substack{Protein \\ degradation}}([Protein]))/2 \qquad (5\text{-}2)$$

Although changes in turnover are indicative of changes in synthesis and degradation, it is not known which component (synthesis or degradation has changed). For example, slowed turnover could result from synthesis, degradation, or both slowing. The combination of change in turnover and change in concentration is needed to identify whether synthesis or degradation is primarily changed between control and experimental conditions for a given protein or group of proteins.

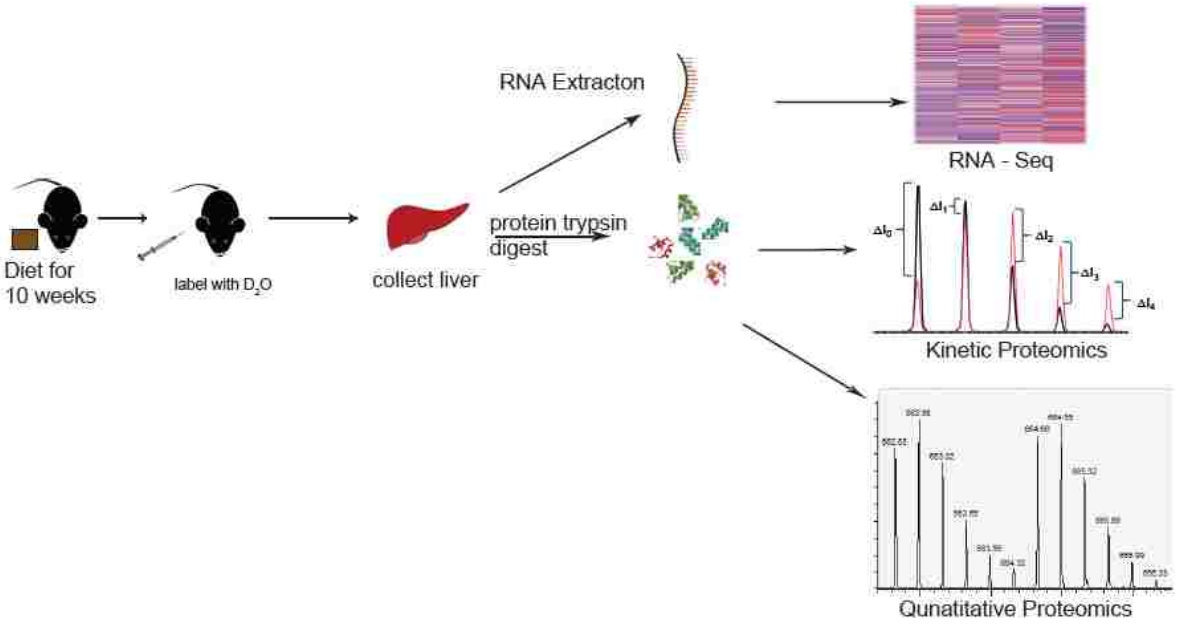

Figure 5-1 Experimental Workflow. Mice were fed experimental diets for 10 weeks and then labeled with D2O. The mice were then sacrificed at various time-points throughout the following month. Liver was taken and prepared for various analyses. Some had the RNA extracted for RNA-Seq, while the rest was fractionated for Kinetic Proteomics or mixed with SILAC standard for Quantitative Proteomics

In order to analyze changes in proteostasis we used RNA-Seq, Quantitative Proteomics, and Kinetic Proteomics, which measure mRNA quantity, protein quantity and protein turnover rate respectively (Figure 5-1). With protein concentrations and turnover rates determined we were able to determine how any measured protein was regulated (synthesis, degradation or both) while the mRNA showed into where the regulation occurred and why.

To analyze changes in proteostasis we chose dietary restriction (DR) as a model. DR involves feeding an organism reduced amounts of food, and extends lifespan substantially[3,4]. Using DR as our test intervention offers two large advantages: First, DR has been studied for decades, and has had multi-omics studies with quantitative and kinetic Proteomics performed previously[5,20], which provides a baseline for comparisons. Second, in those decades of study,

several disruptions to DR have been found. Different genotypes and mutations can prevent DR from prolonging life [23,24]. Different dietary compositions and additives can disrupt DR [25,26]. We can analyze DR disruptions to determine if the disruption is affecting only specific pathways or affecting the proteome in a more general way. By providing insight into what is disrupted, we may identify mechanisms of DR's beneficial effects. We chose to use diets with different protein levels for this study due to the ease of performing the disruption. Previous work has shown that high protein content in a diet can disrupt beneficial DR effects such as insulin sensitivity[26]. Low protein (LP) and High protein (HP) chows were used and each diet had an *ad libitum* (AL) and DR cohort.

We show that a high protein DR diet undoes the global decrease in protein turnover rates and protein quantitation observed in canonical DR. We also show that this change is driven by post-transcriptional control of proteins. Finally, we suggest a method of proteostatic control that may be at work in DR. In the future, we will determine other biological pathways associated with this change, and perform follow up experiments to confirm our observations.

5.4 Methods

5.4.1 Animal Handling

5.4.1.1 Mouse housing, genotype, and diet

Mouse diets, housing, and metabolic labeling were performed according to protocols approved by the Institutional Animal Care and Use Committee of Brigham Young University. Ten-week-old C57/Bl6 male mice were purchased from Charles River Laboratory. They were stored in a pathogen free facility for the duration of the experiment. Mice were fed an AL diet for one week after arrival to acclimate to the facility. Mice were then randomly divided into AL

or DR groups. Mice were housed separately to ensure equal access to food. AL animals had constant access to food, while DR animals were fed daily a pellet of 3g ± .1g in size (65% of expected AL consumption). The HP diet was Harlan 8604 chow; the LP diet was NIH31 chow.

5.4.1.2 Metabolic Labeling

At 10 weeks, the mice were given an intraperitoneal bolus injection of sterile D_2O saline at 35 µL/g body weight. This injection brought the mice up to 5% Molar Percent Excess (MPE) deuterium as previously described[20]. Mice were then provided drinking water containing 8% MPE to maintain the 5% MPE in the animals' body water.

5.4.1.3 Euthanasia and Sample Collection

Mice were anesthetized with CO_2 and then euthanized by cardiac puncture. Mice were then immediately dissected and all tissues except for blood were flash frozen on solid CO_2 and then stored at -80°C. Blood was stored on ice until it could be centrifuged at 800 x g for 10 minutes at 4°C. The centrifugation separated serum and red blood cells, which were stored in separate containers at -80°C.

5.4.1.4 Mouse Weight Determination

Mice were weighed weekly on a laboratory scale. The scale was tared using a sterile plastic bucket. The mouse was placed within the bucket and weighed. After weighing, mice were placed back in their cages. Weighing was performed weekly during one of the daily feedings of DR animals, in order to minimize distress to the animals.

5.4.1.5 Mitochondrial Respiration

Fresh liver tissue was quickly removed from exsanguinated mice and immediately placed in ice-cold mitochondrial respiration buffer 05 (MiR: 0.5 mM EGTA, 10 mM KH_2PO_4, 3

mM $MgCl_2$-6 H_2O, 60 mM K-lactobionate, 20 mM HEPES, 110 mM Sucrose, 1 mg/ml fatty acid free BSA, pH 7.1) and trimmed of connective tissue. Tissue was gently separated and homogenized under a surgical scope (Olympus, ST) to particles of around 1 mg. Homogenate was then transferred to a tube with chilled MiR05 and 50 µg/ml saponin and rocked at 4 °C for 30 min, then washed in MiR05 at 4 °C for at least 15 min before use. High-resolution O_2 consumption was determined at 37 °C using the Oroboros O_2K Oxygraph. Before addition of sample into respiration chambers, a baseline oxygen consumption rate was determined. After addition of sample, the chambers were hyperoxygenated to ~350 nmol/ml. Following this, respiration was determined as indicated. Lastly, residual oxygen consumption was measured by adding antimycin A (2.5 µM) to block complex III action, effectively stopping any electron flow and providing a baseline O_2 consumption rate.

5.4.1.6 Differences between Cohorts

LP and HP cohorts were purchased and treated at different times due to logistical concerns. The LP AL and LP DR cohorts had 9 mice each. The HP AL cohort had 19 mice and the HP DR cohort had 20 mice. Due to the difference in cohort size, sacrifice times were different. Two LP animals from each diet were sacrificed at 1 day, 3 days, 9 days and 27 days after bolus D_2O injection, with one animal from each group sacrificed without receiving a bolus injection or any other D_2O labeling. The HP mice had two animals sacrificed at 9 hours, 1 day, 2 days, 4 days, 8 days, 16 days, and 32 days post injection, with the 4, 8 and 32 day time-points each having a third sacrifice and 2 mice per cohort sacrificed without deuterium injection. The HP DR's extra mouse was sacrificed with no bolus injection.

5.4.2 Kinetic Proteomic Analysis

5.4.2.1 Measurement of MPE

For animals in LP cohorts, serum was distilled to measure MPE as described in Chapter "Mechanisms of *in vivo* Ribosome Maintenance Change in Response to Nutrient Signals". For animals in HP cohorts the serum and 100 mg of liver homogenate (made using MP Biomedicals FastPrep-24 bead beater) were used. These samples were distilled at 90°C overnight and the distillate collected. In both LP and HP, the following steps were identical. The distillate was diluted 1:300 in ddH_2O, and MPE of deuterium was directly measured against a D_2O standard curve using a cavity ring-down water isotope analyzer (Los Gatos Research [LGR], Los Gatos, CA, USA) according to the published method [27].

5.4.2.2 Trypsin Digestion

Liver tissue from each animal was placed in Ammonium Bicarbonate (ABC) solution (25 mM, pH 8.5) along with protease inhibitor cocktail (Sigma) and was homogenized using a MP Biomedicals FastPrep-24 bead homogenizer at 6 m/s for 60 seconds. Volumes were calculated to give approximately 10 mg/mL protein. Protein concentration was measured using a bicinchoninic acid (BCA) protein assay (Thermo Fisher). 300-500 µg of protein were placed on 30 kDa centrifugal filters (VWR). 100 µL of guanidine (6 M, 100 mM Tris-HCl pH 8.5) was added to each sample and centrifuged at 14,000g for 15 minutes. Another wash with guanidine (same volume and centrifuge settings) was performed. Flow-through was discarded. 100 µL of guanidine was added to the filters, and the solution was brought to 10 mM dithiothreitol. The filters with sample were placed in a sand bath at 60 °C for 60 minutes. After 5 minutes of cooling, the samples were brought to 20 mM iodacetamide. The samples were then incubated in the dark for 60 minutes. Afterwards, the samples were centrifuged at 14,000g for 15 minutes.

200 µL ABC was added to the filters, which were spun at 14,000g for 15 minutes. After a second ABC wash (same volume and centrifuge settings), ABC was added to the filters to a final volume of 300 µL. Collection vials were emptied and cleaned. Pierce MS-Grade Trypsin was added to a 1:50 (w:w) in each sample, which were incubated at 37°C overnight. The next morning, samples were centrifuged at 14,000 g for 30 minutes. 100 µL of ABC was added to the filters and they were centrifuged again for 30 minutes at 14,000 g. Filters were discarded and the filtrate was dried using a Speedvac (Sorval) vacuum centrifuge. The dried samples were stored at 4°C until use.

5.4.2.3 HPLC Fractionation

Samples were re-suspended in 10 mM ammonium formate (LC-MS grade pH 9.5). Samples were fractionated using high pH C18 High Performance Liquid Chromatography (HPLC), which is orthogonal to low pH C18 chromatography used in "LC-MS Data Acquisition" allowing for improved protein coverage [28]. Fractionation was performed using the 1260 HPLC Infinity (Agilent) and the Gemini 50 x 2.00 mm C18 column with 3µm beads and 110 angstrom pore size. Peptides were eluted using a 10 mM ammonium formate (pH 9.5) H_2O/acetonitrile gradient from 3% B to 60% B over 40 minutes flowing at 1 mL/min. Buffer A was 97% H_2O, 3% acetonitrile, 10mM ammonium formate pH 9.5. Buffer B was 10% H_2O, 90% acetonitrile, 10mM ammonium formate pH 9.5. 1 mL fractions were collected. 1 mL fractions were pooled into 8 fractions by pooling every 8th fraction. For example, fractions 1, 9, 17, and 25 were pooled into one fraction. Pooling was performed in this manner to spread out high abundance peptides to different fractions. By spreading out peptides in this way, more coverage can be obtained within the dynamic range of the mass spectrometer. It also ensured varied hydrophobicity of peptides within each sample allowing the chromatography for the LC-MS to

be most effective. Pooled fractions were dried with a SpeedVac vacuum centrifuge (Sorval) then suspended in 200 µL of 80% acetonitrile and decanted into a mass spectrometry vial. Samples were again dried with a SpeedVac vacuum centrifuge (Sorval) and suspended in 40 µL of 3% acetonitrile 0.1% formic acid (all LC-MS grade) for LC-MS analysis.

5.4.2.4 LC-MS Data Acquisition

As described previously, protein identification and kinetic acquisition were performed on an Agilent 6530 Q-ToF mass spectrometer coupled to a capillary nanoflow Agilent 1260 HPLC using the chipcube nano-spray source[20,21]. Peptides were eluted from an Agilent C18 Polaris chip at 300 nL/min using an H_2O-acetonitrile gradient acidified to pH 4 by Pierce LC-MS grade formic acid. Buffer A was 3% acetonitrile, 0.1% formic acid. Buffer B was 97% acetonitrile, 0.1% formic acid. The elution gradient was as follows: 0 minutes, 100% A; 0.1 minutes, 95% A; 27 minutes, 40% A; followed by high percentage B column washing and low percentage B re-equilibration. The Agilent 6530 Q-ToF mass spectrometer was run in 2 Ghz high dynamic range mode. Protein identification runs were performed in MS/MS mode using collision-induced dissociation with nitrogen gas. MS and MS/MS data were collected at a maximum rate of 4 spectra/second with CID fragmentation on the top 10 most abundant precursors. Dynamic exclusion was set to 0.2 minutes. Kinetic acquisitions were performed in MS only mode and collected at 1 spectra/second. MS only mode increases signal intensity, improves signal-to-noise, and gives more scan points per elution chromatogram, greatly enhancing isotopomer analysis accuracy. Data were also collected on an Orbitrap Fusion-Lumos mass spectrometer. Samples were resuspended in 0.1% formic Acid (Pierce LC-MS grade) in H_2O (Optima grade Thermo Fischer). Samples were analyzed with a Thermo Lumos Tribrid (Orbitrap). Tryptic peptides were separated using a reverse phase C18 column (Acclaim PepMap™ 100) and a

Thermo Easy-Spray source. Mobile phase for the liquid chromatography was 0.1% formic acid in H_2O (Buffer A) and 0.1% formic acid in 80% acetonitrile (Optima grade Thermo Fischer) with 20% H_2O (Buffer B) on an Easy-nLC 1200 HPLC system. Samples were eluted using a gradient of 5% B to 22% B over 85 minutes, 22% to 32% B over 15 minutes, with a wash of 32% to 95% B over 10 minutes, which was held at 95% B for 10 minutes. Sample loading and equilibration were performed using the HPLC's built-in methods. MS only runs were performed using 2400 V in the ion source, 60000 resolution with a scan range of 375-1700 m/z, 30% RF Lens, Quadrupole Isolation, 8 *10^5 AGC Target and a maximum injection time of 50 ms. MS/MS scans were performed using the same settings as used for MS only scans with 3 seconds allowed per MS/MS after each MS scan. The following filters were used: peptide monoisotopic peak determination, an intensity threshold of 5*10^3, fragmentation limited to charge states +2 to +6, with an error tolerance of 10 ppm high and low, and isotopes excluded. Dynamic exclusion allowed fragmentation of any peak once every 60 seconds. The fragmentation scan used an isolation window of 1.6 m/z, CID fragmentation with an energy of 30%, detection in the linear ion trap in Rapid Scan mode with a AGC target of 1*10^4, a maximum injection time of 35 milliseconds and used the "Inject Ions for All Available Parallelizable Time" option.

5.4.2.5 Protein Identification

Peak lists obtained from MS/MS spectra were identified using Mascot version 2.2.04, OMSSA version 2.1.9, X!Tandem version X! Tandem Sledgehammer (2013.09.01.1), MS-GF+ version Beta (v10282), Comet version 2016.01 rev. 2 and MyriMatch version 2.2.140. The search was conducted using SearchGUI version 3.2.7[29].

Protein identification was conducted against a concatenated target/decoy version of the *Mus musculus* complement of the UniProtKB (Created September 2016 , 16806 (target)

sequences). The decoy sequences were created by reversing the target sequences in SearchGUI. The identification settings were as follows: Trypsin, Specific, with a maximum of 2 missed cleavages 10.0 ppm as MS1 and 0.5 Da as MS2 tolerances; fixed modifications: Carbamidomethylation of C (+57.021464 Da), variable modifications: Oxidation of M (+15.994915 Da), Pyrolidone from Q (--17.026549 Da), Acetylation of protein N-term (+42.010565 Da), Pyrolidone from E (--18.010565 Da), Pyrolidone from carbamidomethylated C (--17.026549 Da), fixed modifications during refinement procedure: Carbamidomethylation of C (+57.021464 Da).

Peptides and proteins were inferred from the spectrum identification results using PeptideShaker version 1.15.1[30]. Peptide Spectrum Matches (PSMs), peptides and proteins were validated at a 1.0% False Discovery Rate (FDR) estimated using the decoy hit distribution. All validation thresholds are listed in the Certificate of Analysis available in the supplementary information. Post-translational modification localizations were scored using the D-score and the phosphoRS score with a threshold of 95.0 as implemented in the compomics-utilities package. A phosphoRS score above was considered as a confident localization.

After protein identification, identification files and the MS-only mass spectrometry data were analyzed with the DeuteRater software package [18]. DeuteRater provided the protein turnover rates used for later analyses.

5.4.2.6 Homology Analysis

Due to sample fractionation and biological variability, some peptide sequences were assigned to different homologous proteins in different experimental groups. To address this, all identifications for every sequence within kinetic proteomics data sets were identified.

Homologous sequences had the accession numbers combined to indicate uncertainty in the identification. DeuteRater analysis was then redone to create homology corrected rates.

5.4.2.7 Filtering Data

Kinetic data required filtration to remove data with extreme outliers or other issues. The kinetic proteomics data comes from a curve fit of relevant data, so all curves with an R^2 less than 0.5, or with 95% confidence interval/ rate value less than 0.2 were removed from further analysis. The confidence interval was divided by the turnover rate to normalize error to the measured value.

5.4.3 Quantitative Analysis

5.4.3.1 Homogenization, Trypsin Digest, and HPLC fractionation

A mouse liver labeled according to a Stable Isotope Labeling by Amino Acids in Mammals (SILAM) (Lys $6C^{13}$, Cambridge Isotopes) was purchased and homogenized as described in the "Trypsin Digestion" section above. We mixed 150 µg of protein from the SILAM homogenate with 150 µg protein from the sample homogenate. We used 3 replicates from each dietary group. Due to isotopic shifts caused by D_2O labeling creating difficulties in peptide identification, only animals within one day of intraperitoneal injection, or those that received no injection, were used for this experiment. The mixtures of SILAM and sample homogenates were prepared identically to those described within the "Kinetic Proteomic Analysis" section until mass spectrometry analysis.

5.4.3.2 Mass Spectrometry Analysis

Samples were re-suspended to 1 µg/µL in .1 % formic acid. Samples were analyzed on a Thermo Lumos Tribrid instrument paired with a Thermo Easy-nLC 1200 HPLC. Solvent A was .1% formic acid 100% water, Solvent B was .1% formic acid, 80% ACN 20% water. All

solvents were LC-MS grade. Gradient was as follows: 0-45 minutes was 5-45 % Buffer B, 45-50 minutes 45-100 % Buffer B, 50-60 minutes 100 % Buffer B. The MS scans were collected at 60,000 Resolution, with 20 MS/MS scans between MS scans. MS/MS fragmentation was done with a 1.6 m/z isolation window, CID fragmentation with 28% fragmentation energy. Fragment ions were measured in the Linear Ion Trap with the "Normal" resolution setting.

5.4.3.3 Data Analysis

Data from the mass spectrometry analysis was analyzed using the MaxQuant software package[31]. All data was analyzed at the same time, with each dietary group analyzed as a single experimental group. Constant modifications were carbamidomethylation for cysteine. Variable modifications allowed were oxidation of methionine and acetylation of the N-terminus. The identification database was the same as that used for the kinetic analysis. Lys6 was added as a heavy label, all other settings were left at default. Unlabeled divided by labeled signal intensities were determined and used to determine amounts of peptide in the sample relative to the SILAM standard. The relative peptide abundances could then be compared between samples.

5.4.4 RNA-Seq

We used the Direct-zol RNA MiniPrep Plus kit from Zymo Research to extract RNA from liver tissue of all animals in this study. Briefly, 10-20 mg of frozen liver tissue from each mouse was processed using a Trizol extraction and the resulting RNA frozen at -80°C. Since we wished to identify changes in the transcriptome that resulted only from dietary differences, RNA from three different mice in the same dietary cohort (but sacrificed at different times) were pooled to form a single sample for RNA-Seq, thus masking any differences resulting from temporal variations. There were three pools per dietary cohort, containing RNA from three mice each. Sample volumes were adjusted to obtain a concentration of 4µg total RNA in 50 µL of

RNase-free water, and submitted to the BYU Sequencing Center. The BYU Sequencing Center constructed cDNA libraries after a poly-A pull-down to enrich for mRNA, and then sequenced them using an Illumina HiSeq 2500 sequencing platform. RNA-Seq bam files were analyzed in R using the DESeq2 package in Bioconductor 3.3 from Bioconductor.org[32], downloaded October 20, 2016.

5.4.5 Multi-omics Data Analysis

5.4.5.1 Differential Expression Determination

Turnover rate data, quantitative MS data, and RNA-Seq data were first filtered in this fashion: Protein/Gene IDs were matched between all dietary groups. Any proteins/gene IDs that were not common to all four diets were excluded from further analysis. 95% confidence intervals were then calculated for each measurement based on data output from DeuteRater, MaxQuant, and DESeq2, for protein turnover data, quantitative data, and RNA-Seq data respectively. Using R scripts, proteins/genes that were significantly different between diets were identified by analyzing overlap between mean values and confidence intervals: in order to be considered different between diets, the mean value of one diet had to lie outside of the confidence interval of the other compared diet, and vice-versa. Any that failed this test were labeled as matching, and assigned a value of zero difference. Permutation tests to guard against false discovery are in process. For comparison between kinetic, quantitative, and RNA-Seq data, any protein that did not occur in all three sets was excluded from analysis. For LP and HP diet comparisons, proteins were excluded if they were not observed in both dietary data sets. Graphical output of the data was performed using JMP12, Microsoft Excel, and RStudio (version 0.99.903).

5.4.5.2 Gene Ontology Analysis

Ontology groupings were determined using DAVID [33,34]; proteins/genes were separated into three general categories: "up," "equal," and "down" according to whether the ratio of DR to AL was greater than one, equal to one, and less than one, respectively. These categories were determined using the non-overlapping confidence interval test described in the "Differential Expression Determination" section. Ensembl IDs from RNA-Seq data were translated to UniProt accession numbers prior to ontology analysis. Gene ontology output from DAVID used background groups comprised of all categories combined together. Ontology groups with Benjamini coefficients less than or equal to 0.05 were retained for analysis; all others were disregarded.

5.4.5.3 RNA-Motif Analysis

RNA motif analysis was performed using the HOMER motif analysis tool[35] in order to detect translational preference due to RNA sequence motifs in the mRNA. Output from HOMER was processed using in-house R scripts.

5.5 Results

5.5.1 High Protein Diet Elicits Canonical Phenotypes

Mice were weighed throughout the experiment to ensure the health of the animals, and to analyze differences in the diets (Figure 5-2 Panel A). We also analyzed the effect of different diets on mitochondrial respiration immediately following euthanasia (Figure 5-2 Panel B-C). The results of both of these tests show that DR is different from AL in phenotypic ways, decreasing in both weight and mitochondrial oxygen consumption. HP-DR evidences more severe weight loss relative to its control than LP-DR, even though the AL groups are very similar. This indicates a disruption of some part of the DR phenotype caused by higher dietary

protein. However, the effect of different amounts of protein in DR on a cellular level required more in-depth analysis to determine.

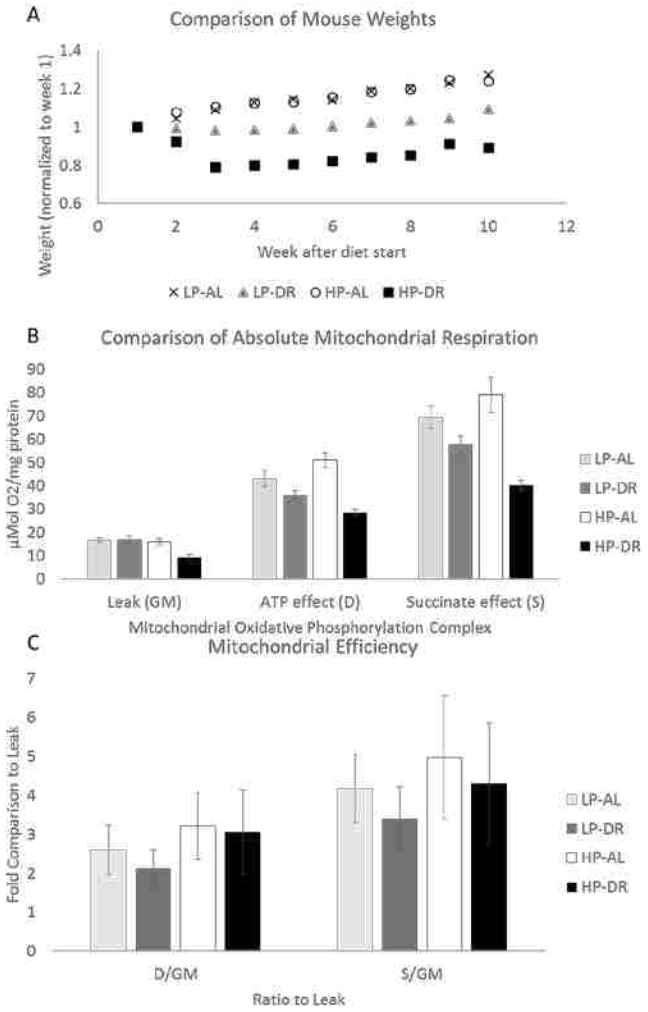

Figure 5-2 Comparison of Weight and Mitochondrial Respiration. Panel A is a comparison of mouse weights over the course of the experiment. Each animals' weight was normalized to its weight at the start of the experiment. Each point on the graph represents an average of the normalized data at that time-point. The AL dietary groups are nearly identical. In both DR groups, weight decreases immediately and eventually increases, but the relative decrease is far larger in HP-DR than LP-DR. Panel B represents the mitochondrial use of oxygen in various conditions. Leak is the mitochondria at rest with oxygen, ATP is the addition of ADP and oxygen to show function of the Electron Transport Chain other than complex 2, and the Succinate effect shows complex 2 added to the rest of the Electron Transport Chain. The AL seems to use more oxygen than DR in both diets. HP-DR seems to use less oxygen compared to its AL than LP in all cases. Panel C shows the relative efficiency of the ATP effect and the Succinate effect compared to mitochondrial leak. The data suggests that the HP diets might have a slight increase in efficiency compared to LP, but the error is too high to be sure.

5.5.2 Protein make-up of diet affects DR globally

A key observation in previous studies of DR has been that DR slows average protein turnover rates and decreases the average protein quantity[5,20]. Our study replicates these previous observations in our low protein groups (Figure 5-3 A and C). In the high protein diet, DR does not have this effect, resulting in minimal change to global protein turnover rates between DR and its AL control (Figure 5-3, B and D). This is important to the protein homeostasis hypothesis of DR. This hypothesis states that the DR benefit to lifespan is the result of more time being spent

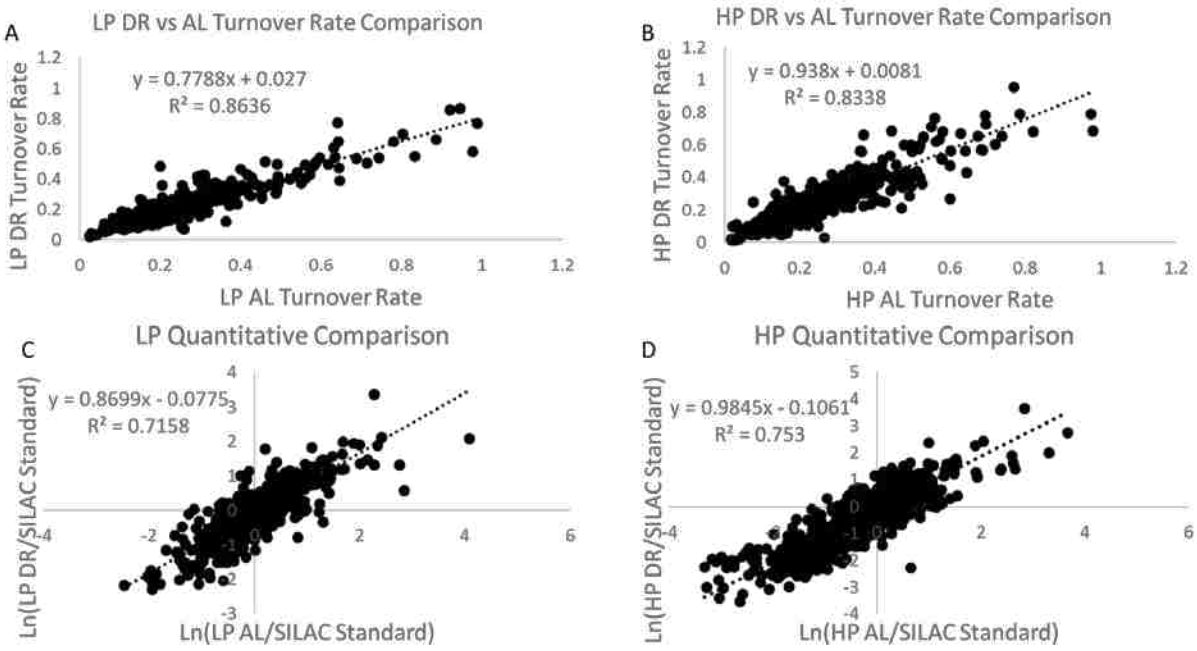

Figure 5-3 Rate and Turnover Comparison. Comparison of Protein turnover rates (A-B) and Quantitation (C-D). If samples are identical, the fit line should have an approximate slope of 1, which is the case in High Protein Quantitation (Panel D, slope = .9845), and is a not far off in HP Turnover rates (Panel B, slope = .938). For LP the slopes are far lower than in their HP counterparts(Turnover: Panel A slope =.7788, Panel C slope = .8699). This indicates that the LP DR is far more different from its AL than the HP DR is from its AL.

on protein translation[20]. The hypothesis is that the decreased demand on the protein translation machinery allows fewer mistakes and more time for the quality control machinery to work. This change in turnover rate may be responsible for the phenotypic changes observed by other groups

[26] but how the turnover rate and phenotypic changes influence each other has not yet been determined. Our previous work[20] and the literature[36,37] have identified the strong connection between reduced mTOR signaling and the DR effect. Conversely, it has been established that mTOR activity is directly connected to amino acid and in particular leucine concentration[38,39]. Therefore, the effect of the high protein diet may be, in part, to activation mTOR in spite of the reduced calorie diet. This would have a direct impact on global synthesis and degradation rates.

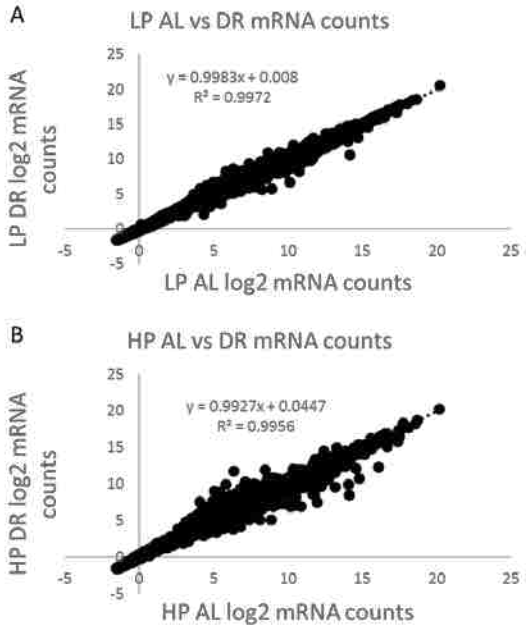

Figure 5-4 Comparison of mRNA amounts. A comparison of DR mRNA (y-axis) counts to AL mRNA counts (x-axis) in both LP (Panel A) and HP (Panel B) diets. A slope of 1 would indicate no change between the diets. Since the slopes are very close to 1, it can be seen that there are no major differences within the diets in terms of mRNA amounts.

5.5.3 The Proteome is Controlled Post-Transcriptionally during DR

The RNA-Seq data showed remarkably little change regardless of dietary changes (Figure 5-4A). This was particularly interesting considering there were statistically significant changes in quantitative and kinetic measurements both for individual proteins and globally in the LP diet (Figure 5-3 A and C). This indicates that the observed changes to the proteome, and presumably the phenotypic benefits, of LP DR are regulated post-transcriptionally.

In an effort to explain how this post transcriptional regulation occurs, we analyzed the RNA-Seq data for evidence that changes in protein concentration or kinetics are correlated with micro-RNA motifs, transcriptional activating factors, or other RNA motifs that are known to regulate mRNA longevity and translation. These tests found no evidence of gene-specific control at this level. This indicates that the post-transcriptional control is unlikely to be driven by RNA sequence based regulation. Using the combination of turnover and concentration changes for each protein, we can identify the primary control mechanism for the mechanism of post-transcriptional regulation that is active during protein translation or degradation.

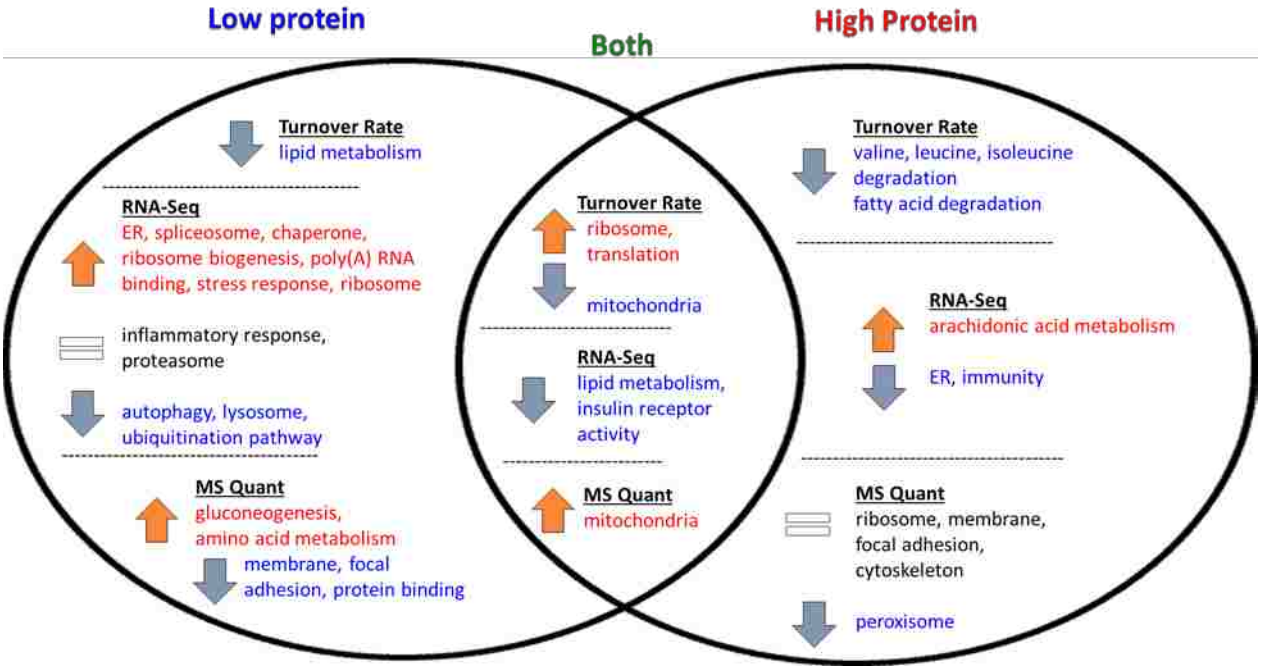

Figure 5-5 Ontology Analysis of HP vs LP Diets. Venn diagram of the differences observed when LP and HP diets were compared. Groupings were determined by the process described in "Gene Ontology Analysis" in the methods section. Comparison is between DR and AL, so if an ontological group shows a red Up arrow under the RNA header, there is more mRNA from that group in DR than AL and vice versa. This figure demonstrates that there are clear differences between diets affecting important cellular pathways

5.5.4 Ontology Groupings

After the global protein trends were determined, we grouped proteins whose kinetics or concentrations responded in similar ways from the various diets and tested whether there was a statistically significant change in the concentration or kinetics for the proteins as a group. Significance of the change for the group was assessed by comparing to the background of all proteins observed. The results of the ontology analysis are shown in Figure 5-5, with all results (up, down or unchanged) being a comparison of DR relative to AL. Our ontology analysis demonstrated that some large functional categories respond similarly to DR regardless of dietary protein, such as mitochondria and the ribosome. It should also be noted that the LP analysis showed more ontologies and more of those detected were changed compared to AL. This fits with the global shifts in protein turnover rate and quantitation observed in LP diets but not in HP diets.

5.5.5 Regulation can be Determined through Multi-Omics

By using our multi-omics approach, we have determined that changes in concentration and turnover of many proteins throughout the proteome during DR with added dietary protein are controlled post-transcriptionally. Although mRNA concentrations were unchanged we observed that many proteins experienced a significant change in concentration. The turnover rate decrease for the majority of observed proteins is consistent with previous literature[20], and when compared against the change in concentration we can identify whether synthesis or degradation is primarily regulated under these conditions.

In comparing LP to HP diets, we have determined that the HP disruption of LP DR extends to global proteome maintenance, expanding beyond the specific pathways previously observed[26]. We have determined that the large decreases in protein turnover and quantity we and

others[8,20] have observed in LP DR compared to its AL control are almost entirely lost during HP DR.

5.5.6 Identification of Possible Regulatory Mechanism

Our ontological analysis (Figure 5-5) indicated that one of the functional groups showing the greatest variation between HP and LP dietary restriction diets was translational machinery. We hypothesized that a large-scale regulatory change in a protein functional group involved in translation could be responsible for the overall slowing of protein synthesis observed in LP dietary restriction. The proteins involved in translational machinery were subdivided based on the general roles they fulfill during protein synthesis (e.g. ternary complex formation, ribosomal structure, tRNA charging), and analyzed for differences between HP and LP dietary restriction diets. Of all of these subgroups, the most striking differences were found in the tRNA synthetases. While the RNA-Seq data for these enzymes was unchanged, similar to the overall RNA-Seq trends, the concentration for many of the tRNA synthetases was significantly lower in LP-DR versus HP-DR diets (Figure 5-6). When we compared the turnover rates, we observed that the majority of the synthetases were being turned over at a faster rate in LP diets, suggesting that these synthetases were undergoing higher degradation rates. However, about one-third of the synthetases were being turned over at a slower rate in LP diets, indicating decreased synthesis.

It has been observed in previous studies that tight regulatory control over protein translation can be enacted through control of the amino acid-charged tRNA pool[40-42]. Stimuli such as cellular stress[43] and lack of nutrition[44]can cause significant changes in the amount and species of tRNA that are produced and charged with amino acids[45]. By manipulating the amount of specific amino-acyl tRNAs, the cell could bias protein production to favor mRNA's

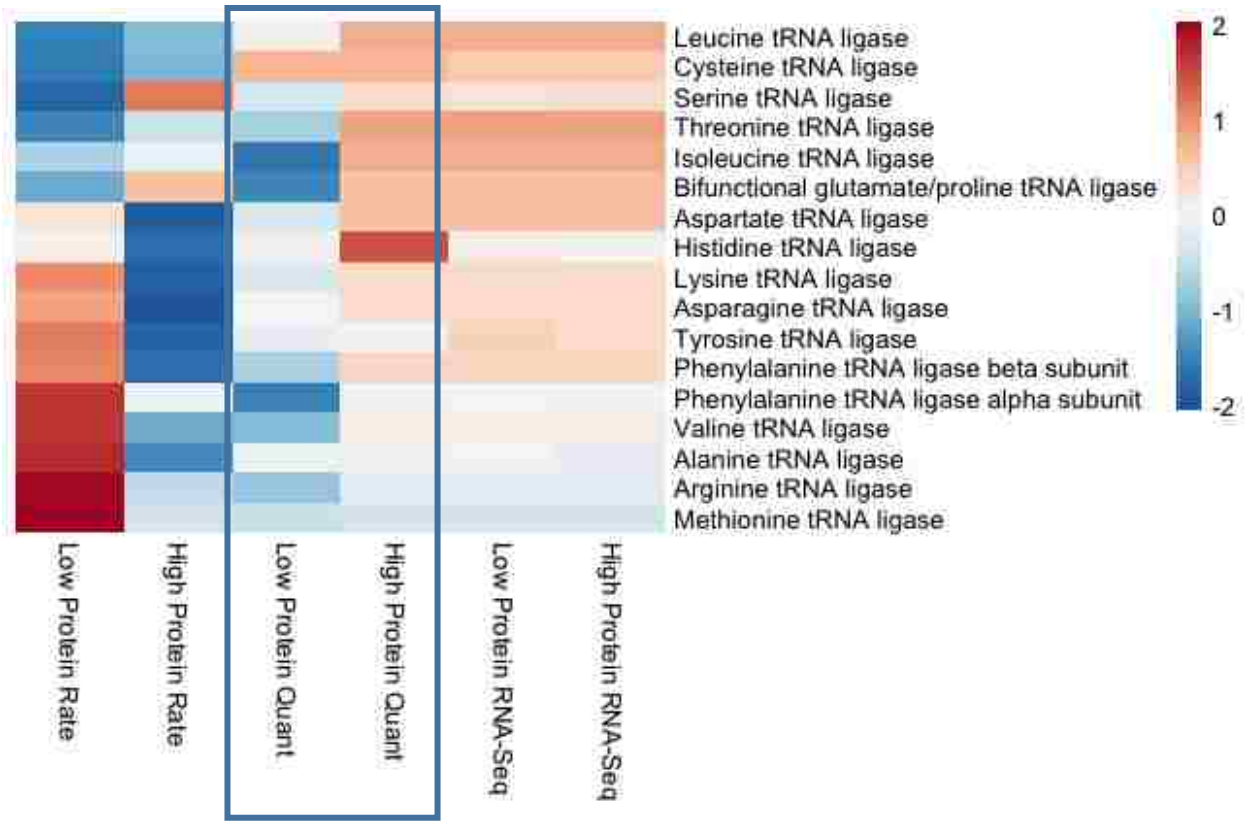

Figure 5-6 Analysis of tRNA Synthetases: When analyzing proteins involved in translation to find a post-transcriptional control mechanism, we observed that concentrations of 18 out of 20 tRNA syntethases were significantly lower in LP-DR, but not HP-DR which could explain the slower general protein translation rate in LP. The changes in turnover rates of the synthetases indicates differential regulation of the individual enzyme concentrations.

containing specific codons, allowing the cell to quickly adjust to changing environmental conditions[45,46]. However, although mechanisms in *E. Coli* and yeast[40,41] have been studied, the methods the eukaryotic cells could use to cause such tRNA biases are not well understood.

Our data suggest that liver cells may do this is by fine-tuned regulation of tRNA synthetase activity. The quantity of a particular tRNA synthetase is expected to have a direct effect on the overall production rate of its amino-acyl tRNA; if the quantity of the charging enzyme goes down, we would expect the concentration of the corresponding amino-acyl tRNA to decrease as well. This would have a wide-scale dampening effect on protein synthesis both through reduction of raw material provided to the ribosome, as well as through the Gcn2

regulatory pathway, which responds to increasing amounts of uncharged cytosolic tRNA[41] (Figure 5-7).

The change in tRNA synthetase regulation could be tied to changes in amino acid availability, which could logically cause decreased cytosolic concentration of tRNA synthetases through regulatory feedback mechanisms. This could be tested by measuring free amino acid and tRNA concentrations in the tissue. Also, direct measurement of the percentage of charged amino-acyl tRNA for all amino acids would test for a tRNA pool perturbation occurring as a result of differential dietary protein amounts. The results of these experiments are expected to confirm whether alterations to the tRNA pool constitute a major cellular mechanism resulting in the phenotypic benefits observed with DR.

5.6 Discussion

Using quantitative and kinetic proteomics, we have shown that we can simultaneously monitor regulation of synthesis and degradation of large numbers of individual proteins *in vivo*. This is particularly important in studying dietary restriction (DR) where RNA-Seq showed that the mRNA concentrations were remarkably unchanged by DR. These results suggest that there is significant post-transcriptional regulation due to dietary changes for most of the proteome. This, along with data on weight and mitochondrial respiration, suggests a major change disruption of DR based on dietary protein level, as well as suggesting a possible mechanism for the disruption. The HP DR animals may be attempting to maintain protein levels and turnover rates with less energy to do so. Maintaining high protein turnover and concentration requires energy and raw materials. Draining resources to try to maintain an AL proteome with DR resource levels could result in animals using more of their body weight as energy. Furthermore, this changed energy response could also affect the mitochondria due to its role in metabolism.

Lending credence to this hypothesis, both the respiration data and ontology analysis suggest that mitochondria were remodeled as part of both DR phenotypes. If the dietary protein creates strain on the mitochondria and the organism more generally, the changed energy requirements could undo the benefits of DR as observed by Solon-Biet, which includes reducing the lifespan back towards AL lifespan[26,47]. Another hypothesis is that DR is beneficial because the lowered protein turnover permits greater quality control of the synthesized proteins [48]. If the dietary protein encourages increased protein turnover rates globally, the hypothesis predicts an AL-like phenotype should be observed. Differentiating between these hypotheses, and identifying differences in signaling between the LP DR and HP DR diets requires further investigation.

A critical clue into the investigation of dietary signalling is the RNA-Seq data. Neither DR treatment shows a significant change from AL, nor does protein level change the correlation between AL and DR. This suggests that whatever DR or dietary protein are signaling to the cell, the signal is affecting the proteome after RNA is transcribed. The logical control points would be the ribosome, which synthesizes all proteins, or the various protein degradation pathways.

Our primary hypothesis currently is the global shift in homeostasis that occurs during DR is orchestrated in large part by control of the tRNA synthetase enzymes. A reduction in the charging of tRNA would cause global shifts in protein synthesis by the ribosome (Figure 5-7). Interestingly, the relative charging percentage of tRNA is carefully monitored and is tied to the activity of the GCN2 kinase. When uncharged tRNAs bind to GCN2 it acts immediately to repress translation by phosphorylation of eIF-2α at serine 51 within 15 min of amino acid deprivation[49]. Therefore, the regulation of the tRNA synthetase enzymes may be a longer-term result of the initial GCN2 signaling. Data suggests individual regulatory mechanisms for different tRNA synthetases, but we have not analyzed the individual mechanisms at this time. In

the future, we will examine the amount of tRNA in the cells. We will also attempt to observe quantity and phosphorylation state of various control proteins through more targeted mass spectrometry or immuno-affinity assays.

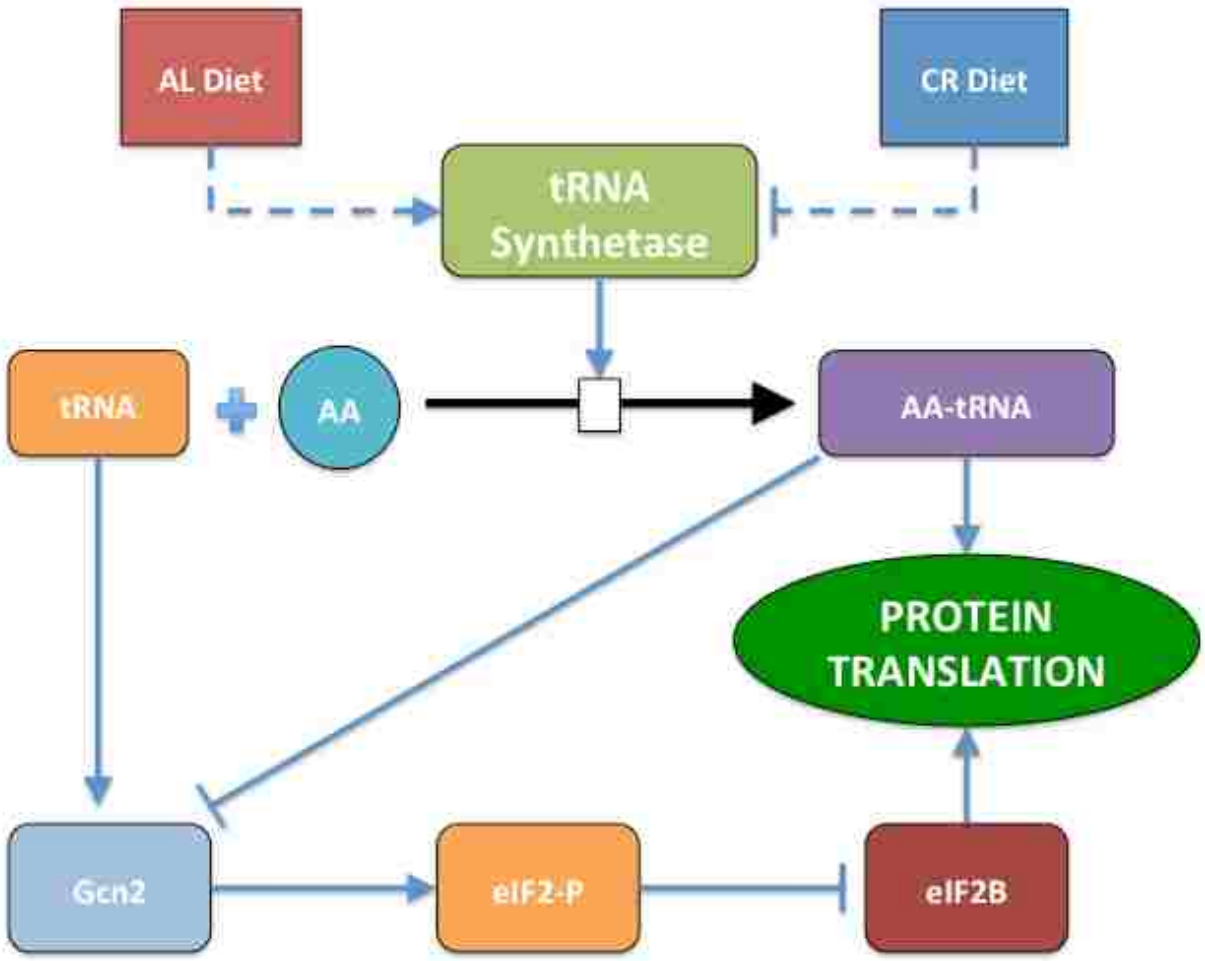

Figure 5-7 Model of tRNA in DR. Known model of tRNA synthetases control of protein translation. Our contribution to the model is the dietary control of the tRNA synthetases.

5.7 Future Directions

Post-transcriptional control of the proteome in DR has been established, and dietary protein has been shown to undo the kinetic and quantitative changes traditionally associated with DR. We have evidence that the tRNA synthetase enzymes are a potential pathway for control of

proteostasis due to dietary signaling. We are in the process of measuring tRNA levels and charging to determine if differences in tRNA synthetase turnover and concentration are responsible, at least in part, for the proteostatic regulation in LP-DR that is undone by high dietary protein.

5.8 Acknowledgements

We are grateful to Dr. Wilcox and the BYU sequencing center for collecting RNA-Seq data from purified RNA, and Earl Albee, Warren Bingham, and the BYU animal care facility for assistance in maintenance of the mice. This work was supported by a grant from the Fritz B. Burns Foundation, BYU startup funds to JCP, Roland K. Robins Graduate Research Fellowships to BCN and RHC, and BYU Undergraduate Research Awards to NK, RP, BJ, and SA.

5.9 Bibliography

1 Ben-Zvi, A., Miller, E. A. & Morimoto, R. I. Collapse of proteostasis represents an early molecular event in Caenorhabditis elegans aging. *Proc. Natl. Acad. Sci. U. S. A.* **106**, 14914-14919, doi:10.1073/pnas.0902882106 (2009).

2 Ke, Z. *et al.* Translation fidelity coevolves with longevity. *Aging Cell* **16**, 988-993, doi:10.1111/acel.12628 (2017).

3 McCay, C. M., Crowell, M. F. & Maynard, L. A. The effect of retarded growth upon the length of life span and upon the ultimate body size. *Nutrition* **5**, 155-171; discussion 172 (1935).

4 Anderson, R. M., Shanmuganayagam, D. & Weindruch, R. Caloric restriction and aging: studies in mice and monkeys. *Toxicol. Pathol.* **37**, 47-51, doi:10.1177/0192623308329476 (2009).

5 Karunadharma, P. P. *et al.* Subacute calorie restriction and rapamycin discordantly alter mouse liver proteome homeostasis and reverse aging effects. *Aging Cell* **14**, 547-557, doi:10.1111/acel.12317 (2015).

6 de Groot, M. J. *et al.* Quantitative proteomics and transcriptomics of anaerobic and aerobic yeast cultures reveals post-transcriptional regulation of key cellular processes. *Microbiology* **153**, 3864-3878, doi:10.1099/mic.0.2007/009969-0 (2007).

7 Miller, B. F., Drake, J. C., Naylor, B., Price, J. C. & Hamilton, K. L. The measurement of protein synthesis for assessing proteostasis in studies of slowed aging. *Ageing Res Rev* **18**, 106-111, doi:10.1016/j.arr.2014.09.005 (2014).

8 Dai, D. F. *et al.* Altered proteome turnover and remodeling by short-term caloric restriction or rapamycin rejuvenate the aging heart. *Aging Cell* **13**, 529-539, doi:10.1111/acel.12203 (2014).

9 Leprivier, G., Rotblat, B., Khan, D., Jan, E. & Sorensen, P. H. Stress-mediated translational control in cancer cells. *Biochim. Biophys. Acta* **1849**, 845-860, doi:10.1016/j.bbagrm.2014.11.002 (2015).

10 Montanaro, L., Trere, D. & Derenzini, M. Nucleolus, ribosomes, and cancer. *Am. J. Pathol.* **173**, 301-310, doi:10.2353/ajpath.2008.070752 (2008).

11 Kolch, W. & Pitt, A. Functional proteomics to dissect tyrosine kinase signalling pathways in cancer. *Nat. Rev. Cancer* **10**, 618-629, doi:10.1038/nrc2900 (2010).

12 Kristiansen, M. *et al.* Disease-associated prion protein oligomers inhibit the 26S proteasome. *Mol. Cell* **26**, 175-188, doi:10.1016/j.molcel.2007.04.001 (2007).

13 Repetto, E., Yoon, I. S., Zheng, H. & Kang, D. E. Presenilin 1 regulates epidermal growth factor receptor turnover and signaling in the endosomal-lysosomal pathway. *J. Biol. Chem.* **282**, 31504-31516, doi:10.1074/jbc.M704273200 (2007).

14 Safar, J. G. *et al.* Prion clearance in bigenic mice. *J. Gen. Virol.* **86**, 2913-2923, doi:10.1099/vir.0.80947-0 (2005).

15 Lee, S. & Notterpek, L. Dietary restriction supports peripheral nerve health by enhancing endogenous protein quality control mechanisms. *Exp. Gerontol.* **48**, 1085-1090, doi:10.1016/j.exger.2012.12.008 (2013).

16 Callister, S. J. *et al.* Normalization approaches for removing systematic biases associated with mass spectrometry and label-free proteomics. *J. Proteome Res.* **5**, 277-286, doi:10.1021/pr050300l (2006).

17 Malmstrom, J. *et al.* Proteome-wide cellular protein concentrations of the human pathogen Leptospira interrogans. *Nature* **460**, 762-765, doi:10.1038/nature08184 (2009).

18 Naylor, B. C. *et al.* DeuteRater: a tool for quantifying peptide isotope precision and kinetic proteomics. *Bioinformatics* **33**, 1514-1520, doi:10.1093/bioinformatics/btx009 (2017).

19 Kasumov, T. *et al.* Measuring protein synthesis using metabolic ^{2}H labeling, high-resolution mass spectrometry, and an algorithm. *Anal. Biochem.* **412**, 47-55, doi:10.1016/j.ab.2011.01.021 (2011).

20 Price, J. *et al.* The Effect of Long Term Calorie Restriction on in Vivo Hepatic Proteostatis: A Novel Combination of Dynamic and Quantitative Proteomics. *Mol. Cell. Proteomics* **11**, 1801-1814, doi:10.1074/mcp.M112.021204 (2012).

21 Price, J. C. *et al.* Measurement of human plasma proteome dynamics with (2)H(2)O and liquid chromatography tandem mass spectrometry. *Anal. Biochem.* **420**, 73-83, doi:10.1016/j.ab.2011.09.007 (2012).

22 Lam, M. P. *et al.* Protein kinetic signatures of the remodeling heart following isoproterenol stimulation. *J. Clin. Invest.* **124**, 1734-1744, doi:10.1172/JCI73787 (2014).

23 Liao, C. Y., Rikke, B. A., Johnson, T. E., Diaz, V. & Nelson, J. F. Genetic variation in the murine lifespan response to dietary restriction: from life extension to life shortening. *Aging Cell* **9**, 92-95, doi:10.1111/j.1474-9726.2009.00533.x (2010).

24 Schleit, J. *et al.* Molecular mechanisms underlying genotype-dependent responses to dietary restriction. *Aging Cell* **12**, 1050-1061, doi:10.1111/acel.12130 (2013).

25 Cai, W. *et al.* Oral glycotoxins determine the effects of calorie restriction on oxidant stress, age-related diseases, and lifespan. *Am. J. Pathol.* **173**, 327-336, doi:10.2353/ajpath.2008.080152 (2008).

26 Solon-Biet, S. M. *et al.* The ratio of macronutrients, not caloric intake, dictates cardiometabolic health, aging, and longevity in ad libitum-fed mice. *Cell Metab.* **19**, 418-430, doi:10.1016/j.cmet.2014.02.009 (2014).

27 Lis, G., Wassenaar, L. I. & Hendry, M. J. High-precision laser spectroscopy D/H and 18O/16O measurements of microliter natural water samples. *Anal. Chem.* **80**, 287-293, doi:10.1021/ac701716q (2008).

28 Wang, Y. *et al.* Reversed-phase chromatography with multiple fraction concatenation strategy for proteome profiling of human MCF10A cells. *Proteomics* **11**, 2019-2026, doi:10.1002/pmic.201000722 (2011).

29 Vaudel, M., Barsnes, H., Berven, F. S., Sickmann, A. & Martens, L. SearchGUI: An open-source graphical user interface for simultaneous OMSSA and X!Tandem searches. *Proteomics* **11**, 996-999, doi:10.1002/pmic.201000595 (2011).

30 Vaudel, M. *et al.* PeptideShaker enables reanalysis of MS-derived proteomics data sets. *Nat. Biotechnol.* **33**, 22-24, doi:10.1038/nbt.3109 (2015).

31 Cox, J. & Mann, M. MaxQuant enables high peptide identification rates, individualized p.p.b.-range mass accuracies and proteome-wide protein quantification. *Nat. Biotechnol.* **26**, 1367-1372, doi:10.1038/nbt.1511 (2008).

32 Love, M. I., Huber, W. & Anders, S. Moderated estimation of fold change and dispersion for RNA-seq data with DESeq2. *Genome Biol.* **15**, 550, doi:10.1186/s13059-014-0550-8 (2014).

33 Huang, d. W., Sherman, B. T. & Lempicki, R. A. Systematic and integrative analysis of large gene lists using DAVID bioinformatics resources. *Nat. Protoc.* **4**, 44-57, doi:10.1038/nprot.2008.211 (2009).

34 Huang, d. W., Sherman, B. T. & Lempicki, R. A. Bioinformatics enrichment tools: paths toward the comprehensive functional analysis of large gene lists. *Nucleic Acids Res.* **37**, 1-13, doi:10.1093/nar/gkn923 (2009).

35 Heinz, S. *et al.* Simple combinations of lineage-determining transcription factors prime cis-regulatory elements required for macrophage and B cell identities. *Mol. Cell* **38**, 576-589, doi:10.1016/j.molcel.2010.05.004 (2010).

36 Blagosklonny, M. V. Molecular damage in cancer: an argument for mTOR-driven aging. *Aging (Albany NY)* **3**, 1130-1141, doi:10.18632/aging.100422 (2011).

37 Kenyon, C. J. The genetics of ageing. *Nature* **464**, 504-512, doi:10.1038/nature08980 (2010).

38 Lynch, C. J. Role of leucine in the regulation of mTOR by amino acids: revelations from structure-activity studies. *J. Nutr.* **131**, 861S-865S (2001).

39 Jewell, J. L. *et al.* Metabolism. Differential regulation of mTORC1 by leucine and glutamine. *Science* **347**, 194-198, doi:10.1126/science.1259472 (2015).

40 Sorensen, M. A. *et al.* Over expression of a tRNA(Leu) isoacceptor changes charging pattern of leucine tRNAs and reveals new codon reading. *J. Mol. Biol.* **354**, 16-24, doi:10.1016/j.jmb.2005.08.076 (2005).

41 Zaborske, J. M. *et al.* Genome-wide analysis of tRNA charging and activation of the eIF2 kinase Gcn2p. *J. Biol. Chem.* **284**, 25254-25267, doi:10.1074/jbc.M109.000877 (2009).

42 Young, S. K., Baird, T. D. & Wek, R. C. Translation Regulation of the Glutamyl-prolyl-tRNA Synthetase Gene EPRS through Bypass of Upstream Open Reading Frames with Noncanonical Initiation Codons. *J. Biol. Chem.* **291**, 10824-10835, doi:10.1074/jbc.M116.722256 (2016).

43 Chan, C. T. *et al.* A quantitative systems approach reveals dynamic control of tRNA modifications during cellular stress. *PLoS Genet.* **6**, e1001247, doi:10.1371/journal.pgen.1001247 (2010).

44 Ferro, I., Liebeton, K. & Ignatova, Z. Growth-Rate Dependent Regulation of tRNA Level and Charging in Bacillus licheniformis. *J. Mol. Biol.* **429**, 3102-3112, doi:10.1016/j.jmb.2017.09.010 (2017).

45 Wilusz, J. E. Controlling translation via modulation of tRNA levels. *Wiley Interdiscip Rev RNA* **6**, 453-470, doi:10.1002/wrna.1287 (2015).

46 Rush, E. C., Chhichhia, P., Kilding, A. E. & Plank, L. D. Water turnover in children and young adults. *Eur. J. Appl. Physiol.* **110**, 1209-1214, doi:10.1007/s00421-010-1621-5 (2010).

47 Solon-Biet, S. M. *et al.* Dietary Protein to Carbohydrate Ratio and Caloric Restriction: Comparing Metabolic Outcomes in Mice. *Cell Rep*, doi:10.1016/j.celrep.2015.05.007 (2015).

48 Mathis, A. D. *et al.* Mechanisms of In Vivo Ribosome Maintenance Change in Response to Nutrient Signals. *Mol. Cell. Proteomics* **16**, 243-254, doi:10.1074/mcp.M116.063255 (2017).

49 Dong, J., Qiu, H., Garcia-Barrio, M., Anderson, J. & Hinnebusch, A. G. Uncharged tRNA activates GCN2 by displacing the protein kinase moiety from a bipartite tRNA-binding domain. *Mol. Cell* **6**, 269-279 (2000).

6. Conclusions

Kinetic proteomics is an emerging field with great potential. Currently the need for specialized analysis tools hinders broad use of the technique. I have led the development of tools that both advance the calculations and are user friendly. By providing these tools, my team has helped researchers unfamiliar with kinetic proteomics enter the field without needing to invest months determining calculations and creating software tools, or needing to collaborate with one of the few labs created the necessary calculation software in house. I have also led the group improving our DeuteRater tool to work on the more complicated calculations needed to perform kinetic proteomics in human subjects. By improving on both our own and existing tools, we have the potential to extend human kinetic proteomics beyond one or two expert groups, and make the technique available to all scientists.

I have also contributed to our knowledge of biology by using kinetic proteomics. Working closely with other graduate students in the Price lab, I have been instrumental in proving ribosomal protein exchange in eukaryotes, and so a possible method of ribosomal maintenance. Not only is ribosomal maintenance critical to normal functioning of the cell, but ribosomal maintenance may be responsible for dietary restriction's (DR) beneficial effects on longevity observed in mice. Finally, I worked closely other graduate students to determine global regulation of the proteome in normal DR and the disrupted state caused by adding dietary protein to DR. While work is still necessary to confirm our findings, it is possible that this study

will shed needed light on the mechanism of DR in laboratory animals. Hopefully, our findings can be translated into further discoveries in humans.

7. Future Directions

The main future directions for this work are preparing DeuteRater-H for distribution, and confirming the tRNA effect observed between High Protein and Low Protein DR. These changes have been elaborated on in their respective chapters.

Other future directions include analyzing the ribosome in other conditions. A ribosomal disease or a different time in the lifespan of a mouse would provide insight into how different damage conditions affect ribosomal maintenance. A similar effort could be performed with DR, examining how ribosomal maintenance changes in conditions that cause DR-like effects or are immune to DR, such as different dietary conditions or different genotypes. Examining turnover in these models could determine if improved ribosomal maintenance is specific to DR, or is important to all metabolic lifespan extension mechanisms. It would also be useful to determine ribosomal turnover in humans to see if the observations in mice translates to humans as well.

Finally, in DeuteRater, a direction we have not explored is improving higher resolutions in the Orbitrap. When using the highest resolution settings on the Orbitrap, both abundance and neutromer spacing decreased significantly in precision, accuracy, and number of proteins observed. My hypothesis is that most of the problems at high resolution are caused by higher resolution scans requiring more time. Instrument run time was identical for all instrument conditions, which likely resulted in fewer scans to average together in data analysis. This lack of data points results in worse signal to noise compared to other resolutions with more scans per analysis run. If that is the case, lengthening the time of the experimental gradient proportionally

to the scan time should correct the issue, and should theoretically drastically improve neutromer spacing metrics due to the increased resolution.